ADHESION AND FRICTION FORCES OF COLLOIDAL PARTICLES IN ATMOSPHERIC SYSTEMS

A Dissertation
Presented to
The Academic Faculty

by

Hyo Jin Kweon

In Partial Fulfillment
of the Requirements for the Degree
Doctor of Philosophy in the
School of Civil and Environmental Engineering

Georgia Institute of Technology
May 2013

ADHESION AND FRICTION FORCES OF COLLOIDAL PARTICLES IN ATMOSPHERIC SYSTEMS

Approved by:

Dr. Sotira Yiacoumi, Advisor
School of Civil and Environmental Engineering
Georgia Institute of Technology

Dr. Costas Tsouris
School of Civil and Environmental Engineering
Georgia Institute of Technology

Dr. Spyros Pavlostathis
School of Civil and Environmental Engineering
Georgia Institute of Technology

Dr. James Mulholland
School of Civil and Environmental Engineering
Georgia Institute of Technology

Dr. Athanasios Nenes
School of Earth and Atmospheric Sciences
Georgia Institute of Technology

Date Approved: January 8, 2013

To my beloved family…

ACKNOWLEDGEMENTS

Above all, I would like to give thanks to my Lord, Jesus Christ, who has been my wonderful guidance and counselor. He has encouraged and comforted me with the greatest love and piece. He is the reason that I live, and I want to praise, worship, and glorify Him forever with everything He has given me.

I am thankful to Professor Sotira Yiacoumi, my advisor at the Georgia Institute of Technology, for giving me a chance to study for my PhD, and to Professors James A. Mulholland and Spyros G. Pavlosthatis in CEE, Professor Athanasios Nenes in ChBE, and Dr. Costas Tsouris at ORNL for being my committee members.

I must express my deep and sincere gratitude to Professor Jaehong Kim in CEE, Carole Moore who is the Assistant Vice Provost for Academic Affairs, Professor Seung Soon Jang in MSE, and other professors in CEE. They helped and supported me with their whole hearts so that I was able to complete the study.

I am very thankful to my friends whom I met in Atlanta and Boston—the members in Sugarloaf Korean Baptist Church, Boston Onnuri Church, Prayer group at MIT, and Yiacoumi's group—for being with me. They have prayed for me and brought me so many joyful moments.

I want to show my earnest appreciation to my mother, Sook Young Lee, and father, Soon Seok Kweon, for their prayer, support, and unconditional love. They have also taken care of my husband and little baby boy so that I was able to focus on this study with no concern. They are the best mother and father in the world.

Finally, I would like to thank my husband, Jeong Woo Han, for being my other half and my little baby boy, David Hoyoung Han, for coming to mama and papa.

Hyo Jin Kweon

12, 5, 2012, Atlanta, USA

TABLE OF CONTENTS

Page

CHAPTER

LIST OF TABLES

LIST OF FIGURES

Page

LIST OF SYMBOLS

A, A_i	Surface area
a	Intermolecular spacing
D	Separation distance between two interacting surfaces; length of a cylinder
E	Electric field
F	Force
F_{ad}	Adhesion force
F_{cap}	Capillary force
$F_{Coulomb}$	Coulomb force
F_{el}	Electrostatic force
F_f	Friction force
F_{img}	Electrostatic image force
F_n	Normal load
$F_{pressure\_difference}$	Force due to the pressure difference across the meniscus
$F_{surface\_tension}$	Force due to the surface tension of water
F_{vdw}	Van der Waals force

F_{tot}	Total adhesion force; the sum of adhesion force and normal load
H_{air}	Hamaker constant in air
H_{water}	Hamaker constant in water
H	Distance between the circular line of the sphere and the substrate
k	Spring constant of the AFM probe
l, r	Principal radii of the meniscus
P/P_o	Relative humidity
Q_i	Surface charge
R	Ideal gas constant
R_p	Radius of the spherical particle or the AFM tip
S	Photodiode sensitivity
T	Absolute temperature
V	Voltage; deflection signal; surface potential
V_i	Surface potential of the *i*-th surface
V_m	Molar volume of water
Z	Separation distance between two spheres
α, β, γ	Weight coefficient

β_m	Angle of the meniscus
γ_w	Surface tension of water
ΔP	Pressure difference across the meniscus
ΔV	Change in the deflection signal of the probe: difference in the surface potential
ε	Relative permittivity
ε_o	Vacuum permittivity
θ_i	Contact angles of surfaces
μ	Friction coefficient
σ, σ_i	Surface charge density
Φ	Electric flux

LIST OF ABBREVIATIONS

AFM	Atomic force microscopy
Bt	*Bacillus thuringiensis*
DLVO	Derjaguin-Landau-Verwey-Overbeek
EFM	Electrostatic force microscopy
HFIR	High flux isotope reactor
ORNL	Oak Ridge National Laboratory
RH	Relative Humidity
SEM	Scanning electron microscopy
SSPM	Scanning surface potential microscopy
STEM	Scanning transmission electron microscopy

SUMMARY

Interactions of colloidal particles with surfaces occur in natural and engineered systems, and they influence the transport of contaminants through diffusion, aggregation, filtration, and sedimentation. To quantify the transport and fate of colloidal particles and their influence on the environment, it is therefore important to understand their interactions with surfaces. Colloidal particles interact with surfaces through adhesion and friction forces, which include van der Waals, capillary, electrostatic, hydration, and hydrophobic interactions. Both adhesion and friction forces can determine how strongly colloidal particles interact with surfaces, and they are influenced by various physical and chemical surface properties, such as hydrophobicity, charge density, and roughness, as well as the conditions of the surrounding environments. In atmospheric systems, relative humidity (RH) induces the capillary force and also influences the contributions of van der Waals and electrostatic forces. To investigate the role of surface properties and RH in the interactions of colloidal particles with surfaces, atomic force microscopy (AFM) was employed to measure the adhesion and friction forces of colloidal particles including *Bacillus thuringiensis* spores, silica, and gold at various experimental conditions with several types of surfaces including mica, silica, and radioactive gold. In addition, the adhesion forces including van der Waals, capillary, and electrostatic forces were theoretically calculated and compared to measured forces.

The interaction of *Bacillus thuringiensis* spores, which are considered models for *Bacillus anthracis,* with surfaces reveals that the influence of RH on the adhesion and friction forces varies for different surface properties including hydrophobicity, roughness, and charge density. The friction force of the spores is greater on a rougher surface than on mica, which is atomically flat. As RH increases, the friction force of the spores decreases on atomically flat surfaces whereas it increases on rough surfaces. The influence of RH on the interaction forces between hydrophobic surfaces is not as strong as for hydrophilic surfaces. The friction force of the spores is linear to the sum of the adhesion force and normal load on the hydrophobic surface. The poorly defined surface structure of the spores and the adsorption of contaminants from the surrounding atmosphere are believed to cause a discrepancy between the calculated and measured adhesion forces.

The role of surface potential was investigated in order to study how radioactivity influences the interaction of colloidal particles with surfaces. Adhesion force measurements for an irradiated gold surface show that radioactivity influences adhesion because radioactive materials acquire surface charge through a self-charging process. They can thus behave differently from natural aerosols in atmospheric systems, giving rise to resuspension and secondary contamination in areas far from the source. Scanning surface potential microscopy was employed to measure the surface potential of radioactive gold foil. Atomic force microscopy was also used to investigate the adhesion force for gold that acquired surface charge either by irradiation or by the application of electrical bias. Overall, the adhesion force increases with increasing surface potential or relative humidity. At high levels of radioactivity, the adhesion force increases when relative humidity increases to medium levels but decreases with a further increase of relative humidity. A comparison between experimental measurements and calculated values revealed that the surface potential promotes adhesion. The contribution of the electrostatic force at high levels of relative humidity was lower than the one estimated by the theoretical calculations due to the effects caused by enhanced adsorption of water molecules when surfaces are highly charged.

In the continuation of the study, the role of electrostatic potential in particle adhesion and the influence of RH on the contribution of electrostatic force were further investigated using micron-sized spherical particles and various planar surfaces including mica, silica, and gold. It was found that the application of a stronger positive electrical bias to the particles induces a stronger total adhesion force. The sensitivity of the system to the changes in the bias is strongest in the system with mica due to its highest surface charge density among the materials investigated. For larger-size particles, the contribution of the electrostatic force is diminished, and therefore the sum of van der Waals and capillary forces becomes the major contributor to the total adhesion force. The role of water adsorption in the total adhesion force and its influence on the contribution of the electrostatic force depends on the hydrophobicity or the contact angle of interacting surfaces. For the hydrophilic surface, water adsorption either attenuates the surface charge or screens the effect of surface potential. The excessive amount of adsorbed water provides a path to surface charge leakage that may cancel out the electrostatic force, leading to a reduction in the adhesion force. Even though model equations have limitations to predict the influence of water adsorption on the electrostatic force, theoretically calculated forces agree well with the measured adhesion forces except for the system with highly localized surface potential.

The results in this thesis provide fundamental information about the interactions of colloidal particles with surfaces at various conditions in atmospheric environments.

Systems of interest include microbial spores and radioactive surfaces. Thus, the results can help better understand the phenomena influenced by the interaction of colloidal particles such as aggregation, coagulation, and transport, and be useful in monitoring and control of contamination in atmospheric systems.

CHAPTER 1

INTRODUCTION

1.1. Interactions of Colloidal Particles with Surfaces

Interactions of colloidal particles with surfaces are of interest in several research areas, including environmental engineering, as colloidal particles and surfaces are abundant in natural and engineered systems and play a determining role in the transport of contaminants and in decontamination processes.[1,2] Immobilization and release of particulate contaminants, wear of mechanical devices, and transport of particles in groundwater and atmospheric systems are a few examples that are influenced by interaction forces of colloidal particles. These forces are also involved in microbial activities such as attachment of biological particles to surfaces and membrane fouling.[3-5] The interaction of colloidal particles with surfaces is also involved in the decrease of energy production because the adhesion of particles to the leaves of broad-leaf trees and solar panels may disrupt the absorption of solar energy. Therefore, the interaction of colloidal particles not only influences the quality of natural environments and human health but also impacts the social economy and future energy production.

Surface interaction forces include van der Waals, capillary, electrostatic, hydration, and hydrophobic interactions.[6] These forces can be categorized into two types according to their direction with respect to the interacting surfaces: adhesion and friction forces. Adhesion is the force normal to interacting surfaces and is defined as the minimum force required for detachment of one surface from another. Friction is the force resisting the lateral motion of an object in contact with a substrate surface, and is divided into two kinds according to the relative movement between the interacting surfaces: static and kinetic friction. Static friction is exerted between two objects with no relative motion while kinetic friction is between two objects with relative motion. To move stationary particles on a surface, a stronger force than the static friction force between the particles and the surface is required.

In atmospheric systems, the van der Waals, capillary, and electrostatic forces are the main components of the interaction of colloidal particles with surfaces. The van der Waals force arises from instantaneous polarization due to dipole moments among non-polar molecules. The electrostatic force occurs when the interacting surfaces acquire surface charge, and it consists of the Coulombic force and the electric image force. The van der Waals and electrostatic forces exist in both air and water. On the contrary, the capillary force exists only in air because it arises from water condensation between interacting surfaces and depends on the relative humidity (RH). The capillary force is the sum of the forces from surface tension of water and the pressure difference across the water meniscus.[1]

Interaction forces, including friction, are generally influenced by the physical and chemical properties of interacting surfaces, such as surface roughness, particle shape, hydrophobicity, and surface charge.[1,7] First and foremost, RH plays an important role because of its effects on the contribution of other properties to the adhesion.[8,9] As RH increases, the surface coverage by water molecules and the thickness of the water layer increase, depending on the affinity of the surface material to water.[10] Adsorbed water molecules may contribute to friction in two opposing ways: (i) by attenuating friction due to the lubrication of surfaces and (ii) by enhancing friction due to the increase of the effective contact area and the capillary force arising from water condensation between interacting surfaces. The surface charge is also considered an important influencing parameter, especially when the system includes conductive or charged surfaces.[11,12] Since moisture dissipates the charge, the electrostatic force can either promote or decrease the friction force, depending on the sign of the charge of the interacting surfaces. Besides adsorption, absorption of water molecules by the interacting bodies can influence the interaction forces by altering surface features such as roughness and particle size.[13,14]

Atomic force microscopy (AFM) is used widely to study interaction forces of colloidal particles at interfaces owing to its capability to image the geometry of a surface and to measure surface interaction forces occurring at microscales and even at nanoscales. Various applications of AFM are reviewed thoroughly elsewhere.[15,16] The interfacial behavior between two contacting surfaces at such scales often cannot be explained by generally accepted knowledge for macroscopic systems due to the significance of the molecular interactions at microscales and nanoscales. For example, the well-known Amontons' Law shows a linear relationship between the friction force, F_f, and the total normal force—that is, the sum of the adhesion force and the normal load—for macroscopic interactions: $F_f = \mu (F_n + F_{ad})$, where μ, F_n, and F_{ad} are the friction coefficient, the normal load, and the adhesion force, respectively. However, based on experimental and computational simulation results, this relationship is nonlinear at microscales and nanoscales.[3,17-19] Adhesion characteristics and surface roughness are key components determining the nature of the relationship between friction and normal forces.[19] Therefore, the macroscopic perception cannot simply be applied to such interactions at small scales.

In this thesis, the interactions of the spores of *Bacillus thuringiensis* and of radioactive materials with various types of surfaces are investigated. The influence of bacteria, among other colloidal particles, is inevitable in environmental and human activities because of their ubiquitous interactions with living or nonliving surfaces except in cautiously controlled clean systems.[20] Particularly, biofilms and spores are of great concern in food science, pathology, and environmental sciences because they are highly resistant to various disinfectants.[20,21] Typically in aquatic systems or with an abundant amount of moisture in atmospheric systems, bacteria tend to accumulate on surfaces and form biofilms by which they can survive and protect themselves more effectively due to the higher nutrient levels on surfaces than in bulk media.[20] A spore (or endospore), which is another method of self-defense for spore-forming bacteria, is an effective means of bacterial dispersal in air and water. When bacteria face life-threatening conditions such as extreme temperature, dehydration, nutrient depletion, and disinfectant chemicals, they produce spores that are highly resistant to such conditions. Most spore-forming bacteria reside in soil, and when they encounter moisture- and nutrient-rich conditions, they turn back into vegetative cells. In air, bacterial spores can be transmitted to humans by inhalation, consumption of contaminated products, and skin contact because they transfer in the environment with other airborne particles.[20,22] Therefore, the behavior of spores depends upon environmental conditions such as temperature and RH, as well as the physical and chemical properties of interacting surfaces in atmospheric systems.

Transport of radioactive particles plays an important role in spreading radioactivity.[23] Like other particulate matter, radioactive particles deposited onto the soil and plants can be resuspended by natural and anthropogenic activities, including wild fires and human-initiated burning,[24,25] propagating radioactive contamination to an initially uncontaminated area. Because of health issues and long-term effects associated with aerosols contaminated with adsorbed isotopes,[26] it is essential to monitor and control the transport of radioactivity. However, traditional particle diffusion models fail to predict the behavior of radioactive particles in atmospheric systems arising from changes in their electrical state owing to self-charging.[24,25,27-29] The self-charging process can be one of the most important features of radioactive particles, which acquire surface charge through two processes: (1) ionization due to the emission of either charged particles or electrons during radioactive decay, and (2) absorption of ions generated in the surrounding medium.[23,30-33] More specifically, the net surface charge depends on particle activity and the ion concentration of the surrounding medium.[31,33] Another factor influencing the surface charge of radioactive particles is their size. The smaller the particle size, the higher is the surface charge density.[12,32] Therefore, the transport of colloidal radioactive particles can be very different from that of larger particles. Surface charge acquired during the decay processes can extend the travel distance of particles, leading to unexpected radioactive contamination of areas far from the source of the radioactivity. Furthermore, the surface charge may attract particles to other surfaces, resulting in a higher concentration of deposited radioactive particles. Enhancement in the deposition of particles may be due to the increased interaction force by the additional electrical Coulomb or image forces.[33] Therefore, a study of such forces for colloidal radioactive particles is needed so that a predictive model that accurately describes the behavior of radioactive aerosols can be developed.

Anticipating an accidental or intentional release of particulate contaminants, including bacterial spores and radioactive particles, we must be able to predict microscopic surface interactions as well as their macroscopic transport behavior so that our response will be effective and efficient. In this view, a study of the adhesion and friction forces of colloidal particles can help prevent and control surface contamination.

In the present work, the interaction forces of various colloidal particles and planar surfaces are studied using AFM under various conditions in atmospheric systems. Along with the experimental results, theoretical force calculations using available mathematical models for the van der Waals, capillary, and electrostatic forces are performed. The calculated results are compared with the experimental measurements to better understand the contributions of the main force components to the total interaction force.

1.2. Research Objectives

The present work aims at understanding interaction forces of micron-size organic/inorganic particles with several types of planar surfaces under various environmental conditions. To achieve the main goal, the following research objectives were set as building blocks.

- ✓ Investigate the influence of surface properties of interacting surfaces including roughness, particle size and shape, electrical potential, and contamination on the adhesion and friction forces
- ✓ Assess the role of the relative humidity and adsorption of water molecules to surfaces in the adhesion and friction forces.
- ✓ Probe how radioactivity exerts an effect on the interaction forces.

- ✓ Identify the relationship between adsorption of water molecules on surfaces and surface potential, and evaluate how this relationship influences the interaction forces.
- ✓ Examine the validity of existing theoretical models available for interaction forces under various conditions and suggest directions to modify the models in order to describe more accurately the interaction forces.

To achieve these research objectives, the adhesion and friction forces of spherical inorganic (silica and gold) and microbial (spores of *Bacillus thuringiensis*) particles on various planar surfaces including mica, silica, gold, and radioactive gold were measured using AFM. Comparisons of the experimental data with calculated results obtained from existing mathematical models for interaction forces were performed.

1.3. Organization of Thesis

Chapter 1 presents fundamental principles on the interaction of colloidal particles in atmospheric systems, and addresses the importance of the study to the understanding of interaction forces at microscales and nanoscales. The objectives of this research are included as well.

Chapter 2 describes experimental methods and theoretical calculations for interaction forces. The operation procedure of AFM for measurements of adhesion and friction forces is explained, and the mathematical equations for the van der Waals, capillary, and electrostatic forces are introduced.

In Chapter 3, the friction force of a bacterial spore and a spherical silica particle against mica, silica, and gold surfaces is studied in atmospheric systems. The influence of surrounding conditions and surface properties on the force is examined. By comparing the friction coefficient, the validity of macroscopic concepts on the microscopic and nanoscopic interactions is discussed.

The influence of radioactivity and surface potential of radioactive gold on the adhesion force is investigated in Chapter 4. Two different cases of force measurements are compared: (1) irradiated gold surface that acquires surface potential via a self-charging process and (2) gold surface that acquires surface potential via the application of electrical bias. The role of relative humidity is also examined.

How the surface potential and relative humidity influence the adhesion force is investigated in Chapter 5. The surface potential is acquired by applying electrical bias through either a conductive particle or a conductive surface. In addition, the role of adsorption of water molecules in the adhesion force and its influence on the contribution of electrostatic force to the total interaction force is identified.

Chapter 6 includes major conclusions of the thesis and provides recommendations for future studies.

CHAPTER 2

INTERACTIONS OF COLLOIDAL PARTICLES WITH SURFACES: EXPERIMENTAL METHODS AND THEORETICAL MODELS

2.1. Experimental Methods

Interfacial interaction forces of colloidal particles at microscales and nanoscales are measured by atomic force microscopy (AFM). An AFM probe is either a tipped cantilever made with various materials, such as silicon nitride, silicon, and carbon nanotubes, or an AFM probe made by attaching a particle to the end of a tipless cantilever. A conductive AFM probe can be prepared by making or coating the probe with conductive materials such as gold and platinum. The surface potential of substrates can be measured by electrostatic force microscopy (EFM).

2.1.1. Atomic Force Microscopy (AFM)

Atomic force microscopy is a novel tool that can be used not only to image the surface morphology but also to measure interaction forces between a probe and a substrate.[34] AFM has been used to study interaction forces of colloidal particles, including bacteria to substrate surfaces.[21] In the AFM operation, it is possible to control the medium conditions providing a habitat-like environment to bacteria. By using AFM, both adhesion and friction forces can be measured.[16]

In order to measure the interaction force between a colloidal particle and a substrate, a particle is attached to the end of a tipless cantilever. Images of AFM probes in which a colloidal particle or a microbial probe are attached to the end of tipless cantilevers are shown in Figure 2.1. By varying the experimental conditions, such as the type of substrate material and the chemistry of the medium, the contribution of various parameters to the interaction forces can be examined. The adhesion force is measured by first bringing the AFM probe in contact with the substrate surface, and then moving it away from the surface as the schematic shows in Figure 2.2. The force is calculated using Hooke's law: $F = k \times S \times \Delta V$ where F, k, S and ΔV are the force, the spring constant of the AFM probe, the photodiode sensitivity, and the deflection of the probe, respectively.

Two different methods have been proposed for friction measurements using AFM. The first method is the "Parallel Scanning Method." It was introduced by Ruan and Bushan (1994)[35] and was modified by Wang et al (2007)[36] by adding the angle of the mounted cantilever to the calculation of the friction coefficient. A friction coefficient can be obtained by this method so that the friction force can be calculated after the adhesion force is measured. Based on experimental observations, however, this method was determined to be unsuitable for atmospheric systems, where the relative humidity (RH) is not fixed, because the friction coefficient changes as RH changes. The second method that has been proposed is the "Perpendicular Scanning Method" which was introduced by Meyer and Amer (1990).[37] The friction force is measured by obtaining the change in voltage (ΔV) between trace and retrace motions of an AFM probe that is brought in contact with the surface as illustrated in Figure 2.3. The advantage of the perpendicular scanning method is that the friction signal is measured directly by AFM. In this thesis, the friction force is measured by employing the perpendicular scanning method. The spring constant and photodiode sensitivity are calculated using beam mechanics.[38,39]

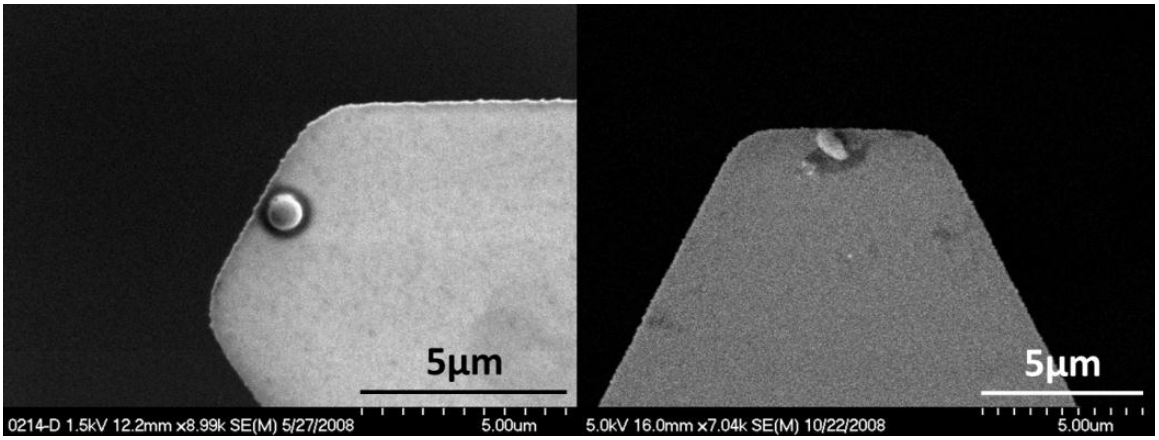

Figure 2.1. Images obtained with Scanning Electron Microscopy (SEM): 1-µm silica particle (left) and *Bacillus thuringiensis* spore (right) were attached to the end of a tipless cantilever.

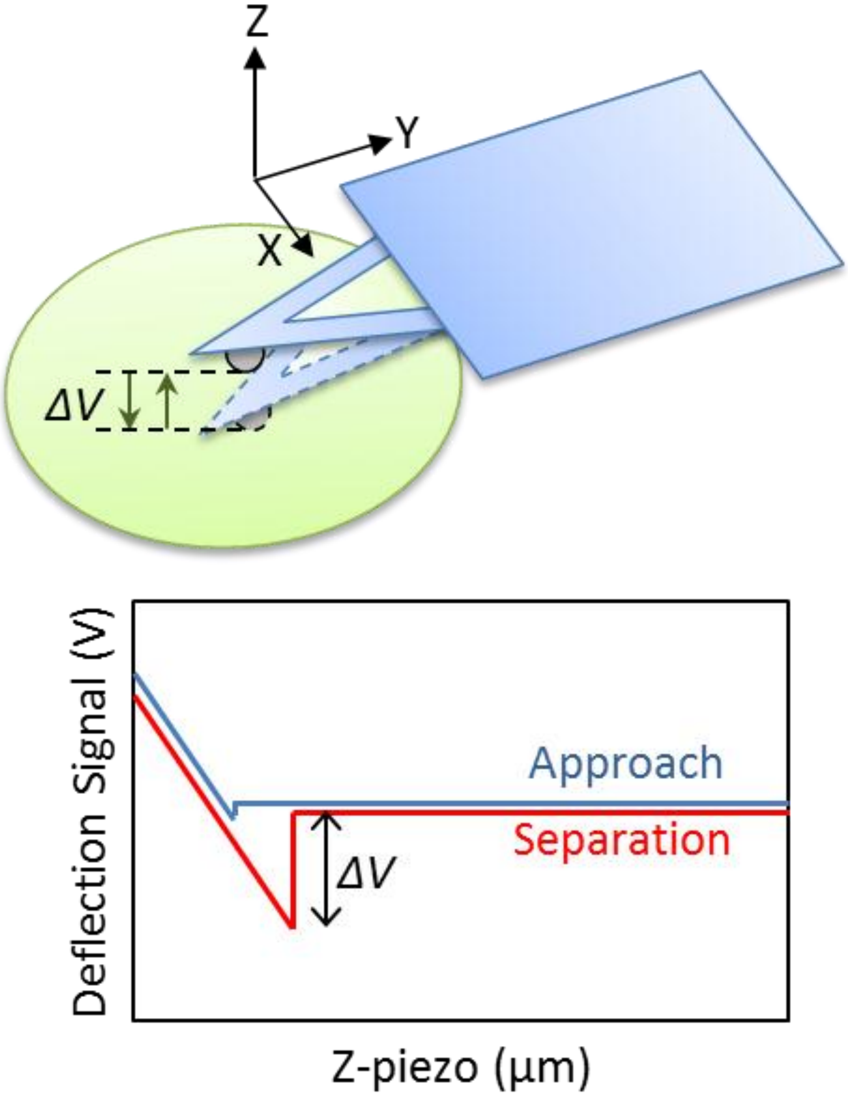

Figure 2.2. Schematic of adhesion force measurements using AFM. An AFM probe is brought in contact with the substrate surface and then is moved away from the surface. The deflection of the cantilever due to interaction forces is recorded as voltage signal (V), which is used to estimate the adhesion force based on Hooke’s law.

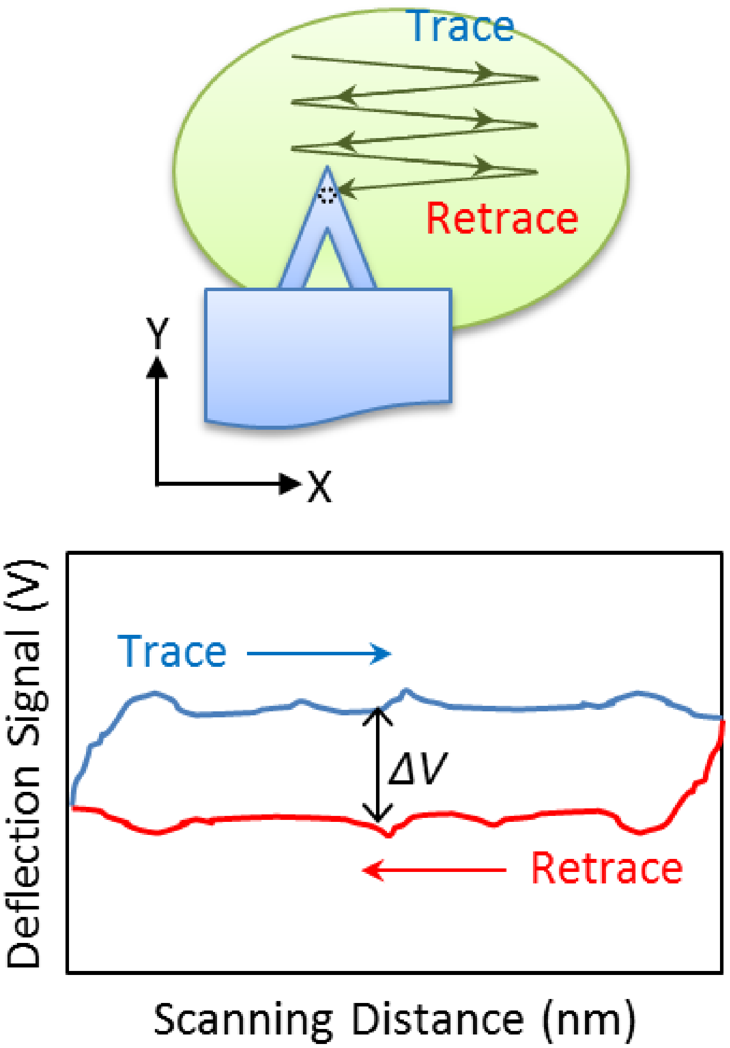

Figure 2.3. Schematic of the perpendicular scanning method for friction force measurements using AFM. The friction force is measured by acquiring the change in voltage (ΔV) between trace and retrace motions of an AFM probe that is brought in contact with the surface.

In addition to the adhesion and friction force measurements, AFM can be used to apply electrical bias to a system that involves conducting materials, through either the substrate or the particle. The electrical bias is adjusted by controlling one of AFM operating parameters. This method can be employed to modify the charge density on surfaces.

2.1.2. Scanning Surface Potential Microscopy (SSPM)

Scanning Surface Potential Microscopy (SSPM) is a technique that combines the tapping mode and lift mode of AFM with the goal to provide information about topography and local surface potential. First, the AFM tip obtains the topographic information using tapping mode (Figure 2.4, left), and then distinguishes the difference of local surface potential between the tip and the substrate at constant height using lift mode (Figure 2.4, right). The second scan using lift mode eliminates the topographic artifacts from the potential information. The surface charge density of a substrate is calculated by applying Gauss's Law. According to Gauss's Law, the electric flux through a unit area is given by $\Phi = EA = \frac{\sigma A}{\varepsilon_o}$ where Φ, E, A, σ, and ε_o represent the electric flux, electric field, surface area, surface charge density, and vacuum permittivity, respectively. When the electric field is constant, it can also be defined as the change in voltage (ΔV) per distance, d: $E = \frac{\Delta V}{d}$. Therefore, the surface charge density of the substrate is calculated by the following equation.

$$\sigma_{substrate} = \frac{V_{substrate} - V_{tip}}{z_{substrate} - z_{tip}} \times \varepsilon_o \qquad (2.1)$$

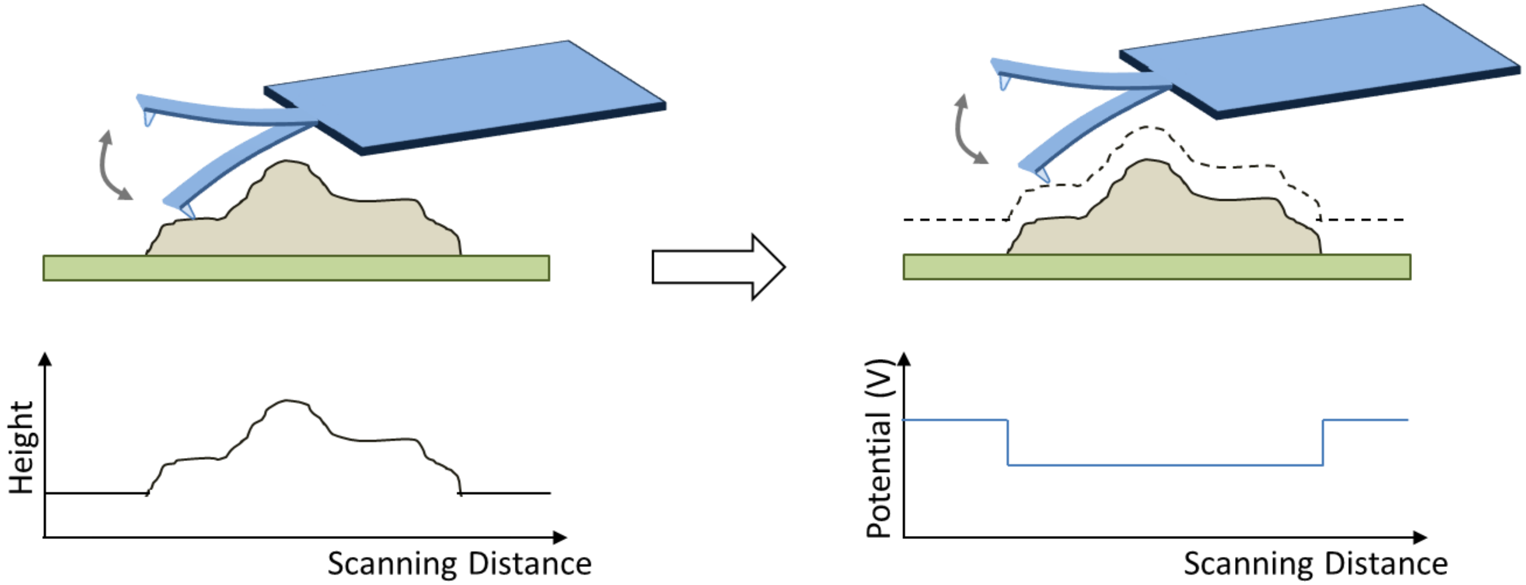

Figure 2.4. Schematic of surface potential measurements using SSPM. The first scan using tapping mode (left) obtains the topographical information and the second scan using lift mode (right) obtains the surface potential information.

where $V_{substrate} - V_{tip}$ and $z_{substrate} - z_{tip}$ represent the difference in voltage and the separation distance between the substrate and the tip, respectively. The geometry of the system (i.e., a spherical particle versus a planar surface) may influence the charge density. In the present work, the geometry of the system was ignored, and a constant electric field between the tip and the substrate was assumed.

2.2. Theoretical Models

2.2.1. Adhesion Forces in Atmospheric Systems

The adhesion force of particles has been studied for decades.[9] The sources of the adhesion force depend on the physical and chemical characteristics of interacting surfaces, such as polarity, hydrophobicity, and existence of functional groups on the surface.[1] In atmospheric systems, the relative humidity (RH) plays an important role in the interfacial interaction of colloidal particles because water molecules adsorb on the interacting surfaces and thus form a water meniscus between them. Therefore, the van der Waals (F_{vdw}), capillary (F_{cap}), and electrostatic (F_{el}) forces are considered as the major contributors to adhesion in atmospheric systems.[9,40] The RH not only determines the capillary force but also influences the other two forces. These forces are also influenced by the shape, size, and surface roughness of interacting surfaces. To simplify the calculations, however, ideal conditions are typically assumed: perfectly smooth surfaces, a circular shaped meniscus, and no surface contamination. Figure 2.5 presents a schematic of a spherical particle positioned on a planar substrate surface in atmospheric systems.

The van der Waals force is calculated by integrating the force between the circular line that comprises the sphere and the substrate surface as a function of the

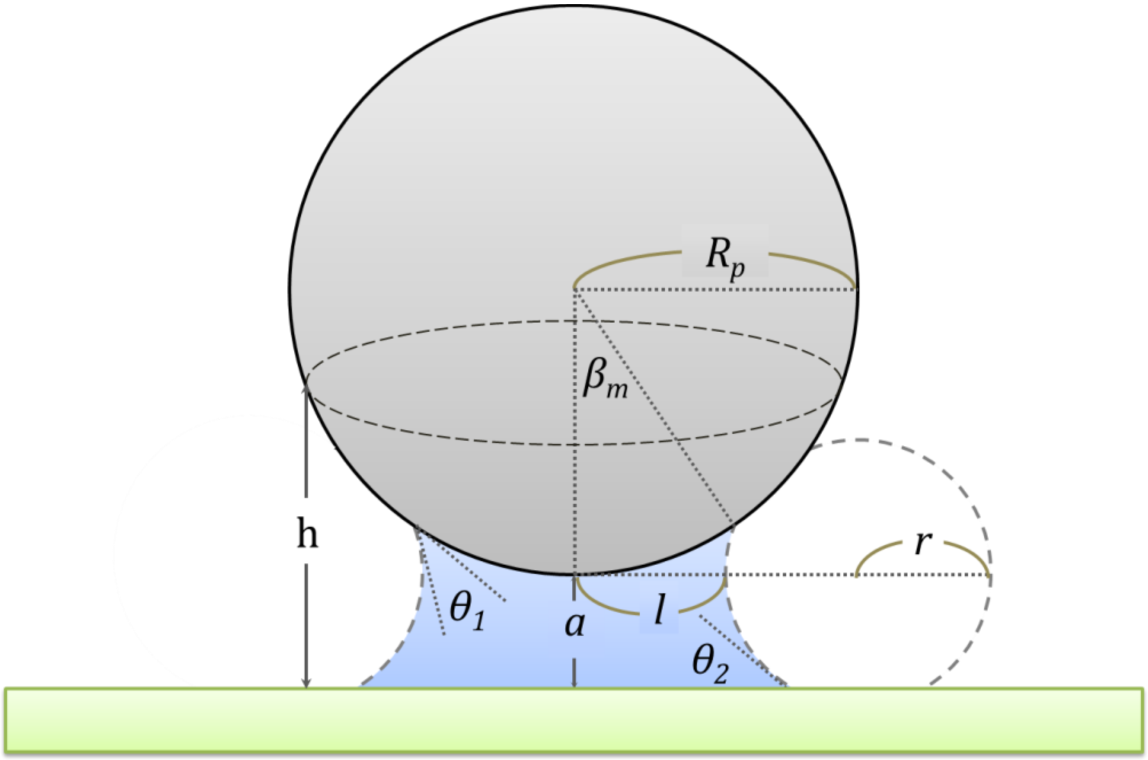

Figure 2.5. Schematic of a spherical particle on a planar substrate surface in atmospheric systems. The water meniscus formed in between is due to the adsorption of water molecules. The distance between the particle and the substrate surface is enhanced.

surrounding conditions. Due to the formation of the meniscus between the sphere and the planar surface, the force for the meniscus domain is integrated separately from the origin of the meniscus. Using the parabolic approximation for the distance between the circular line and the substrate, i.e., $h = a + {x^2}/{2R_p}$, the mathematical formula for the van der Waals force is expressed as:

$$F_{vdw} = \frac{H_{water} R_p}{6a^2} + \frac{H_{air} - H_{water}}{6a^2} R_p \times \frac{a^2}{\left(a + R_p - R_p \cos\beta_m\right)^2} \tag{2.2}$$

where H_{water} and H_{air}, a, R_p, and β_m represent the Hamaker constant in water and air, intermolecular spacing, radius of the particle, and angle of meniscus, respectively.[1,9,41]

The capillary force arises due to the surface tension of water and the pressure difference across the meniscus:

$$F_{cap} = F_{surface\_tention} + F_{pressure\_difference} = 2\pi l \gamma_w \left(\theta_1 + \beta_m\right) + \pi l^2 \Delta P \tag{2.3}$$

where γ_w is the surface tension of water, and r and l are the principle radii of the meniscus. The pressure difference, ΔP, is expressed with the principle radii, r and l, while the relationship between the RH and principle radii is described using the Kelvin equation:

$$\Delta P = \pi l \gamma_w \left(\frac{1}{r} - \frac{1}{l}\right) \quad \text{and} \quad \ln\left(\frac{P}{P_o}\right) = -\frac{\gamma_w V_m}{RT}\left(\frac{1}{r} - \frac{1}{l}\right) \tag{2.4}$$

where P/P_o, V_m, R, and T represent the RH, molar volume of water, ideal gas constant, and absolute temperature, respectively. Using the Young's Modulus and the Kelvin equation, the mathematical formula of the capillary force is expressed as:[9,41]

$$F_{cap} = \pi l \gamma_w \left[-\frac{lRT}{\gamma_w V_m} \ln\left(\frac{P}{P_o}\right) + 2\sin\left(\theta_1 + \beta_m\right) \right]$$

$$\text{where } l = R_p \sin\beta + r\left[\sin\left(\theta_1 + \beta_m\right) - 1\right] \text{ and } r = \frac{R_p\left(1 - \cos\beta_m\right) + a}{\cos\left(\theta_1 + \beta_m\right) + \cos\theta_2} \qquad (2.5)$$

where θ_1 and θ_2 are the contact angles of the particle and the substrate, respectively.

The electrostatic force is calculated using Coulomb's Law. Although Coulomb's Law applies only for point charges, it can also be used for uniformly charged identical spheres. To simplify the calculations, the electrostatic force in this work was estimated by using Coulomb's Law and considering that the two interacting surfaces behave like two identical spheres that are uniformly charged.

$$F_{el} = -\frac{Q_{substrate\ surface} Q_{particle}}{4\pi\varepsilon_o d^2} \qquad (2.6)$$

In this equation, Q_i, ε_o, and d are the surface charge, vacuum permittivity, and distance between two spheres, respectively. Distance d is expressed as $d = 2R_p + z$ where z is the separation distance between two surfaces. Since the surface charge is the product of surface charge density (σ_i) and the surface area of the particle, the equation can be written as:

$$F_{el} = -\frac{Q_{substrate\ surface} Q_{particle}}{4\pi\varepsilon_o d^2} = -\frac{\sigma_{substrate\ surface}\sigma_{particle} 4\pi R_p^4}{\varepsilon_o \left(2R_p + z\right)^2} \tag{2.7}$$

If a dielectric material exists between the two interacting surfaces, the relative permittivity (ε) is used instead of the vacuum permittivity. The relative permittivity is the product of the dielectric constant and the vacuum permittivity.

For the electrostatic interaction between a charged insulating surface and a grounded conducting surface, the method of image charges or the method of mirror charges can be employed. The charge on the insulating surface induces the polarization of the conducting surface. The mirror charge due to polarization has the same magnitude but opposite sign compared to the charge on the insulating surface. Therefore, the electrostatic image force is always attractive. The mathematical formula of the electrostatic image force is:

$$F_{img} = -\alpha \frac{\left(\sigma_{particle} A_{particle}\right)^2}{16\pi\varepsilon_o R_p{}^2} + \beta\sigma_{particle} A_{particle} E - \gamma\pi\varepsilon_o R_p{}^2 E^2 \tag{2.8}$$

where E is the externally applied electric field. The coefficients α, β, and γ are functions of several parameters, such as the dielectric constant and particle geometry.[14,42,43]

The surface charge density can be calculated using Gauss's Law: $\Phi = Q/\varepsilon_o$ where Φ is the electric flux. Since the electric flux is defined as the product of electric filed (E) and the surface area (A), i.e., $\Phi = EA$, the electric field is expressed with the surface charge density: $E = {Q}/{\varepsilon_o A} = {\sigma}/{\varepsilon_o}$. If the particle and the substrate surface are assumed as two infinite plates, the system can be treated as two charged sheets. Then, the electric field is given by: $E = {\sigma}/{2\varepsilon_o}$. The electric field is also related to the difference in surface potential (ΔV) by the relationship, $E = {\Delta V}/{d}$, where d is the distance between the two plates. Therefore, the final expression for the surface charge density is as follows:

$$\sigma = 2\varepsilon_o \frac{\Delta V}{d} \tag{2.9}$$

2.2.2. Friction Coefficient

Amontons' Law provides the friction coefficient (μ) as a relationship between the friction force (F_f) and the sum of the adhesion force (F_{ad}) and normal load (F_n):

$$\mu = \frac{F_f}{F_n + F_{ad}} \tag{2.10}$$

Through AFM, both the friction and the adhesion forces can be measured. Note that the measured friction force is the kinetic friction force because it is measured while the AFM probe is moving. Once the friction and adhesion forces are measured, the friction coefficient can be obtained using equation (2.10) at each RH. Such an approach may be used to examine the linearity between the friction force and the adhesion force at different levels of RH.

CHAPTER 3

FRICTION AND ADHESION FORCES OF *BACILLUS THURINGIENSIS* SPORES ON PLANAR SURFACES IN ATMOSPHERIC SYSTEMS

3.1. Introduction

Surface adhesion and friction forces are of interest in various areas of research, including environmental science and engineering, because colloidal particles and surfaces are present everywhere and their interactions play a determining role in the transport of contaminants and decontamination processes in natural and engineered systems.[1,2] Immobilization and release of particulate contaminants, wear of mechanical devices, and transport of particles in groundwater and atmospheric systems are a few examples that are influenced by adhesion and friction forces. These forces are also involved in microbial activities such as attachment of biological particles to surfaces and membrane fouling.[3-5]

The influence of bacteria, among other colloidal particles, is inevitable in environmental and human activities because of their ubiquitous interactions with living or nonliving surfaces except in cautiously controlled clean systems.[20] Particularly, biofilms and spores are of great concern in food science, pathology, and environmental sciences because they are highly resistant to various disinfectants.[20,21] Typically in aquatic systems or with an abundant amount of moisture in atmospheric systems, bacteria tend to accumulate on surfaces and form biofilms by which they can survive and protect themselves more effectively due to the higher nutrient levels on surfaces than in bulk media.[20] A spore (or endospore), which is another method of self-defense for spore-forming bacteria, is an effective means of bacterial dispersal in air and water. When bacteria face life-threatening conditions such as extreme temperature, dehydration, nutrient depletion, and disinfectant chemicals, they produce spores that are highly resistant to such conditions. Most spore-forming bacteria reside in soil, and when they encounter moisture- and nutrient-rich conditions, they turn back into vegetative cells. In air, bacterial spores can be transmitted to humans by inhalation, consumption of contaminated products, and skin contact because they transport with other airborne particles.[20,22] Therefore, the behavior of spores depends upon environmental conditions such as temperature and relative humidity (RH), as well as the physical and chemical properties of interacting surfaces in atmospheric systems.

Atomic force microscopy (AFM) is used widely to study bacterial behavior at interfaces owing to its capability to image the geometry of a surface and to measure surface interaction forces occurring at microscales and even nanoscales. The various applications of AFM are reviewed thoroughly elsewhere.[15,16] The interfacial behavior between two contacting surfaces at such scales often cannot be explained by generally accepted knowledge for macroscopic systems due to the significance of the molecular interactions at the microscales and nanoscales. For example, the well-known Amontons' Law shows a linear relationship between the friction force, F_f, and the total adhesion force—that is, the sum of the adhesion force and the normal load—for macroscopic interactions: $F_f = \mu (F_n + F_{ad})$, where μ, F_n, and F_{ad} are the friction coefficient, the normal load, and the adhesion force, respectively. However, based on experimental and computational simulation results, this relationship is sublinear at the microscales and nanoscales.[3,17-19] Adhesion characteristics and surface roughness are key components determining the nature of the relationship between friction and normal forces.[19] Therefore, the macroscopic perception cannot simply be applied to such interactions at small scales.

Interaction forces, including friction, are generally influenced by the physical and chemical properties of interacting surfaces, such as surface roughness, particle shape, hydrophobicity, and surface charge.[1,7] First and foremost, RH plays an important role because of its interconnectivity with other properties.[8,9] As RH increases, the surface coverage by water molecules and the thickness of the water layer increase, depending on the affinity of the surface material to water.[10] Adsorbed water molecules may contribute to friction in two opposing ways: (i) by attenuating friction due to the lubrication of surfaces and (ii) by enhancing friction due to the increase of the effective contact area and the capillary force arising from water condensation between interacting surfaces. The surface charge is also considered an important influencing parameter, especially when the system includes conductive or charged surfaces.[11,12] Since moisture dissipates the charge, the electrostatic force can either promote or decrease the friction force, depending on the sign of the charge of the interacting surfaces. Besides adsorption, absorption of water molecules by the interacting bodies can influence the interfacial forces by altering surface features such as roughness and particle size.[13,14]

Anticipating an accidental or intentional release of particulate contaminants including spores, we must be able to predict microscopic surface interactions as well as their macroscopic transport behavior so that our response will be effective and efficient. In this view, the study of the friction and adhesion forces of spores can help prevent and control surface contamination. Despite an awareness of its importance, the friction force at small scales has not been studied as much as the adhesion force for various environmental systems.[3,44,45]

We previously investigated the adhesion behavior of *Bacillus thuringiensis* (*Bt*) spores on model surfaces in atmospheric systems.[4] Building on the knowledge acquired in that effort, this work focuses on the friction behavior of *Bt* spores. AFM was exploited to measure both friction and adhesion forces, and the results were used to investigate the friction coefficient and its linearity. The role of the geometry and appendages of spores was investigated by comparing the interaction forces of spores with silica particles. Lastly, the measured adhesion force was compared with the values calculated using force equations.

3.2. Experimental Methods and Force Calculations

3.2.1. AFM Probes: a Silica Particle and a *Bt* Spore

AFM probes of a *Bt* spore and a 1 µm spherical silica particle, which serves as a model particle for comparison, were prepared for the force measurements, following a procedure described in our previous work.[4] *Bt* spores were purchased from Raven Laboratories (Omaha, NE). A single spore or silica particle was attached at the end of a v-shaped tipless cantilever made of silicon nitride. Particle attachment was performed by Novascan Technologies (Ames, Iowa). The procedure involves handling of the particles using micro-manipulators and attachment on cantilevers using a thin film of glue. The orientation of the spore attached on a tipless cantilever is shown in Figure 3.1 along with a simple schematic of the adhesion of a *Bt* spore on a planar surface. The contact angle of

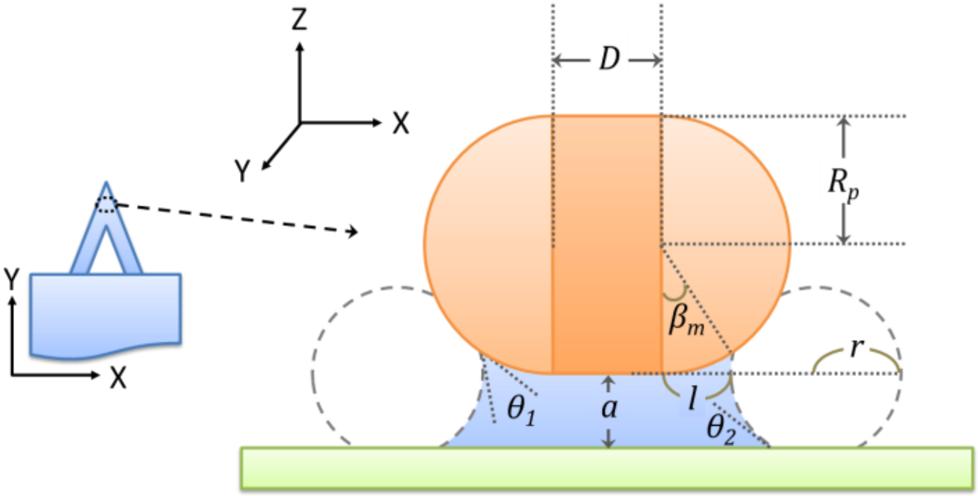

Figure 3.1. Simple schematic of *Bt* spore adhesion on a planar surface with a meniscus formed between the two objects. The size of the intermolecular spacing is magnified. For modeling purposes, the spore is represented by two hemispheres and a cylinder in between. The symbols represent the length of the cylinder (D), radius of the spherical part (R_p), angle of meniscus (β_m), contact angles (θ_i), intermolecular spacing (a), distance from the center of one spherical part to the meniscus (l), and radius of the meniscus (r).

Bt spores (80°) was obtained from the literature,[4,45,46] and the size of spores was estimated using scanning electron microscopy and reported by Chung et al.[4]

3.2.2. Surface Preparation

Mica, silica (fused quartz), and gold (deposited on mica) were prepared as substrate surfaces. Mica was cleaved using two-sided adhesive tape before each measurement. Silica was soaked in concentrated sulfuric acid for more than 24 hours, and gold was cleansed with ethanol and acetone. Then, both silica and gold were rinsed thoroughly with a copious amount of deionized (DI) water. Cleansed silica and gold surfaces were dried and stored in silica gel dehydrators for 3 to 7 days. The contact angle of each substrate surface was measured with DI water using a contact angle meter (CAM Plus, Mentor, Ohio) prior to the experiments. The surface roughness of each substrate surface was measured simultaneously with the friction force using AFM (MultiMode V, Veeco Instruments, Plainview, New York). The electrostatic potential of particles and surfaces was obtained from other studies based on measurements using scanning surface potential microscopy, which is one of the various modules of AFM (MultiMode IIIa, Veeco Instruments, Plainview, New York).[47]

3.2.3. AFM Force Measurements and the Friction Coefficient

The friction and adhesion forces between the particle and the substrate surface were measured using AFM. The friction force was measured as the probe scanned the surface along the x-axis at room temperature (19-21ºC). This method enabled us to exclude the influence of the surface geometry, which has a size much larger than the probe.[37] Considering that the measured friction force is the kinetic force, because it is measured while the probe is in motion, we can assume that meniscus formation between the particle and the substrate surface does not reach equilibrium. To match the conditions of the friction force measurements, we also measured the adhesion force prior to complete formation of the meniscus. This is done by taking the adhesion force measurement immediately after the two surfaces are brought into contact. It should be noted here that the threshold RH level at which condensation of water at the point of contact occurs is a function of the contact angles of the two surfaces. For each substrate (gold, mica, silica) we obtained 10 sets of friction force measurements and 5 sets of adhesion force measurements for different RH values. Each set of measurements contained repetitive measurements (12 for friction forces and 22 for adhesion forces) so that we could analyze the variation of the data. In order to check the damage of particle probes, the spring constant (k) of the probe was measured for each experiment because it changes when the particle detaches from the cantilever due to the loss of the particle mass.

The deflection signal (volt) recorded during the motion of the probe was converted to force (nanonewtons) using Hooke's law: $F = k \times S \times \Delta V$, where F, k, S, and ΔV are the force, spring constant, photodiode sensitivity, and change in deflection signal, respectively. AFM was used to measure the spring constant and photodiode sensitivity for the adhesion force while the same properties for the friction force were calculated using theory of beam mechanics, which is to estimate the deflection of a beam (a cantilever in our case) using various parameters including the mechanical properties of the beam.[38,39] For RH control, all force measurements were performed in a cylindrical glass chamber that completely covered the AFM head and scanner. RH was controlled by mixing different flow rates of dry and water-saturated air gas streams before entering the chamber; the RH was increased from 0 to 80% in increments of 20%. The friction coefficient for each system was obtained by dividing the friction force by the total adhesion force.

3.2.4. Calculation of the Adhesion Force

For the adhesion force calculation, the spore was considered as a perfectly smooth rod-shaped particle as shown in Figure 3.1, based on scanning/transmission electron microscopy (STEM) and scanning electron microscopy (SEM) images obtained previously.[4]

The van der Waals (F_{vdW}), capillary (F_{cap}), Coulomb ($F_{Coulomb}$), and electrostatic image (F_{img}) forces were calculated using the following equations.[1,9,14,41]

$$F_{vdw} = F_{vdw,\,water} + \left(F_{vdw,air} - F_{vdw,water}\right) \times \frac{a}{\left(a + R_p - R_p \cos\beta_m\right)^2}$$

$$\text{where } F_{vdw,i} = F_{vdw,i,cylinder} + F_{vdw,i,sphere} = \frac{H_i D \sqrt{R_p}}{12\sqrt{2}a^{2.5}} + \frac{H_i R_p}{6a^2} \qquad (3.1)$$

The van der Waals force (F_{vdW}) was calculated for the cylindrical ($F_{vdW,i,cylinder}$) and spherical ($F_{vdW,i,sphere}$) parts separately. In eq 3.1, i, a, R_p, β_m, H_i, and D represent the type of medium (air or water), intermolecular spacing, radius of the spherical part, angle of meniscus, Hamaker constant, and length of the cylinder, respectively (see Figure 3.1).

As described in our previous work,[4] F_{cap}, $F_{Coulomb}$, and F_{img} were calculated for a spherical particle of the same volume as that of a rod-shaped particle.[4,14]

$$F_{cap} = \pi l \gamma_w \left[-\frac{lRT}{\gamma_w V_m} \ln\left(\frac{P}{P_o}\right) + 2\sin\left(\theta_1 + \beta_m\right) \right] \tag{3.2}$$

$$\text{where } l = R_p^{'} \sin\beta + r\left[\sin\left(\theta_1 + \beta_m\right) - 1\right] \text{ and } r = \frac{R_p^{'}\left(1 - \cos\beta_m\right) + a}{\cos\left(\theta_1 + \beta_m\right) + \cos\theta_2}$$

In eq 3.2, γ_w, R, T, V_m, P/P_o, θ_1 and θ_2, and R'_p denote surface tension of water, ideal gas constant, temperature, molar volume of water, RH, contact angle of the particle and substrate surface, and radius of a sphere of volume equal to that of a rod-shaped particle, respectively.

$$F_{Coulomb} = -\frac{\sigma_{substrate}\sigma_{particle}}{2\varepsilon_0} A_{particle} \tag{3.3}$$

$$F_{img} = -\alpha \frac{\left(\sigma_{particle} A_{particle}\right)^2}{16\pi\varepsilon_o R_p^{'\,2}} + \beta\sigma_{particle} A_{particle} E - \gamma\pi\varepsilon_o R_p^{'\,2} E^2 \tag{3.4}$$

In eqs 3.3 and 3.4, σ_i, ε_o, $A_{particle}$, and E are the surface charge density, permittivity, surface area of the particle, and externally applied electric field, respectively. The coefficients, α, β, and γ, represent several parameters such as the dielectric constant and geometry of the particle. Previously obtained surface potential–RH profiles[47] were used to estimate the Coulomb and image forces. The detailed calculation procedures are described in our previous work.[4,14]

3.3. Results and Discussion

3.3.1. The Force Measurements

For data analysis, experiments were repeated at the same conditions using the same surface and particle, and the variation of the force measurements was less than 5%. Larger variations of the force measurements were obtained when experimental runs using different surfaces and particles of the same material were compared, which were caused by highly heterogeneous surface properties including roughness, charge, and possible surface contamination.[11] The variation is largest on silica followed by gold and mica. Variations may also arise from the inherent variability in cantilever properties, the complex surface characteristics of the spore, and differences in laser alignment for each measurement. However, the trends of both friction and adhesion forces with RH for all measurements were consistent. Therefore, the results presented in this study for a set of conditions are the average values of all force measurements at those conditions.

Figure 3.2 shows the friction force of spores and silica particles as a function of RH. The trends of the friction force for the two types of particles are comparable. However, the spore experienced a smaller friction force than the silica particle on each substrate through the entire range of RH. This behavior is attributed to the shape of the spore, which leads to a smaller contact area and a longer distance between the spore and the substrate surface during force measurements.[1,48] The spore has a larger contact area to a planar surface than does the silica particle when they are not moving. However, the x- and z-axes of both particles are tilted due to the torsion during force measurements, so the contact area of the spore decreases and the distance increases, whereas the contact area and distance of the silica particle remain the same because of its spherical geometry.

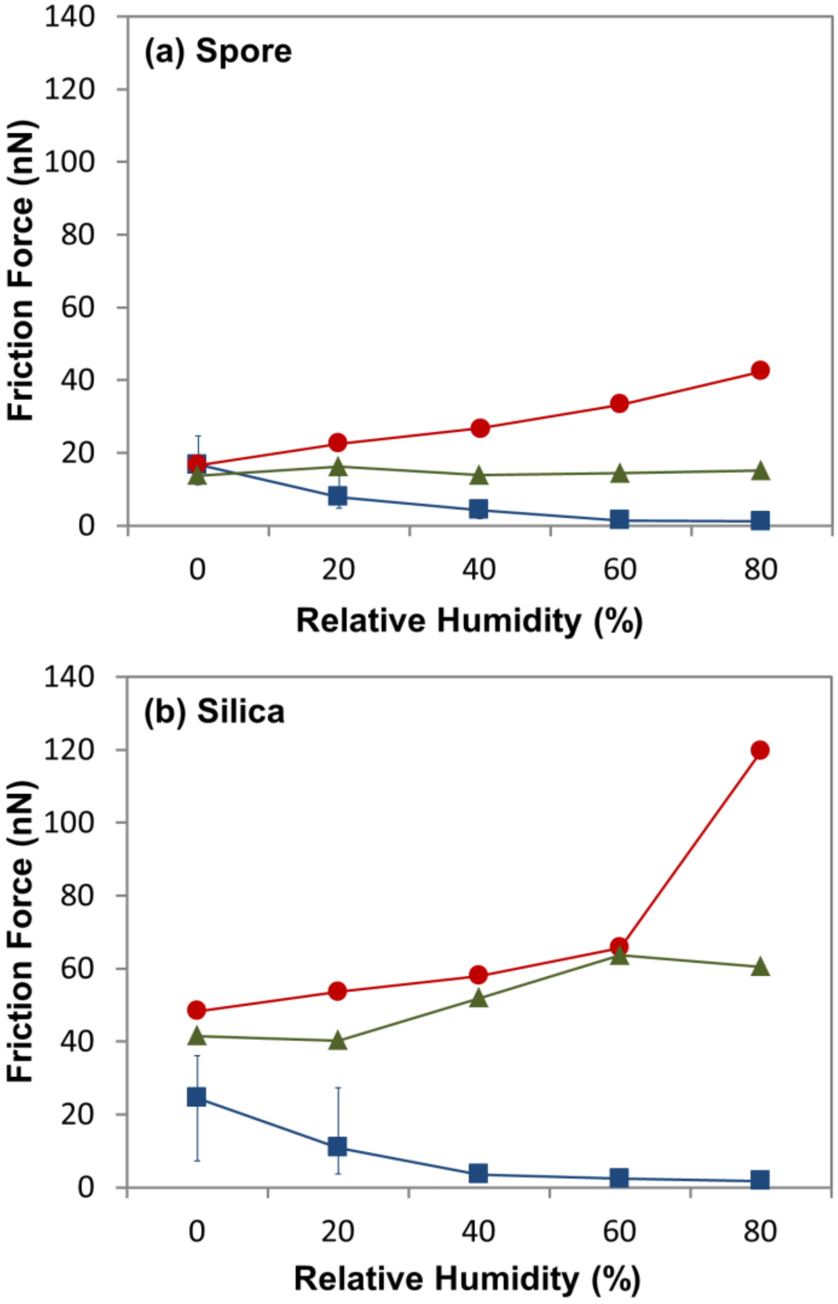

Figure 3.2. Average friction force of the spore (a) and silica particle (b) on mica (square), silica (circle), and gold (triangle). Vertical bars for mica represent the range of the friction force at each RH due to different cleavage rate.

The trend of the friction force for the spore on each substrate surface is comparable to that for the silica particle. Hence, the role of the exosporium and appendages (short hair-like projections and/or filaments) of spores in the interaction forces is considered to be limited for the tested spore probes regardless of their existence.

The contributions of RH, surface roughness, and adhesion force to variations in the friction force are described here in detail for each substrate surface.

3.3.1.1. Mica

Mica has negative surface charge at low RH upon cleavage because potassium ions that balance the net charge between mica sheets are removed.[49-51] It was reported that spores of *Bacillus thuringiensis* are negatively charged whereas silica is almost neutral, and thus a repulsive force or a very small adhesion force exists between spores and a freshly cleaved mica surface at low RH.[47] Therefore, the friction force was expected to be negligible. However, a significant friction was observed for the spore with a wide range of variation at low RH. From the force curve (Z position vs. Force, Figure 3.3(a)), a long-range attraction instead of a repulsive force was found between the spore and mica; such an attraction induces a strong friction force by adding to the normal load on the spore during the friction force measurements.

The long-range attraction persists even after the spore comes in contact with mica. A large friction force and a long-range attraction were also detected for the silica particles, and there is no distinctive difference between the spores and the silica particles in spite of size differences. The spore length is 1.54 ± 0.2 μm and the spore height is 0.82 ± 0.1 μm, while the diameter of the silica spherical particle is 1 μm. This observation suggests that the long-range attraction does not come from the particles. If the interaction between

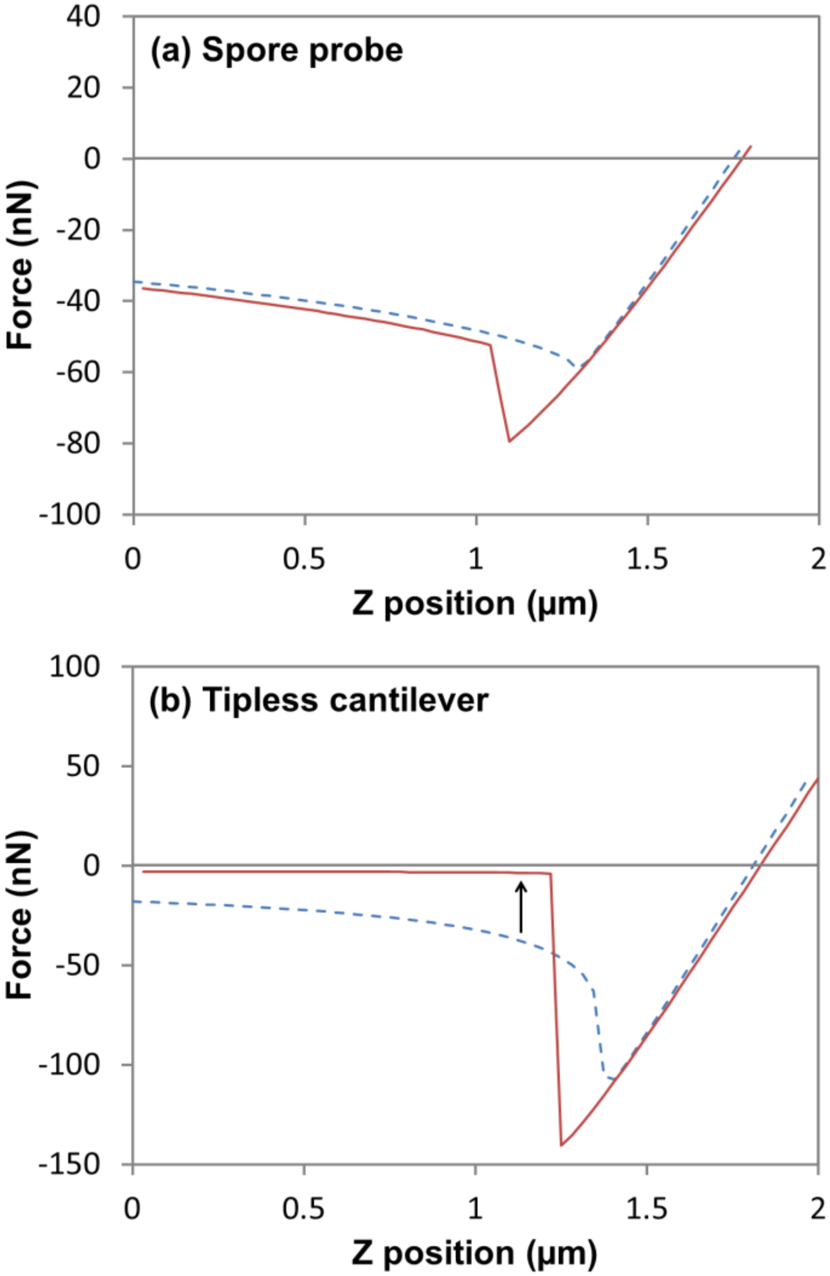

Figure 3.3. Randomly chosen force curves (Z position vs. Force) for the spore (a) and the tipless cantilever (b) on freshly cleaved mica at 20% RH. The broken and solid lines indicate the force curves during the extending and retracting of the probe, respectively. The long-range attraction disappears after the tipless cantilever comes in contact with mica.

the particle and substrate surface induces the long-range attraction, then the intensity of the attraction will change with the size of the particle. Jones et al.[11] also reported a long-range attraction that exists between a spherical glass particle and a hydrophobic glass surface, and its intensity does not change with the size of the particle. To verify the origin of the attraction, we obtained the force curve between a tipless cantilever, similar to the one we used to make the particle probes, and mica. Figure 3.3 shows the approaching (broken line) and retracting (solid line) of the spore probe (a) and the tipless cantilever (b). The approaching curve indicates that a long-range attraction also exists for the tipless cantilever. This measurement confirms that the surface charge of mica induces an attraction, through polarization, to an uncharged cantilever made of silicon nitride. In spite of the fact that the tipless cantilever is nonconductive, the retracting curve shows that the long-range attraction disappeared after the cantilever came in contact with mica (Figure 3.3(b), solid line) whereas it persisted for the spore probe (Figure 3.3(a), solid line). This behavior is attributed to the fact that the cantilever and the mica substrate are in contact when no particle is attached to the end of the cantilever. Because the strength of the electric field is inversely proportional to the distance, the electric field at the end of the cantilever is 2.6 times stronger for the tipless cantilever (normal thickness = 0.6 μm) than for the particle probe (the sum of the height of the particle and the cantilever thickness = 1.6 μm). Therefore, it is possible for the surface charge to discharge through the gold coating on the backside of the cantilever.

When the surface charge density was low, the long-range attraction was not observed even at low RH. Variation in the surface charge density of mica can be caused by the inconsistent cleavage rate and the heterogeneity of the local surface charge density arising from irregular removal of potassium ions (K^+) during cleavage.[52] The long-range attraction was not detected at over 40% RH, at which half coverage of the first water monolayer on mica occurs,[53-55] because the adsorbed water molecules dissipate the surface charge.

Regardless of the intensity of the long-range attraction at low RH, the friction force of the spore on mica decreased as RH increased, which is consistent with the friction results between two mica surfaces.[56] Mica is atomically flat with approximately 0.2 nm of surface roughness (root mean square, rms) based on AFM data, and very hydrophilic (less than 5° contact angle), so water molecules are readily adsorbed onto a mica surface. Prior to complete formation of the water monolayer, water molecules form islands on mica.[53] As the area of water islands increases, lubrication between the spore and the mica also increases. Consequently, the friction force on mica decreases as RH increases. On the contrary, the adhesion force of the spore and the silica particle increased with RH (Figure 3.4). The opposite responses that friction and adhesion forces exhibited to increasing RH suggest that the adhesion force does not contribute to changes in the friction force of the spore on mica. Even though the total normal force decreased from 0 to 40 or 60% RH due to the contribution of a long-range attraction, it increased with further increasing RH. This observation clearly shows that Amontons' Law, $F_f = \mu (F_n + F_{ad})$, does not hold for the interaction of spores and silica particles on mica.

3.3.1.2. Silica and Gold

The magnitude of the friction force for spores and silica particles on silica and gold is noticeably different from that on mica. Figure 3.2 clearly shows that the friction force is much higher on silica and gold, except when the strong long-range attraction

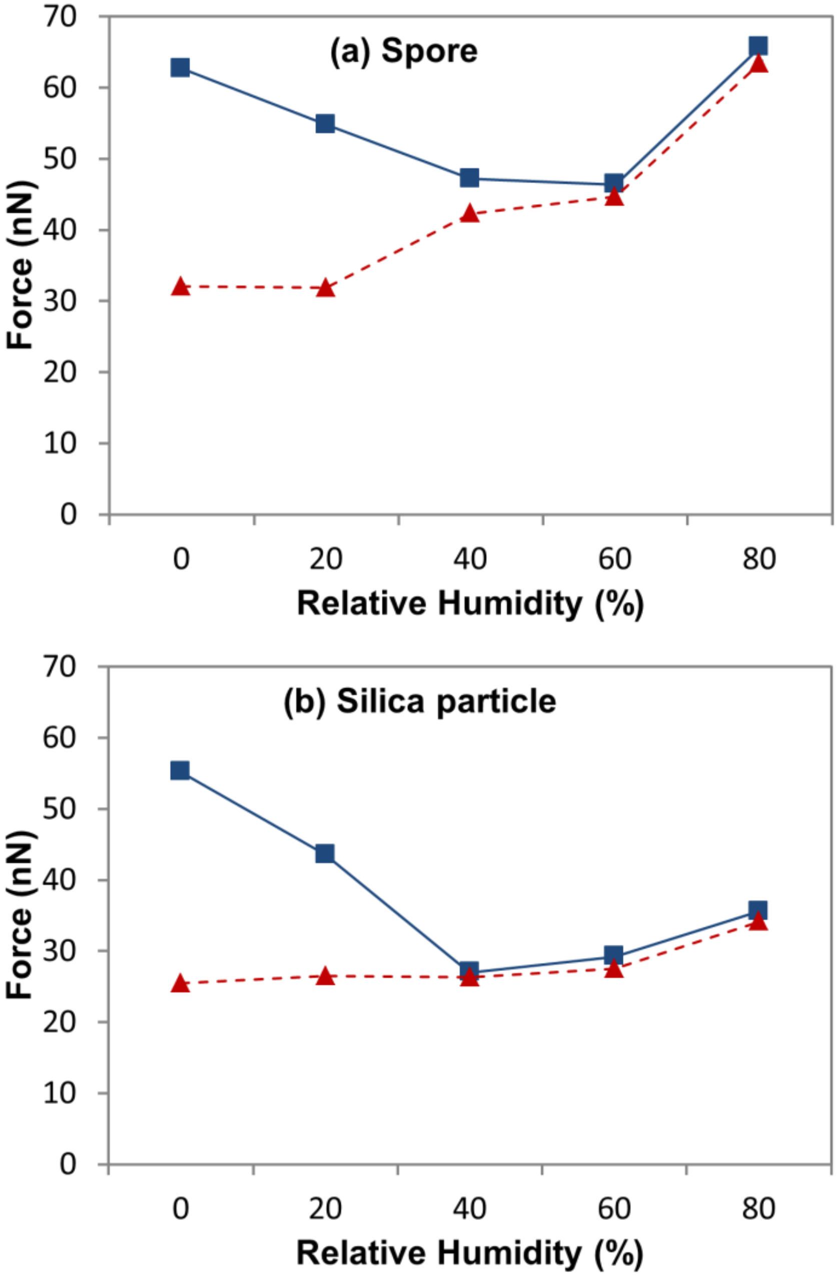

Figure 3.4. Adhesion force (triangles) and total normal force (squares) of the spore (a) and silica particle (b) on mica.

appeared on mica for the spore. This behavior is attributed to surface roughness. If both the particle and the substrate surface are atomically flat, only one contact point should exist. With rough surfaces that can be defined as non-atomically flat surfaces, however, more than one contact point can exist, leading to a larger contact area if the length scale of surface roughness is much smaller than the size of the particle. From AFM data, the surface roughness (rms) of silica and gold is 2–3 nm, which is much smaller than the size of the spore and the silica particle.

Silica is less hydrophilic than mica, so meniscus formation between the spore and the silica occurs at higher RH according to theoretical calculations (Table 3.1). However, an increase in RH influenced the friction force of the spore before the predicted RH level for meniscus formation was reached. In addition, friction continued to increase with RH, which is opposite of the behavior in the spore–mica system. This behavior suggests that the number of adsorbed water molecules is not enough to lubricate the silica surface even at 80% RH. To lessen the friction between interacting surfaces, enough water molecules need to be adsorbed onto the surfaces so that they penetrate the area of contact and separate one surface from another.[57] Surface roughness also contributed to this behavior. Water molecules preferably adsorb onto concave sites that acquire higher surface energy,[11,58,59] so a higher RH is required to yield the same surface coverage at the area of contact on a rough surface than on a smooth surface. Besides, capillary force is not the only factor that contributes to increases in friction force—viscous resistance of adsorbed water also contributes.[60-62] Considering the response of friction to increases in RH prior to meniscus formation, adsorbed water molecules in an amount insufficient to form a meniscus resist the motion of a spore on silica.

Table 3.1. Contact angle and RH level for meniscus formation between the spore and each substrate surface. The RH level for meniscus formation for each substrate was calculated using eq 3.2.

Material	Contact Angle (°)	RH (%) for meniscus formation
Mica	5	10–15
Silica	60	35–40
Gold	80	60–65

The friction force of a silica particle on silica also increased as RH increased (Figure 3.2(b)). Distinctively different from the behavior of the spore, the increase in friction of the silica particle was sudden at 60 to 80% RH. Although it is unclear what induced this behavior, the different chemical composition of silica and spore particles can be considered responsible. Barnette *et al.*[63] proved, via experimental and computer simulation methods, that the adsorption of water on SiO_2 makes the surface more vulnerable to wear by breaking Si–O–Si bonds. Therefore, a critical level of RH for the threshold of friction increase may exist due to chemisorption of water on both the silica particle and the silica surface.

The friction force of the spore on gold was not significantly influenced by RH. Owing to the largest contact angle among the examined substrate surfaces, the spore–gold system is the least susceptible to changes in RH. According to adhesion force calculations, meniscus formation between the spore and gold occurs at much higher RH values (Table 3.1) and its influence is less significant. It was also reported that the lateral resolution of AFM images for hydrophobic surfaces is less influenced by RH.[11,64] Hence, the friction of the spore on gold is quite consistent with increasing RH although what induces a small change in the force is unclear. Besides, the difference in the friction force between spore–gold and spore–silica systems increases as RH increases. This behavior may indicate that surface roughness is a major contributor to the friction force between interacting surfaces at low RH, outweighing the role of other material properties such as chemical composition and contact angle. Different from the spore–gold system, the friction of silica particles on gold slightly increased with increasing RH because silica particles are more hydrophilic than spores.

The adhesion forces of the spore and the silica particle, which were measured prior to meniscus formation, did not change as significantly on silica or gold with increases in RH as the friction forces did. This behavior indicates that adsorbed water molecules cannot influence the adhesion force until a meniscus is formed, contrary to the case of friction force. This observation also supports the importance to friction force of two other mechanisms: viscous resistance of adsorbed water molecules and chemical reaction of water on the substrate surface.

3.3.2. Friction Coefficient

The friction coefficient (μ) was estimated using Amontons' Law (Figure 3.5). The data sets containing the long-range attraction for mica were excluded in order to exhibit only the interaction of the spore. Since the normal load was maintained comparatively low for all friction force measurements, the total adhesion force (F_{tot}) is very close to the adhesion force (F_{ad}). The profile of μ–RH is very similar to the friction force behavior for both spores and silica particles because the adhesion force is not as sensitive to RH as the friction force is. On the other hand, the magnitude of μ is determined by the adhesion force, which is exceedingly higher than the normal load for all experiments. Therefore, one needs to consider the adhesive characteristics when using the friction coefficient for the study of interaction forces at microscales and nanoscales with minimal loading force. As can be expected from the response of the friction force to RH, a linear relationship between the friction and the total adhesion forces was observed for gold ($r^2 = 0.82$). This result agrees well with simulation results using a multi-asperity model by Mo et al.,[19] who concluded that the linearity is violated when any surface interaction force in addition to the van der Waals force is involved in the adhesion force.

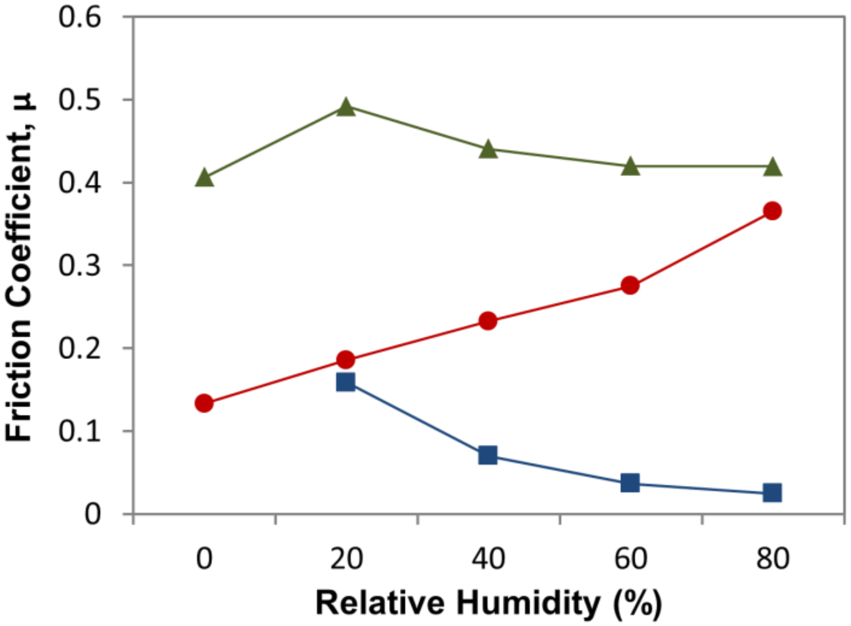

Figure 3.5. Friction coefficient–RH profile for the spore on mica (squares), silica (circles), and gold (triangles).

3.3.3. Calculation of the Adhesion Force

For adhesion force calculations, variation in spore size was considered. The electrostatic force was also taken into account because a considerable amount of charge was observed on each surface. The surface charge was calculated from the electrostatic potential of surfaces following the procedure by Chung et al.[14] The electrostatic potential for the particles and surfaces used in this study was measured using scanning surface potential microscopy and reported elsewhere.[47]

Since the equation for capillary force considers the equilibrium state, that is, formation of a complete meniscus between two interacting surfaces, measured and calculated values were compared only at 0% RH, at which water adsorption is not expected. Figure 3.6 shows the results for each substrate surface. The inclusion of the electrostatic force improves the calculation especially for mica and silica, indicating the significance of the surface charge to surface interactions.

However, the difference between the calculated and the measured forces on gold is significant. Since the difference was also observed for the silica particle, which has a well-defined surface structure compared to that of the spore, surface contamination was considered. Substrate surfaces acquiring high surface energy, such as mica and metals, can easily be covered by water, carbon dioxide, hydrocarbons, and other unknown organic materials. Adsorption of impurities reduces surface energy as a result of changes in surface properties.[1,65-67] Surface contamination was assumed to be minimal on mica because of the preparation procedure for substrate surfaces, so the van der Waals force was recalculated only for silica and gold, assuming hydrocarbons as the surface contaminants.[68] As a result, the force reduction on gold was considerable, whereas

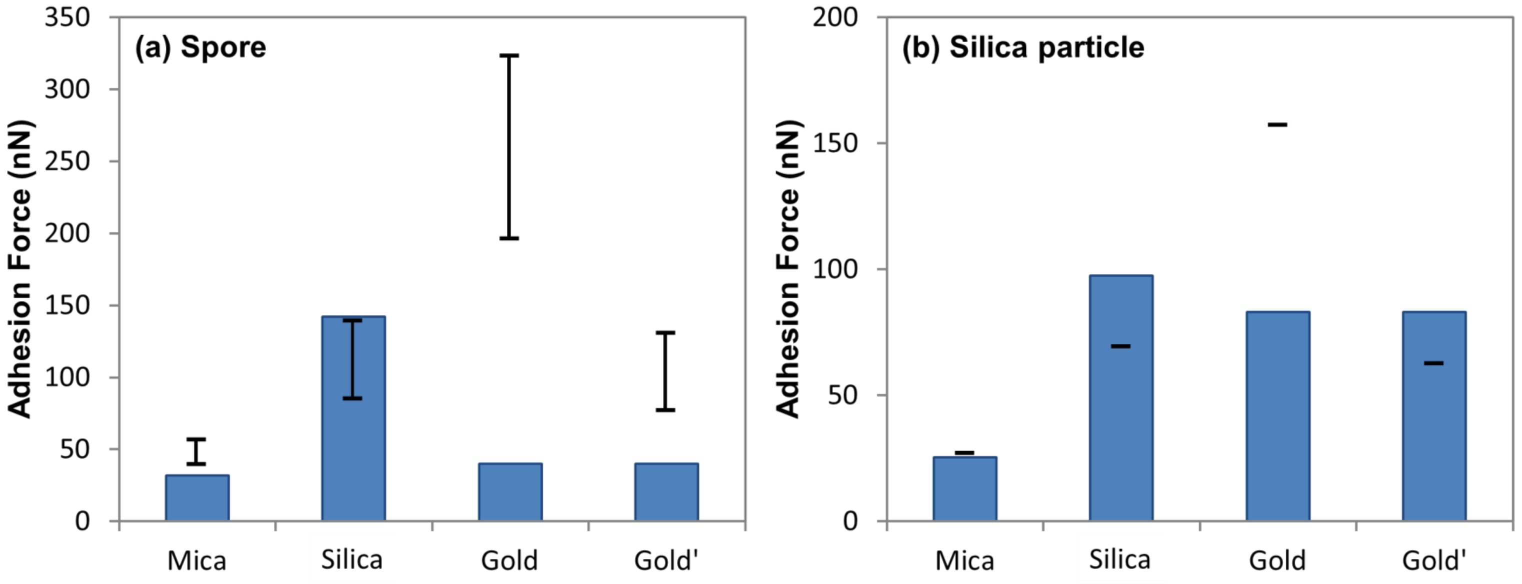

Figure 3.6. Comparison of the calculated adhesion force (vertical range lines in (a) and horizontal bars in (b)) and measured adhesion force (bars) for the spore (a) and the silica particle (b) at 0% RH. Gold´ represents contaminated gold

the force reduction on silica was trivial. This difference is attributed to the Hamaker constant that was used to determine the van der Waals force for each material. While the Hamaker constant of silica (6.5×10^{-20} J) is close to that of hydrocarbon (5.0×10^{-20} J), the Hamaker constant of gold ($30 \sim 50 \times 10^{-20}$ J) is 6~10 times larger.[1] These observations indicate that surface contamination arising from exposure to ambient conditions can reduce substantially the surface energy and, eventually, the surface interaction forces. Therefore, surface contamination and its concentration, as well as the physical and chemical properties of interacting surfaces, should be taken into account when estimating the interaction forces between surfaces in ambient environments.

3.4. Conclusions and Implications

The friction and adhesion forces of spores of *Bacillus thuringiensis* on planar surfaces in atmospheric systems were investigated at various RH levels. The strong surface charge density of mica at low RH induces a long-range attraction between the cantilever and the mica, which leads to strong friction forces for the spores and the silica particles. As the RH increases, water molecules readily adsorb onto the atomically flat, hydrophilic mica surface, causing friction force to decrease. On the other hand, RH increases on a rough silica surface lead to friction force increases, a result of increases in the viscous resistance of adsorbed water molecules and a stronger capillary attraction. As the hydrophobicity of interacting surfaces increases, the significance of RH declines. The friction force of the spore shows a linear relationship to the total adhesion force on a hydrophobic surface. In regard to adhesion force, comparisons between calculated and measured values indicate the importance of surface charge and contamination.

The measurements on single particle interactions with surfaces under controlled relative humidity, as described here, are extremely useful in understanding the behavior of populations of particles. Particle-particle interactions are also important and need to be considered in the case of high concentrations of particles. This study is expected to provide insight for the development of effective methods to prevent and control surface contamination by biological particles, including spores and other organic and inorganic particles.

3.5. Summary

The kinetic friction force and the adhesion force of *Bacillus thuringiensis* spores on planar surfaces in atmospheric systems were studied using atomic force microscopy. The influence of relative humidity on these forces varied for different surface properties including hydrophobicity, roughness, and surface charge. The friction force of the spore was greater on a rougher surface than on mica, which is atomically flat. As the relative humidity increases, the friction force of the spores decreases on mica whereas it increases on rough surfaces. The influence of relative humidity on the interaction forces between hydrophobic surfaces is not as strong as for hydrophilic surfaces. The friction force of the spore is linear to the sum of the adhesion force and normal load on the hydrophobic surface. The poorly defined surface structure of the spore and the adsorption of contaminants from the surrounding atmosphere are believed to cause a discrepancy between the calculated and measured adhesion forces.

CHAPTER 4

INFLUENCE OF SURFACE POTENTIAL ON THE ADHESION FORCE OF RADIOACTIVE GOLD SURFACES

4.1. Introduction

The influence of radioactivity on human health has raised concerns about radioactivity transport in the environment, which have increased since the events in Chernobyl, Ukraine (April 26, 1986) and more recently in Fukushima Daiichi, Japan (March 11, 2011). Problems related to radioactivity after such incidents may continue for several decades because of the generation of long-lived isotopes and the transport of radioactive particles in the environment. Radioactive fallout contaminates not only air but also water and soil, making contamination effects more serious. Like other particulate matter, radioactive particles deposited onto the soil and plants can be resuspended by natural and anthropogenic activities, such as wild fires and human-initiated burning,[24,25] propagating radioactive contamination to initially uncontaminated areas. Because of health issues and long-term effects associated with aerosols contaminated by adsorbed isotopes,[26] it is essential to monitor and control the transport of radioactivity.

Transport of radioactive particles plays an important role in spreading radioactivity.[23] The traditional models of particle transport, however, fail to predict the behavior of radioactive particles in atmospheric systems, arising from changes in their electrical state owing to self-charging.[24,25,27-29] The self-charging process can be one of the most important features of radioactive particles, which acquire surface charge through two processes: (1) ionization due to the emission of either charged particles or electrons during radioactive decay, and (2) absorption of ions generated in the surrounding medium.[23,30-33] More specifically, the net surface charge depends on particle radioactivity and the ion concentration of the surrounding medium.[31,33] Another factor that affects the surface charge of radioactive particles is their size; the smaller the particle size, the higher the surface charge density.[12,32] The transport of colloidal radioactive particles can therefore be significantly different from that of larger particles. Surface charge acquired by the particles during the decay processes can extend their travel distance, leading to unexpected radioactive contamination of areas far from the source of the radioactivity. Furthermore, the surface charge may attract particles to other surfaces, inducing an increase in the deposition rate of radioactive particles. The enhancement in the deposition of particles may be due to the increase of interaction force by the additional electrical Coulomb or image forces.[33] Therefore, in order to develop a predictive model that accurately describes the behavior of radioactive aerosols, a study focused on surface forces of colloidal radioactive particles is required.

The relative humidity (RH) plays an important role in the transport of particles in atmospheric systems. In general, a higher RH promotes particle adhesion by forming a water meniscus between a particle and another interacting surface. At the same time, however, it can decrease the electrostatic force by dissipating the surface charge. In addition, a high surface charge density may lead to enhanced adsorption of water molecules from the surrounding atmosphere.[69] Charge buildup due to the humidity has also been reported.[70] Therefore, a possible relationship between the effects of RH and radioactivity on the behavior of radioactive particles needs to be considered.

The interaction forces of colloidal particles can be studied using atomic force microscopy (AFM). AFM has been used in our previous work to study the interaction forces between bacterial spores and various planar surfaces.[4,71] The interaction forces of an individual particle and different surfaces were quantified under various conditions by obtaining the force-distance profile between the particle and the planar surface. The data were then analyzed by considering various mechanisms acting on the particles and surfaces, including van der Waals attraction, electrostatic interaction, and capillary forces. The present study aims at providing a fundamental understanding of the influence of radioactivity and RH on the interaction of colloidal radioactive particles by means of adhesion force measurements using AFM and theoretical calculations. The influence of RH on the contribution of radioactivity to adhesion is also investigated.

4.2. Experimental and Modeling Methods

4.2.1. Surface Preparation

4.2.1.1. Activation of Gold by Neutron Irradiation

A pure gold foil was activated by neutron capture and used to measure surface potential and surface forces. A detailed procedure for the activation of gold can be found in previous work.[72] In brief, small square pieces of gold foil were cleaned with ethanol to remove any traces of organic contamination. A single piece encased in a polyethylene vial was transported by pneumatic transfer tube PT-2 into the High Flux Isotope Reactor (HFIR) at Oak Ridge National Laboratory (ORNL). Co-irradiated monitors were used to determine the neutron fluence. Both the gold sample and the monitor were carefully placed in the HFIR “rabbit” and irradiated for a few seconds. The resulting radioactivity of each gold sample was 150 to 500 µCi (microcuries), depending on the duration of irradiation. The dominant produced isotope was ^{198}Au, which decays through beta and gamma emissions, with a half-life of 2.7 days. The sample was allowed to decay outside the reactor to a level of radioactivity permitting safe handling outside a glove box. The foil was transported to an analytical laboratory at ORNL and attached to an AFM magnetic puck with double-sided tape, which securely held the sample on the AFM stage during the force measurements. The AFM head was located in a contamination zone, with shielding provided by a 6-mm-thick Lucite box positioned on a floating table.

4.2.1.2. Application of Electrical Bias to Modify the Surface Potential of Gold

A small rectangular piece (approximately 2 mm × 3 mm) of nonradioactive pure gold foil was attached onto a magnetic stainless steel disc with silver paint, which allowed the application of electrical bias to the foil. Prior to each measurement, the prepared sample was cleaned with ethanol and acetone, and then thoroughly rinsed with deionized water. The clean sample was stored in a silica gel dehydrator about 24 hours prior to the experiments.

4.2.2. Surface Potential Measurements

The surface potential of irradiated gold and its corresponding surface topography were obtained by scanning surface potential microscopy (SSPM) and an AFM Nanoscope IIIa (Veeco Instruments, Plainview, NY) located at ORNL. Surface topography was first mapped by AFM in tapping mode, and then the surface potential was measured by SSPM at a predetermined distance from the gold surface for the area where the topography was obtained. The distance between a metal-coated Si tip and the substrate surface (gold or silicon nitride) was maintained at 50 nm to minimize short-range interaction forces, such as the van der Waals force. The approximate radius of the tip apex was 100 nm. This procedure allowed the measurement of the surface potential value within a maximum error of 5%.[73,74]

4.2.3. Adhesion Force Measurements

The adhesion force of the gold surface, prepared as discussed in Section 4.2.1, was measured by AFM using a cantilever with a silicon nitride (Si_3N_4) tip at room temperature (19-21ºC). For the irradiated gold, the AFM Caliber (Veeco Instruments, Plainview, New York) located at ORNL was used, whereas for the nonradioactive gold, the AFM MultiMode V (Veeco Instruments, Plainview, New York), which allows the application of electrical bias and the direct measurement of the cantilever spring constant, was used. The deflection signal, recorded in volts during the probe motion, was converted to force (nanonewtons) through Hooke's law: $F = k \times S \times \Delta V$, where F, k, S, and ΔV are the force, spring constant, photodiode sensitivity, and change in deflection signal, respectively.

Unlike the MultiMode V, the Caliber does not have a feature to directly measure the spring constant. Since the same silicon-nitride-tip cantilever was used for both AFM instruments, the spring constant measured by MultiMode V was used to calculate the force by Hooke's law for the irradiated gold. The adhesion force was measured over a period of weeks following the irradiation window. During the measurements, RH was controlled between <5 and 92% in a rectangular Lexan box that completely covered the whole body of the AFM. For the nonradioactive gold, the surface bias varied by changing one of the parameters of the AFM operation, and the RH was controlled in a cylindrical glass chamber that completely covered the AFM head and scanner.

4.2.4. Adhesion Force Calculations

The electrostatic force is the main component of the adhesion force that is used in the comparisons between measured forces and calculated values. For the electrostatic force calculations, a silicon nitride tip, which has a quadrangular pyramid shape, was considered to be equivalent to a spherical particle with the same surface area as the tip. A schematic that illustrates the silicon nitride tip and its dimensions, as well as the adhesion of a spherical particle on a planar surface, is shown in Figure 4.1. The tip was assumed to be a square pyramid, and its surface area was calculated using the tip height (Figure 4.1a) and the length of the cross line of the base square (Figure 4.1b); dimensions were provided by the manufacturer. A smooth surface was also assumed for both gold and silicon nitride tips. The electrostatic force of the equivalent spherical particle that has the same surface area as that of the tip with a substrate surface was calculated using the following equation:

$$F_{el} = -\frac{\sigma_{substrate\ surface}\sigma_{particle}}{2\varepsilon_0} A_{particle} \qquad (4.1)$$

In eq 4.1, σ_i, ε_o, and $A_{particle}$, are the surface charge density, permittivity, and surface area of the particle, respectively. The surface charge density was calculated from the SSPM measurements for each surface (i) using the following equation where ψ and z denote the surface potential and the distance between the SSPM tip and gold or silicon nitride surface (i), respectively.[14]

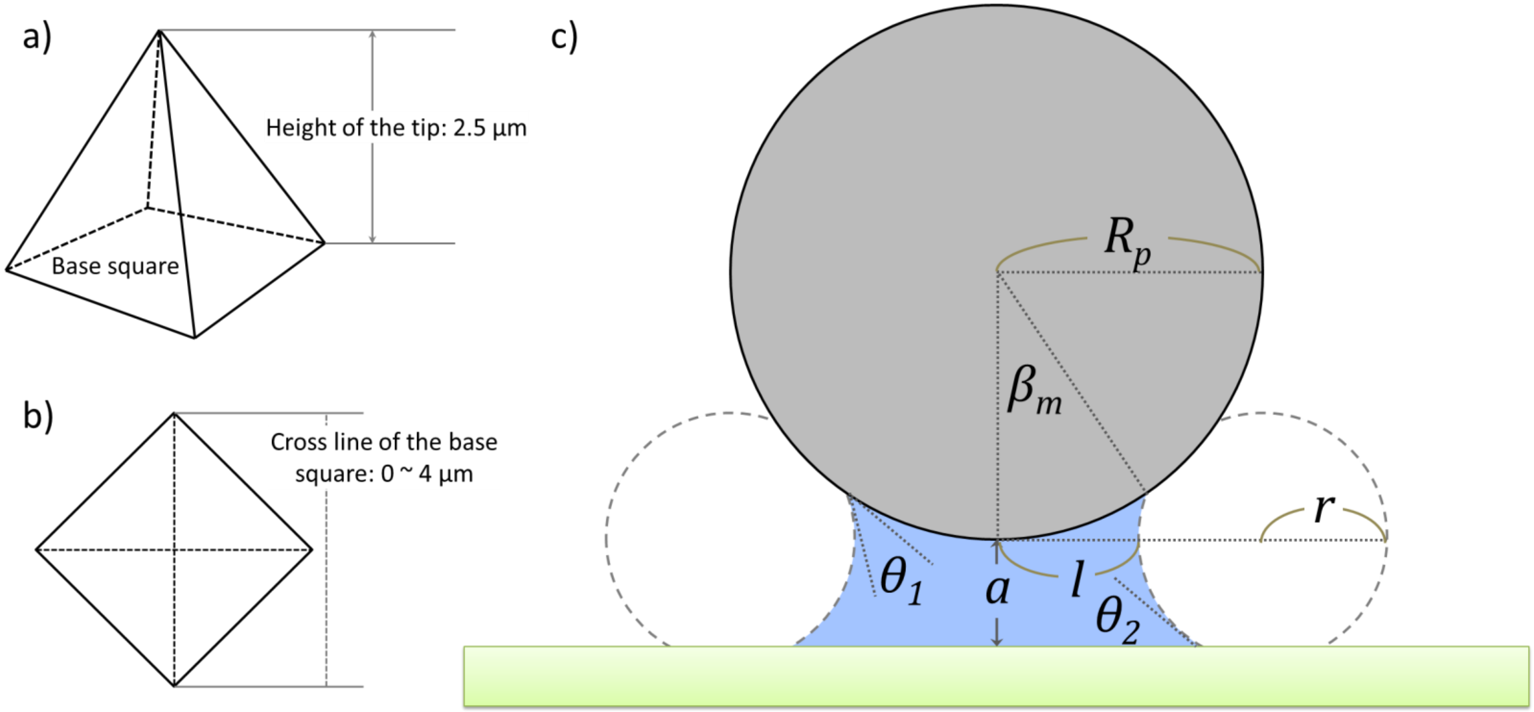

Figure 4.1. (a) Side view and (b) top view of an AFM tip. c) Simple schematic of the adhesion of a spherical particle on a planar surface.

$$\sigma_i = 2\varepsilon_o \frac{\partial \psi}{\partial z} = 2\varepsilon_o \frac{\psi_i - \psi_{SSPM\ tip}}{z} \tag{4.2}$$

The van der Waals (F_{vdW}) and capillary (F_{cap}) forces were also calculated to generate the other components of adhesion force of a spherical particle on a planar surface, and the following equations were used:

$$F_{vdw} = \frac{H_{water} R_p}{6a^2} + \frac{H_{air} - H_{water}}{6a^2} R_p \times \frac{a^2}{\left(a + R_p - R_p \cos\beta_m\right)^2} \tag{4.3}$$

In eq 4.3, H_{water} and H_{air}, a, R_p, and β_m represent the Hamaker constant in water and air, intermolecular spacing, radius of the tip, and angle of meniscus, respectively.[1,9,41]

$$F_{cap} = \pi l \gamma_w \left[-\frac{lRT}{\gamma_w V_m} \ln\left(\frac{P}{P_o}\right) + 2\sin\left(\theta_1 + \beta_m\right) \right]$$
$$\text{where } l = R_p \sin\beta + r\left[\sin\left(\theta_1 + \beta_m\right) - 1\right] \text{ and } r = \frac{R_p\left(1 - \cos\beta_m\right) + a}{\cos\left(\theta_1 + \beta_m\right) + \cos\theta_2} \tag{4.4}$$

In eq 4.4, γ_w, R, T, V_m, θ_1 and θ_2, and P/P_o denote the surface tension of water, ideal gas constant, temperature, molar volume of water, contact angle of the particle and substrate surface, and RH, respectively.[9,41]

4.3. Results and Discussion

4.3.1. Surface Potential of the Irradiated Gold Surface

After obtaining the surface topography of the irradiated gold foil with AFM, its surface potential was measured by SSPM for radioactivity ranging from 492 µCi to 9.4 µCi (for the whole surface of the Au substrate, i.e., 25 mm^2) at 35, 55, and 85% RH. The measurements revealed no effects of radiation on the surface topography of the gold foil. However, SSPM measurements showed that radiation strongly influences the electrical characteristics of the gold. For radioactivity greater than 80 µCi, the measured surface potential was constant at 10 V, which is the maximum measurable level by our SSPM instrument. Therefore, it is considered that the surface potential for radioactivity greater than 80 µCi is higher than 10 V. The surface topography and surface potential at 30.2 µCi and 55% RH are shown in Figures 4.2a and 4.2b, respectively, while the surface topography and potential at a different location at 108 µCi and 55% RH are shown in Figures 4.2c and 4.2d, respectively. The surface potential is 2.5 V in most of the imaged area of Figure 4.2b, with a few variations in some regions. Since the control sample of nonradioactive gold showed uniform surface potential without variation (result not shown), the variation for the irradiated gold may be originated from the heterogeneous charge distribution due to radiation.

Figure 4.3 shows the change of surface potential as a function of radioactivity at 35, 55, and 85% RH. The surface potential was linearly decreased as the radioactivity decreased from 65 to 10 µCi with a decay rate of 0.15 V/µCi, and the potential was constant with further decreasing surface radioactivity. Clement et al.[31] also reported that the mean charge of particles, which depends on the surface charge density of particles,[14]

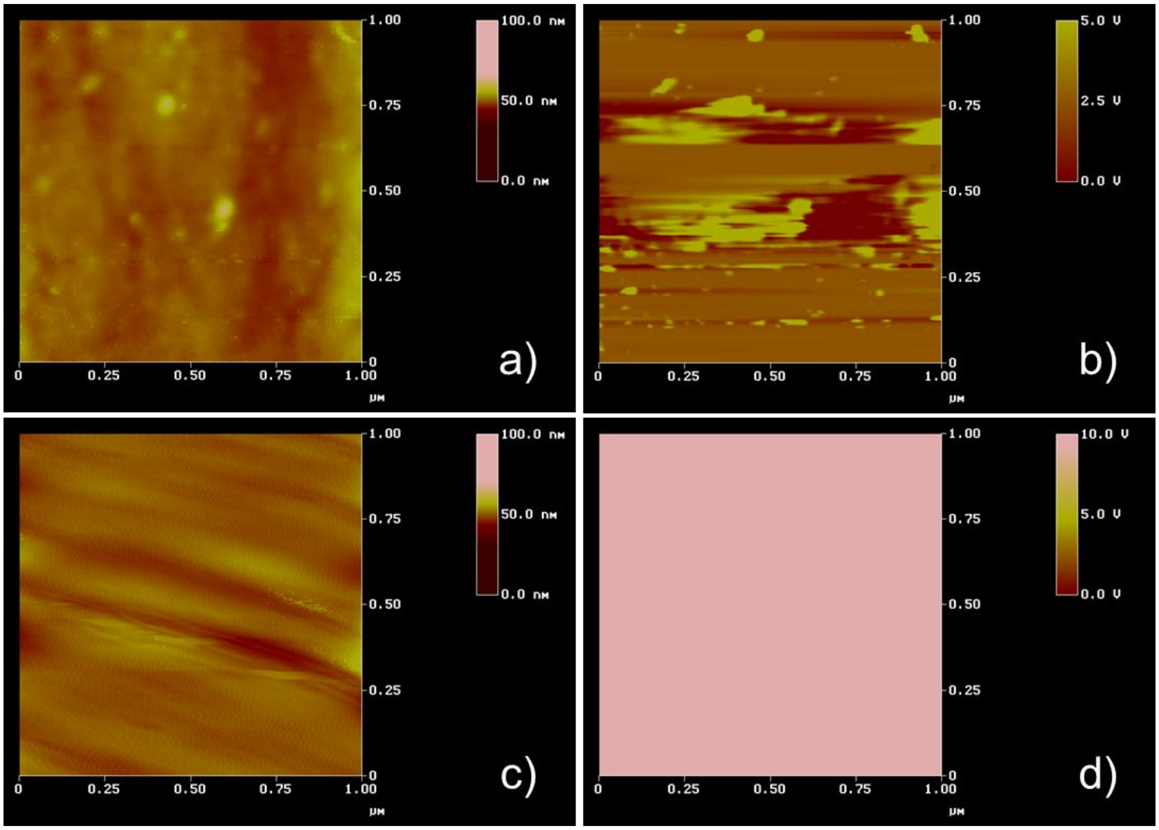

Figure 4.2. (a) Surface topography and (b) surface potential at 30.2 µCi and 55% RH; (c) surface topography and (d) surface potential at 108 µCi and 55% RH. The values of the surface potential in (d) are greater than 10 V, which is the saturation limit of the SSPM instrument.

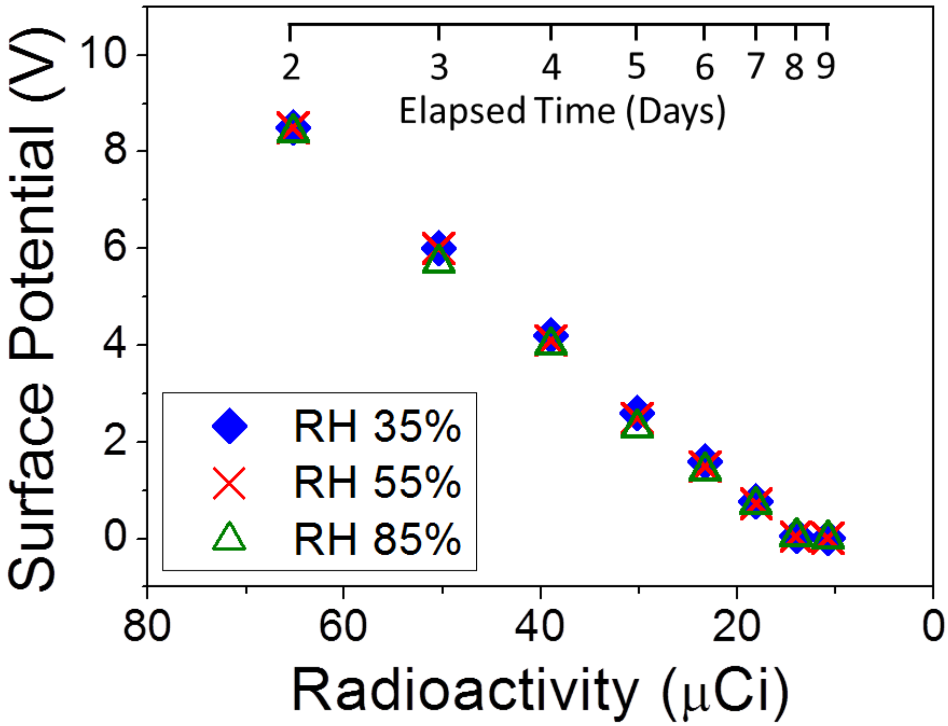

Figure 4.3. Influence of radioactivity on the surface potential at 35, 55, and 85% RH.

is proportional to radioactivity.

In Figure 4.3, the RH at each radioactivity level does not significantly influence the surface potential of irradiated gold. The surface potential decreased less than 5% when the RH increased from 35 to 85% for radioactivity values greater than 30 μCi. In general, the surface potential is reduced at high RH values because the surface charge is attenuated by moisture in the atmosphere. Since radioactive decay is an ongoing process, however, the surface potential caused by the self-charging mechanisms of irradiated gold during decay reaches steady state, and so is not considerably influenced by RH. From the SSPM measurements, it can also be concluded that the effect of the radioactivity does not depend on RH.

4.3.2. Adhesion Force Measurements at Different Levels of Surface Potential of the Gold Surface

Force measurements were carried out through two different procedures. In Case 1, a gold foil acquired surface potential by irradiation. RH was controlled at high (~90%), medium (55-70%), and low (5-15%) values at a certain level of radioactivity, and the force was measured at randomly chosen areas with the AFM Caliber. In Case 2, the surface potential was directly applied to the gold foil by an electrical bias through the AFM stage. The surface potential was controlled from 0 to 10 V at 0, 40, and 80% RH in an ascending order, and the force was measured at randomly chosen areas with the AFM MultiMode V. In both cases, the same type of silicon nitride tip was used.

4.3.2.1. Case 1: Irradiated Gold Surface

Figure 4.4 shows the average value of the adhesion force, and the corresponding radioactivity and surface potential over a period of weeks following the irradiation.

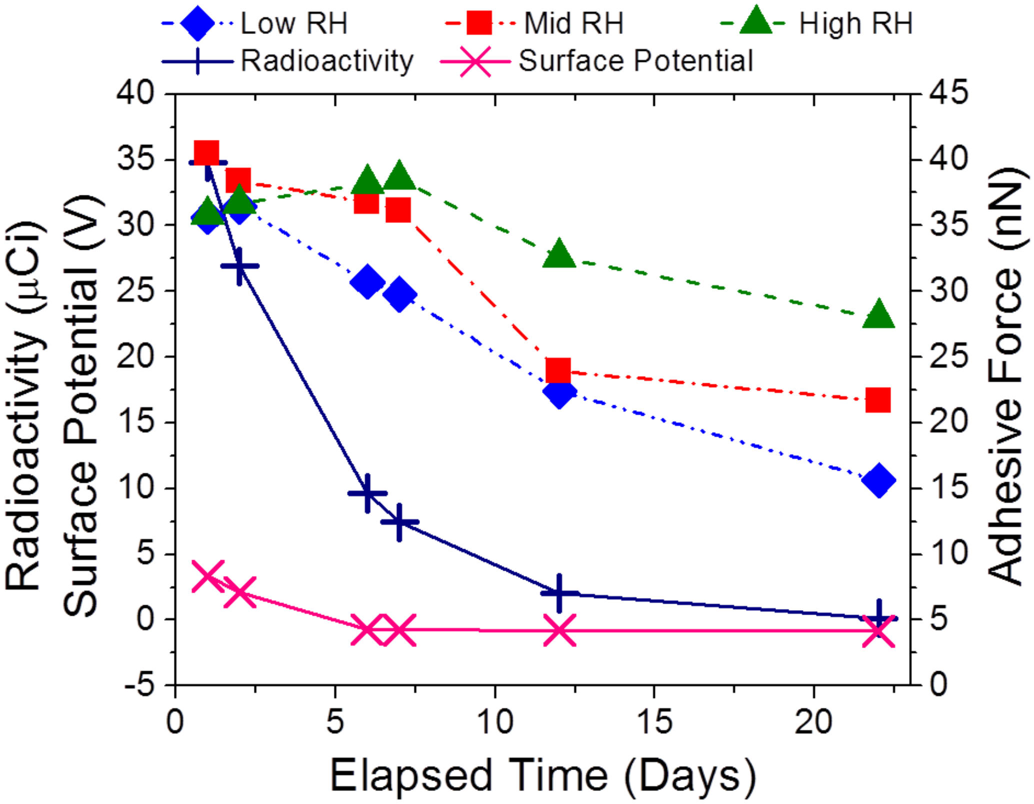

Figure 4.4. Adhesion force measurements between the AFM silicon nitride tip and the irradiated gold (Case 1) as a function of radioactivity over time.

The radioactivity of the gold decreased exponentially, following first-order kinetics, while the surface potential decreased gradually until a radioactivity level of 9.6 µCi was reached, below which the surface potential was maintained near 0 V. Force measurements showed a standard deviation of less than 10%, which is attributed to the heterogeneous charge distribution acquired upon irradiation as shown in Figure 4.2. An exceptionally higher variation (standard deviation of 30%) was observed at one point when the radioactivity level was 2.1 µCi at high RH. It is possibly due to the random formation of microscopic pools of water from the aggregation of adsorbed water molecules prior to the complete formation of water layer.[53]

When the radioactivity was greater than 9.6 µCi, the adhesion force was the highest at the medium level of RH and a similar magnitude of adhesion force was observed at the low and high levels of RH; however, the difference in the adhesion force due to the change in RH decreased as the radioactivity was reduced from 34.8 to 26.9 µCi. By comparing the measurements with theoretically calculated values, the influence of RH and surface potential generated by radioactivity on the adhesion force as well as their relationship can be identified. For this purpose, the theoretical electrostatic force for 34.8 µCi, calculated by eqs 4.1 and 4.2, was added to the last measurement at 0 µCi, and the result is shown in Figure 4.5. A range of theoretical values was found due to the range of dimensions of the AFM cantilever tips provided by manufacturer, as shown in Figure 4.1. The surface potential of silicon nitride and calculation and the parameters used in the calculations are listed in Table 4.1 and Table 4.2, respectively.

Figure 4.5 shows experimentally measured and theoretically calculated forces at low, medium, and high levels of RH. Although the measured forces are within the range

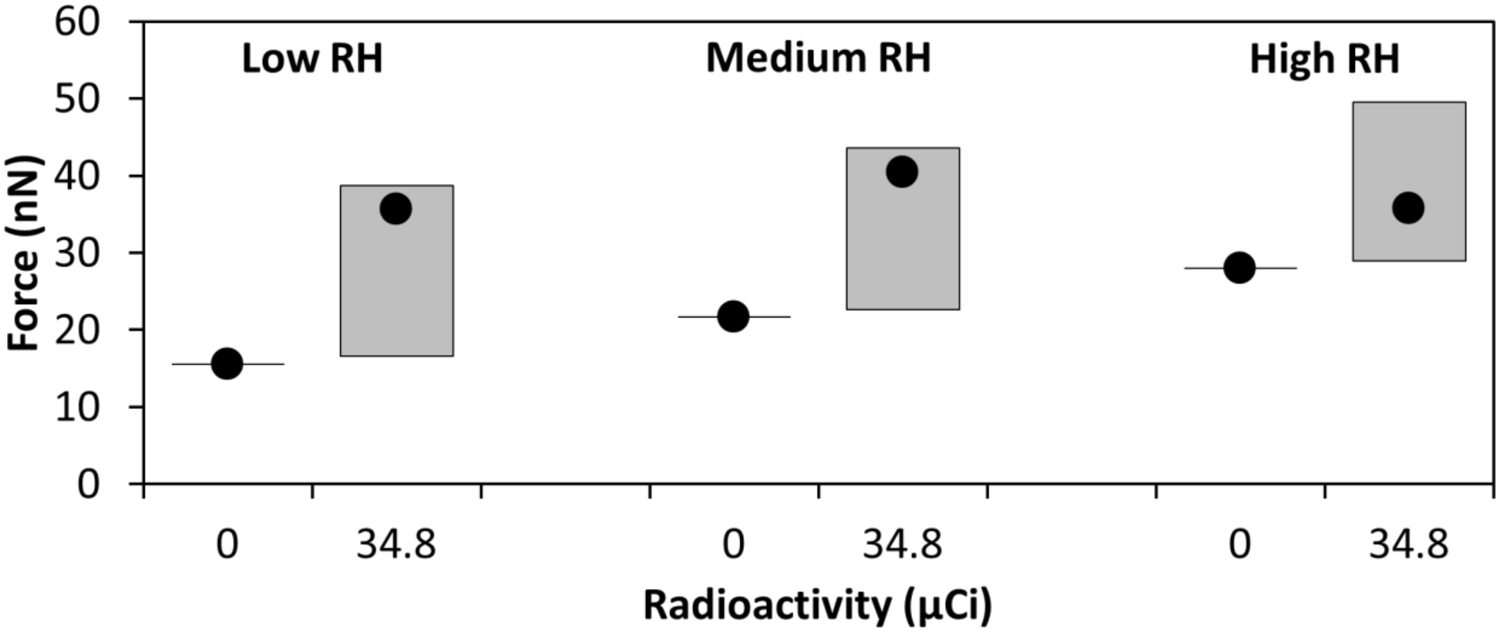

Figure 4.5. Comparison between experimentally measured and theoretically calculated forces. The vertical bars and circles represent the ranges of the theoretical values and the measured forces, respectively. The theoretical values were obtained by adding the contribution of electrostatic force to the measured force at 0 µCi. The range of theoretical values was obtained based on the range of dimensions of the silicon nitride tip.

Table 4.1. Surface potential of silicon nitride measured by SSPM. The error of each measurement is 8–12%.

RH (%)	Surface Potential (V)
0	-0.125
20	-0.112
40	-0.095
60	-0.082
80	-0.081

Table 4.2. Parameters needed in the calculation of the electrostatic forces shown in Figure 4.5 and Figure 4.8.

Hamaker constant in air and water ($\times 10^{-20}$J)	Gold-silicon nitride: 23.3 and 8.2
Voltage bias (V)	0 and 3.4V for irradiated gold; 0, 3, and 10 V for nonirradiated gold

of calculated values, the contribution of electrostatic force at high RH is less than that at low and medium RH, indicating the influence of water adsorption and surface potential on the adhesion force. Water is a bipolar molecule, positively charged on the hydrogen side and negatively charged on the oxygen side, and thereby it is attracted to both positive and negative charges. The irradiated gold, ^{198}Au, decays through beta and gamma emissions that produce positive charges on the surface.[75,76] The positive surface charges were also confirmed by the SSPM measurements for ^{198}Au in Figure 4.4. As verified by SSPM experiments, the surface charge was not dissipated by the adsorption of water molecules onto the gold surface. Therefore, it is possible that the surface charge generated by radioactivity made the gold surface highly hydrophilic, so that it attracted more water molecules than the nonradioactive gold surface.

Adsorbed water molecules can promote adhesion by enhancing the capillary force. However, excessive amount of water adsorption can decrease the adhesion force as shown in Figure 4.6. The figure presents theoretical calculations of the total adhesion force that includes the van der Waals force given by eq 4.3 and the capillary force given by eq 4.4 for a highly hydrophilic surface. The theoretical results show that the capillary force is decreased at a level of RH higher than 80% due to the reduction in pressure difference across the meniscus (see Figure 4.1). In addition, adsorbed water molecules either screen the strength of surface potential[77] or provide a passage for surface charge leakage, especially when a water layer is formed. Since a complete coverage of the substrate surface by water molecules can occur at less than 60% RH for a highly hydrophilic surface such as mica,[53,55,65] the latter explanation is more relevant to the reduction of the adhesion force at 34.8 µCi and high RH. Water is a good conductor that

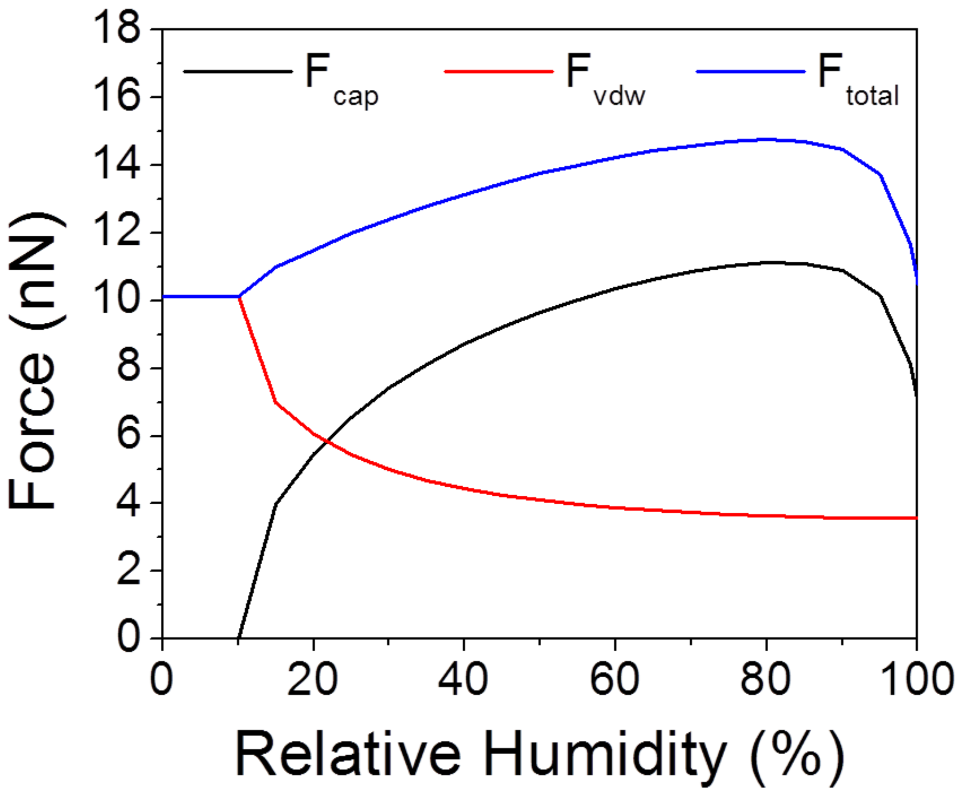

Figure 4.6. Theoretically calculated adhesion force between a silicon nitride spherical particle with radius of 20 nm and a highly hydrophilic gold surface with no surface potential. The force includes van der Waals and capillary forces. The contact angles of the surface and the particle are 0 and 50º,[78,79] respectively.

has a high dielectric constant, i.e., 80 at 20ºC.[1] Since the amount of water adsorption increases with the RH, the surface charge on the gold surface can instantaneously flow through the adsorbed water molecules when the tip comes into contact with the gold surface. The reduction in charge density was not observed in the SSPM measurements at high RH due to the experimental method employed: the SSPM tip is lifted at a certain distance during the measurements, while in the AFM measurements the tip is in contact with the substrate surface.

When the radioactivity decreased below 9.6 µCi, the adhesion force was reduced with decreasing RH. In addition, the adhesion force at each level of RH decreased continuously with a gradual reduction in the radioactivity. This observation was unexpected because the surface potential was near 0 V when the radioactivity decreased to less than 9.6 µCi (see Figure 4.4). However, ^{198}Au still decays even at an overall surface potential of near 0 V, so the changes in the adhesion force can be related to the localized effects of decreasing radioactivity.

4.3.2.2. Case 2: Gold Surface with Application of Electrical Bias

The adhesion force was measured for gold while surface potential was applied by an electrical bias directly through the AFM stage, and the bias was controlled by one of the AFM operating parameters. The bias was increased to higher values than the surface potential corresponding to the highest radioactivity in Case 1 in an effort to detect any distinguishable observations that could be expected at higher radioactivity levels. Figure 4.7 shows the measured adhesion force in Case 2.

The adhesion force increased with the increase of RH similar to Case 1 at a radioactivity less than 9.6 µCi. Unlike Case 1, however, the adhesion force increased

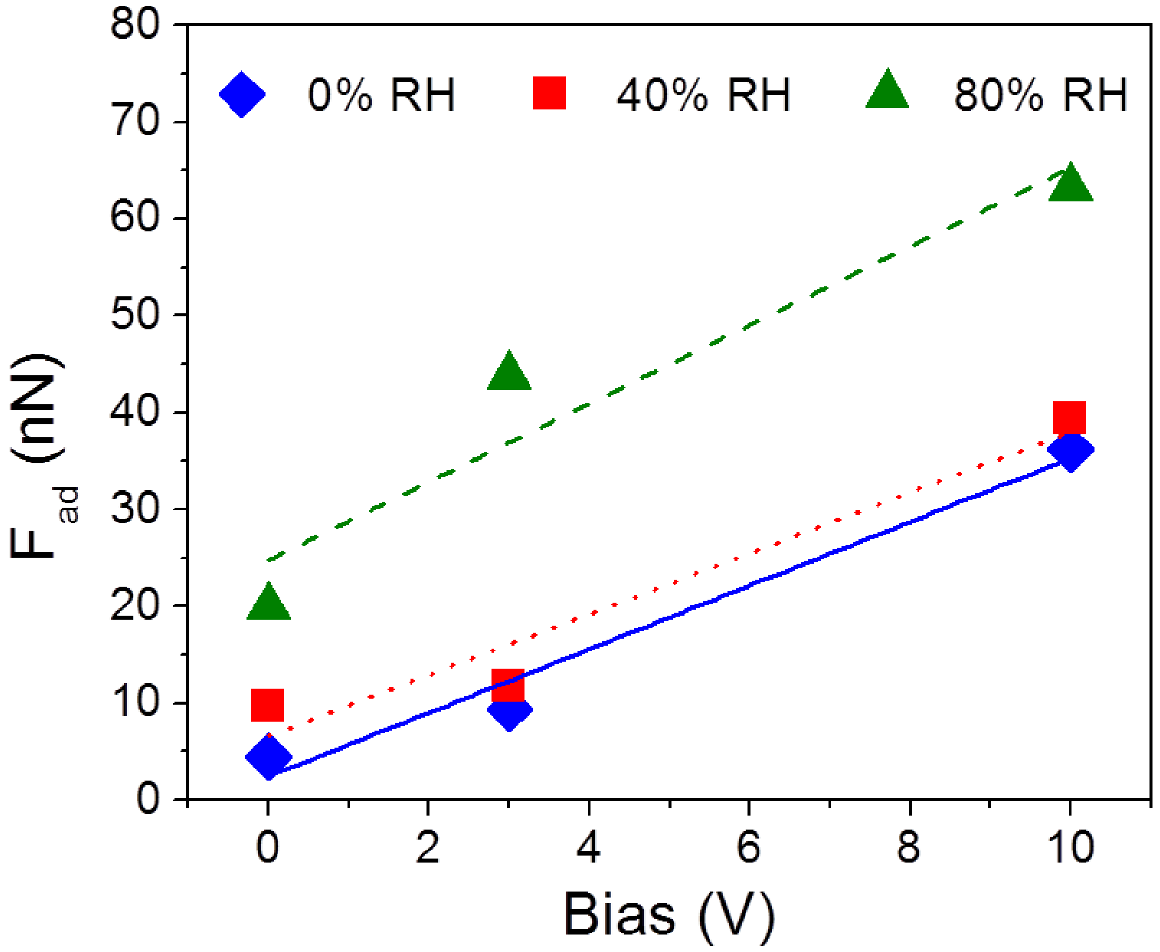

Figure 4.7. Adhesion force of the AFM silicon nitride tip on a gold foil as a function of surface bias and RH in Case 2.

linearly with increasing electrical bias. In addition, a sudden increase in the adhesion force was observed at 3 and 10 V of electrical bias when the RH was increased from 40 to 80%. Figure 4.8 presents a comparison between measured and theoretically calculated adhesion forces at three different RH and applied electrical bias. Since the electrical bias is the only variable among the three measurements obtained at each RH level, the contribution of electrostatic force to the total adhesion force was compared at each RH level in a similar way shown in Figure 4.5. For this purpose, the theoretical electrostatic force for 3 and 10 V, calculated by eqs (4.1) and (4.2), was added to the measured force at 0 V and the results are shown in Figure 4.8. Calculation parameters are listed in Table 4.5. A range of theoretical values was obtained due to the range of dimensions of the AFM cantilever tips provided by the manufacturer, as shown in Figure 4.1.

Figure 4.8 shows that the measured forces fall within the range of the theoretical calculations, but the contribution of electrostatic force is slightly higher than the theoretical value calculated at 3 V and 80% RH. This discrepancy implies a close relationship between the surface potential and the adsorption of water molecules. It is possible that the adsorption of water molecules is enhanced when the electrical bias is applied to the gold foil, as seen in Case 1. It is therefore thought that adsorbed water molecules first increase the adhesion force by promoting the capillary action between the tip and the gold surface. The increase of adhesion force from 40 to 80% RH was, however, slightly reduced at 10 V. Charge leakage through the accumulated water molecules is not likely because such an event was not observed in the AFM force-distance curves. Thus, we can conclude that the electrostatic force is reduced because the applied surface potential is possibly screened by the adsorbed water molecules.

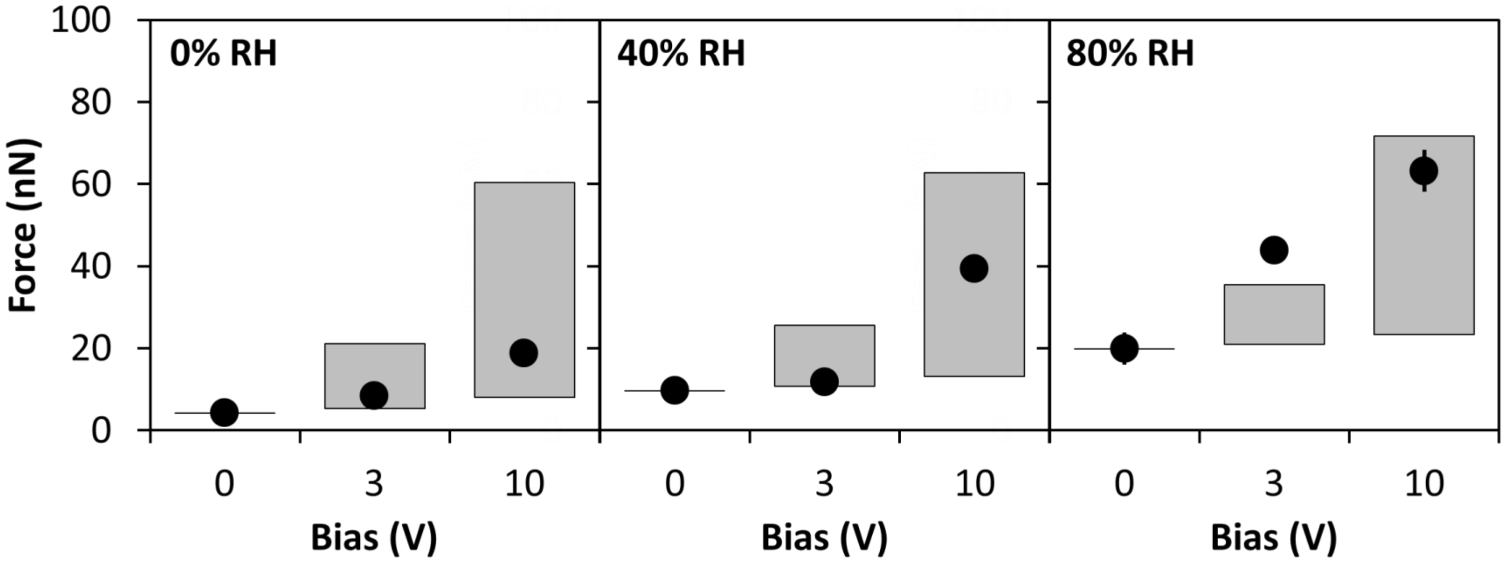

Figure 4.8. Adhesion force versus surface bias in Case 2. The vertical bars represent the ranges of theoretical adhesion forces at 0, 40, and 80% RH. The diamonds represent the measured adhesion forces. The black horizontal squares inside the bars represent the median of the theoretical values to guide the comparison. The range of theoretical values was obtained based on the range of dimensions of the silicon nitride tip.

This explanation agrees with the experimental results of Sugimura et al. who showed a reduced surface potential due to water adsorption.[77] Based on the reduction in the contribution of the electrostatic force at a much lower surface potential in Case 1, it is possible that applying electrical bias to the gold results in a smaller value of surface potential than what is expected because of the electrical resistance of the system, while the surface potential in Case 1 was generated by the self-charging process and directly measured by SSPM.

The adhesion force measurements obtained in this work indicate that enhanced adsorption of water molecules on the gold surface and/or the AFM cantilever tip attenuate the surface potential, leading to a lower than calculated contribution of the electrostatic force to the total adhesion force.

4.4. Conclusions and Implications

The adhesion force of two types of gold surfaces was studied to provide a fundamental understanding of the interaction of self-charging radioactive particles with other particles and surrounding environmental surfaces in atmospheric systems. By employing AFM, force measurements were obtained for gold that acquired surface potential either by radioactive decay or by the application of electrical bias. Radioactivity influences the adhesion force of the irradiated gold because the surface potential generated by the decay adds a significant contribution of electrostatic force to the total adhesion force. Comparisons of the experimental measurements with theoretical values revealed a possible relationship between surface potential and water adsorption, which may cause an increase in the capillary force or a reduction in the contribution of the electrostatic force by either screening the surface potential or providing a passage for charge leakage.

This study examines the interaction between positively charged radioactive and negatively charged nonradioactive surfaces (i.e., two differently charged surfaces). Since the electrostatic force acts on surface interactions, regardless of the RH, the question is how particle interactions influence the transport of radioactivity far from the source. Figure 4.9 shows calculations of the electrostatic force between two spherical particles under different scenarios: interaction between particles with like charges and opposite charges. The parameters used in the calculations are listed in Table 4.3. As shown in Figure 4.9, an electrostatic repulsive force should exist between radioactive particles of likely charged surfaces, making it difficult for these particles to aggregate and/or settle down on environmental surfaces. Radioactive particles may also adhere to surfaces that are neutral or oppositely charged. Based on Figure 4.9, particles acquiring a higher surface charge density (i.e., particles of a higher decay rate) should more readily interact with surfaces. This result means that nonradioactive surfaces can easily be contaminated by radioactive particles because of the high interaction forces. Our results here can therefore be used to provide a better understanding of the behavior of radioactive particles in atmospheric systems.

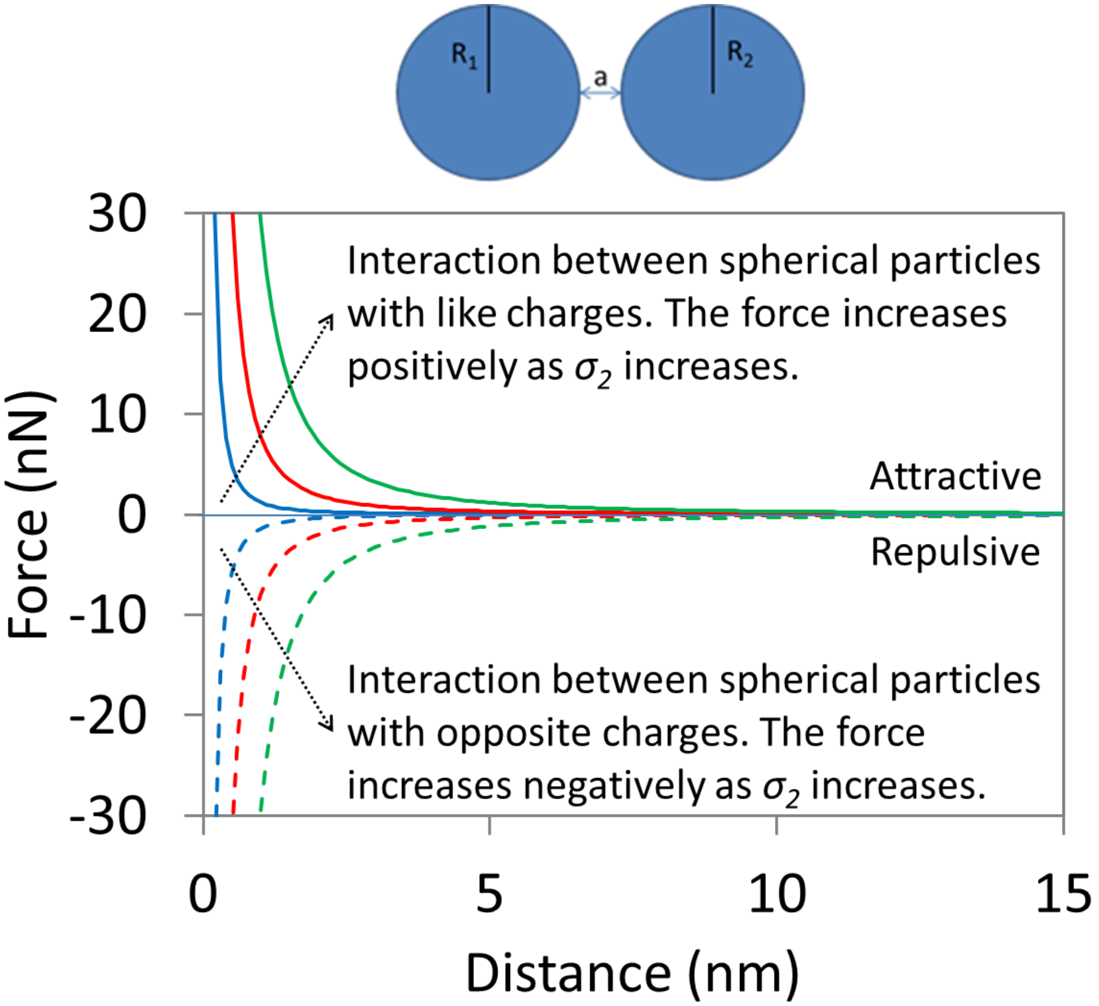

Figure 4.9. The interaction force, including electrostatic (F_{el}) and van der Waals (F_{vdw}) forces, between two spherical particles with radius of 20 nm at 0% RH. F_{el} and F_{vdw} were calculated as a function of the distance between the two particles using the following equations: $F_{el} = -k_e \frac{\sigma_1 \sigma_2}{a^2} A_1 A_2$ and $F_{vdw} = \frac{H_{air} R_1 R_2}{6(R_1 + R_2)a^2}$, where k_e, σ_i, A_i, a, R_i, and H_{air} represent the Coulomb's constant, surface charge density, surface area, distance between two particles, radius, and the Hamaker constant in air, respectively. Calculation parameters are shown in Table 4.3. A repulsive force exists between the particles of like charges, while an attractive force appears for oppositely charged particles. As the absolute value of the surface potential of either or both particles increases, the force also increases in both cases.

Table 4.3. Parameters needed in the calculation of the force-distance profile shown in Figure 4.9.

R_1 and R_2	20nm
H_{air}	6.5×10^{-20} J
σ_1 (C/m^2)	$\pm 1.5\times10^{-4}$
σ_2 (C/m^2)	1.5×10^{-4}
	9.1×10^{-4}
	33.9×10^{-4}

4.5. Summary

Radioactive particles may acquire surface potential through a self-charging process. They can thus behave differently from natural aerosols in atmospheric systems, giving rise to resuspension and secondary contamination in areas far from the radioactive source. Scanning surface potential microscopy was employed to measure the surface potential of radioactive gold foil. Atomic force microscopy was used to investigate the adhesion force for gold that acquired surface charge either by irradiation or by the application of electrical bias. Overall, the adhesion force increases with increasing surface potential or relative humidity. However, a behavior that does not follow the general trend was observed for the irradiated gold at a high decay rate. A comparison between experimental measurements and theoretical values revealed that the surface potential promotes adhesion. The contribution of the electrostatic force at high levels of relative humidity was lower than the one found using theoretical calculations due to the effects caused by enhanced adsorption of water molecules under a high surface charge density. The results of this study can be used to provide a better understanding of the behavior of radioactive particles in atmospheric systems.

CHAPTER 5

THE ROLE OF ELECTROSTATIC CHARGE IN THE ADHESION OF SPHERICAL PARTICLES ONTO PLANAR SURFACES

5.1. Introduction

Interfacial forces such as van der Waals, capillary, and electrostatic forces play an important role in atmospheric transport of aerosol particles, especially when the particle size is in the micrometer range. Among the interfacial forces, the electrostatic force is a major contributor to the behavior of charged particles. Radioactive particles are a relevant example because they acquire charge through self-charging processes.[12,23,25,27,30] Arising from surface charge, the electrostatic force leads to the transport of radioactivity far from radioactive sources and the accumulation of contamination on soil and plant surfaces.[80] Electrical household appliances are a significant source of ultrafine charged particles, which affect indoor air quality.[81-85] Electrostatic interactions prevent the aggregation of charged aerosol particles and allow them to carry various air pollutants including microorganisms, dust, and sometimes radon progeny to long distances.[80] Since charged particles are stabilized and thus do not fall down, their surface charge can enhance the transport of air pollutants. The surface charge may also increase the concentration of pollutants on surfaces, such as computer displays, printers, and power cables.[80,86]

Relative humidity (RH) is another variable that affects the behavior of particles in the atmosphere. As the RH is increased, more water molecules adsorb onto surfaces, and a water meniscus may form between the interacting surfaces in contact. Adsorption of water molecules promotes the adhesion of particles due to the surface tension of water and the pressure difference across the meniscus.[9,41] Since water is a polar molecule which can be attracted by a charged surface, the presence of surface charge considerably affects water adsorption onto surfaces. It has also been reported that water adsorption contributes to charge build-up,[70,87] which contradicts the role of water in dissipating the charge by increasing the conductance of the material.[70,88] Thus, it is essential to consider not only the effects of surface charge and RH upon the adhesion force of micron- and submicron-size particles in atmospheric systems, but also the interactions between surface charge and RH.

Atomic force microscopy (AFM) has been used to study the interaction forces between micron-size particles and different substrate surfaces. The various AFM applications have been reviewed elsewhere.[15,16] AFM is a suitable tool to study particle interaction forces in atmospheric systems because it enables the simulation of the natural environment by controlling such variables as RH and surface potential. AFM has been used in our previous work for the study of micron- and submicron- size particles including a silicon nitride cantilever tip, spherical silica particles of varying diameter, and bacterial spores with various planar surfaces.[4,71,89] The contribution of the electrostatic force was identified by scanning surface potential microscopy (SSPM) measurements and through comparisons of AFM force measurements with calculated values using mathematical models for the van der Waals, capillary, and electrostatic forces.[14,90] Kweon et al. measured the interacting forces of a silicon nitride tip with a radioactive gold surface.[89] It was found that the electrostatic force arising from the surface potential of Au (198) contributes to the total adhesion force. In addition to radioactive particles, there are many examples in which the electrostatic force plays a critical role because aerosol particles can naturally or artificially acquire surface charge.[80,81,86]

This study aims at investigating the contribution of the electrostatic charge and the influence of RH on the adhesion force of various materials. AFM was used to measure the adhesion force of silica or gold particles with various planar surfaces including mica, silica, and gold, which can be readily found in both natural and engineered environments. Mica and silica are insulating materials whereas gold is conductive, but mica can acquire a relatively higher surface charge density than silica does. In order to investigate the effect of particle size on the interaction forces, two different-size particles, 1 µm and 2.5 µm in diameter, were used. The interaction forces were also calculated using established models for the van der Waals, capillary, and electrostatic forces. Comparisons between experimental data and theoretical calculations can be used to improve the models.

5.2. Experimental and Modeling Methods

5.2.1. Surface Preparation

Mica, silica (fused quartz), and gold foil were used as planar surfaces in this study. Prior to cleaning, mica and silica were fixed onto a magnetic disc that adjusts substrate surfaces on the AFM stage using two-sided adhesive tape. In order to minimize surface contamination that could result in the modification of surface properties, mica was cleaved just before each force measurement. Silica was stored in concentrated sulfuric acid for more than 24 hours and was rinsed thoroughly with a large amount of deionized water. A pure gold foil of square shape was attached to the magnetic disc using silver paint, which enabled the application of electrical bias to the gold foil. Electrical bias was applied to modify the electrostatic charge on the surfaces. The prepared gold kit was cleansed with ethanol and acetone, and rinsed thoroughly with a large amount of deionized water. Cleaned silica and gold surfaces were dried and stored in silica gel dehydrators for 3 to 5 days.

5.2.2. AFM Probes

AFM probes of a spherical silica particle and a gold particle were prepared for interaction force measurements. A single spherical silica particle was attached at the end of a v-shaped tipless cantilever made of silicon nitride. A gold probe was prepared by coating a silica probe with gold. Particle attachment and gold coating were performed by Novascan Technologies (Ames, Iowa). The procedure involves handling of the particles with micro-manipulators and attachment on cantilevers with a thin film of glue. A gold coating film enabled the application of the electrical bias to the particle. Two different particle sizes (1 µm and 2.5 µm) were used to prepare both probes of silica and gold particles.

5.2.3. AFM Force Measurements

The interaction force between three different substrate surfaces (mica, silica, and gold) and the prepared particle probes was measured by using the AFM MultiMode V (Veeco Instruments, Plainview, New York) at room temperature (19-21ºC). The application of the electrical bias is allowed through the substrate surface and the particle probe. Since mica and silica are both electrically insulating materials, the electrical bias was introduced through the gold particle. For the system consisting of gold foil, electrical bias was applied through either the gold foil or the gold-coated particle. A silica particle probe was also used in the measurements with the gold foil. The magnitude of the electrical bias was controlled by changing one of the AFM operating parameters. The deflection of the particle probe due to the interaction forces between the probe and the surface was recorded in volts (V), and it was converted to force (nN) using Hooke's law; $F = k \times S \times \Delta V$, where F, k, S, and ΔV are the force, spring constant, photodiode sensitivity, and change in deflection signal, respectively. The relative humidity (RH) was controlled in a cylindrical glass chamber that completely covered the AFM head and scanner.

The normal load (F_n), adhesion force (F_{ad}), and total adhesion force (F_{tot}, i.e., the sum of normal load and adhesion force) can be estimated from the force-distance curve obtained by AFM. Figure 5.1 shows a typical force-distance curve for two cases: interaction between a particle and a surface without a long range attraction (solid line) and with a long range attraction (broken line). In general, the normal load (F_n) is the difference between the set-point, one of the AFM operating parameters, and point d. The adhesion force (F_{ad}) is the difference between points c and d. With the existence of the long-range attraction, however, it is not easy to distinguish F_n from the curve due to the influence of long-range attraction on both F_n and F_{ad}. Moreover, the probe is deflected until the force measurement is completed. In this work, therefore, F_n is defined as the difference between the set-point and point d or d', regardless of the existence of a long-range attraction. The comparison of F_n for different experimental conditions shows the influence of electrical bias applied to either the particle or the substrate surface. In addition, it is more appropriate to compare F_{tot}, the difference between the set-point and point c, instead of F_{ad} because it is difficult to distinguish how much the electrical bias or

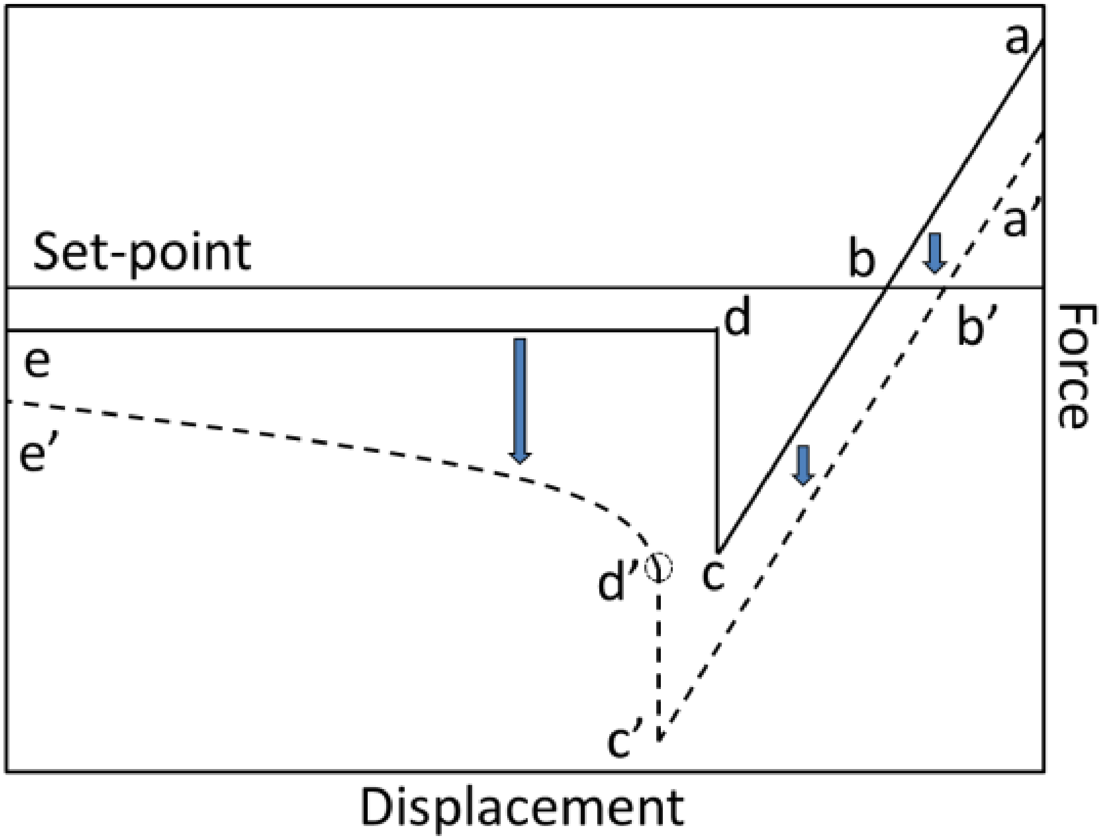

Figure 5.1. A typical retracting force-displacement curve (solid) and the curve with the presence of a long-range attraction (broken). A particle probe travels from a to e. The probe maintains the contact with the surface due to the adhesion force (b to c). When the adhesion force is overcome, the particle is detached from the surface (c to d). As the probe moves further, the deflection of the probe immediately returns to its original state (d to e). When a long-range attraction exists, the curve shifts towards the attraction region, and the deflection of the probe gradually returns to its original state (d’ to e’).

5.2.4. Force Calculations

To investigate the role of surface potential in the adhesion of a spherical particle on a planar surface, as shown in Figure 5.2, the electrostatic force was theoretically calculated and compared to measured forces. For simplicity, a smooth surface was assumed for both the particle and the substrate surface. The electrostatic force is calculated by Coulomb's Law. Although the Coulomb's Law is derived for point charges, it is also applicable to uniformly charged identical spheres. To simplify the calculations, the two interacting surfaces were assumed as two uniformly charged spheres with similar diameters:

$$F_{el} = -\frac{Q_{substrate\ surface} Q_{particle}}{4\pi\varepsilon_o d^2} \tag{5.1}$$

In eq 5.1, Q_i, ε_o, and d are the surface charge, vacuum permittivity, and distance between two spheres, respectively. Distance d is expressed as $d = 2R_p + z$, where z is the separation distance between two surfaces. In addition, the surface charge is the product of surface charge density (σ_i) and surface area of the particle. Thus, eq 5.1 can be written as:

$$F_{el} = -\frac{Q_{substrate\ surface} Q_{particle}}{4\pi\varepsilon_o d^2} = -\frac{\sigma_{substrate\ surface}\sigma_{particle} 4\pi R_p^4}{\varepsilon_o \left(2R_p + z\right)^2} \tag{5.2}$$

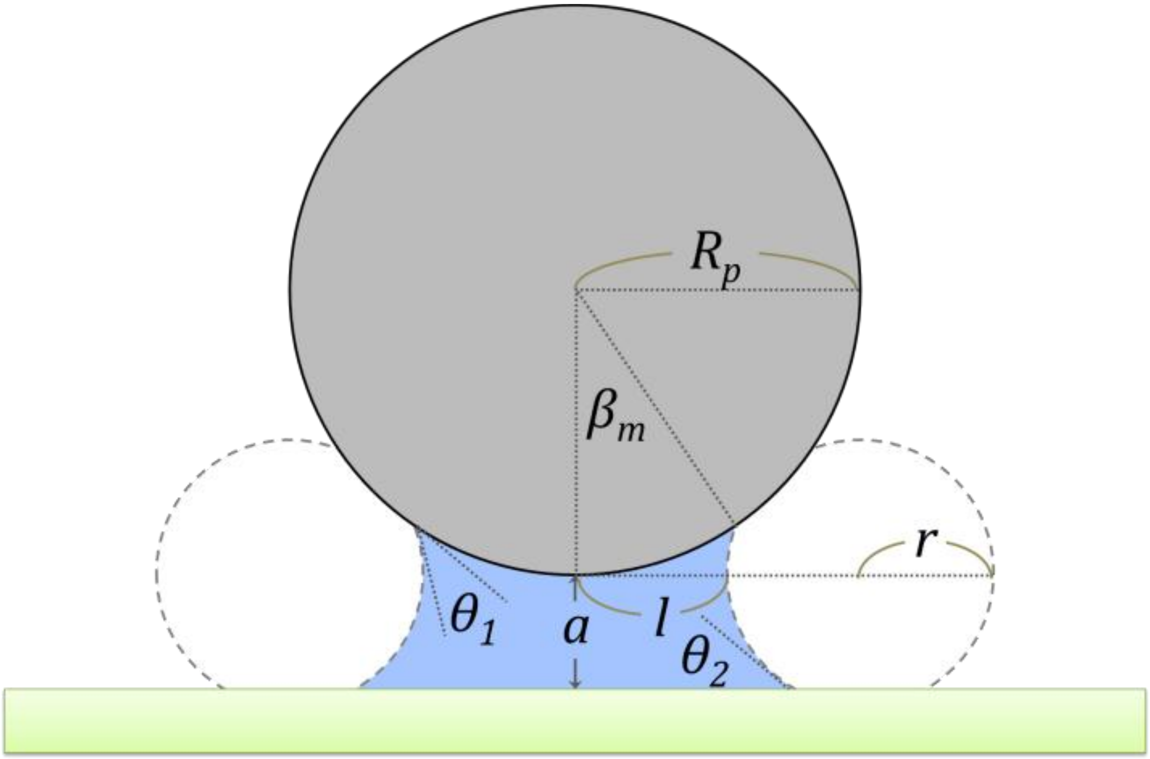

Figure 5.2. Simple schematic for the adhesion of a spherical particle on a planar surface.

If a dielectric medium exists between two interacting surfaces, the relative permittivity (ε) is used instead of the vacuum permittivity. The relative permittivity is the product of the dielectric constant and the vacuum permittivity.

The values of surface potential for mica and silica at different RH levels were taken from the literature and our own measurements,[14,88,90] and were either interpolated or extrapolated (Table 5.1). The surface charge density was calculated using Gauss's Law, $\Phi = Q/\varepsilon_o$, where Φ is the electric flux. Since the electric flux is defined as the product of the electric filed (E) and the surface area (A), i.e., $\Phi = EA$, the electric field is expressed as the surface charge density, $E = Q/\varepsilon_o A = \sigma/\varepsilon_o$. If we assume the particle and the substrate surface as two plates, the system can be treated as one of two charged sheets. Then, the electric field is given by: $E = \sigma/2\varepsilon_o$. The electric field also has the following relationship with the difference in surface potential (ΔV), $E = \Delta V/d$, where d is the distance between the two plates. Therefore, a final expression for the surface charge density at applied electrical bias (ΔV) is as follows:

$$\sigma = 2\varepsilon_o \frac{\Delta V}{d} \tag{5.3}$$

The van der Waals (F_{vdW}) and capillary (F_{cap}) forces were also calculated with the following equations.

Table 5.1. Charge density of mica and silica as a function of RH. The surface potentials of mica and silica at various levels of RH were taken from the literature, and were either interpolated or extrapolated in this study to obtain the charge densities at 0, 40, and 80% RH.[14,88,90]

RH (%)	Charge density (C/m^2)	
	Mica	Silica
0	-0.0030	-0.0001
40	-0.0019	-0.0005
80	-0.0017	-0.0009

$$F_{vdw} = \frac{H_{water} R_p}{6a^2} + \frac{H_{air} - H_{water}}{6a^2} R_p \times \frac{a^2}{\left(a + R_p - R_p \cos \beta_m\right)^2} \tag{5.4}$$

In eq 5.4, H_{water} and H_{air}, a, R_p, and β_m represent the Hamaker constant in water and air, intermolecular spacing, radius of the tip, and angle of meniscus, respectively.[1,9,41]

$$F_{cap} = \pi l \gamma_w \left[-\frac{lRT}{\gamma_w V_m} \ln\left(\frac{P}{P_o}\right) + 2\sin\left(\theta_1 + \beta_m\right) \right]$$
$$\text{where } l = R_p \sin\beta + r\left[\sin\left(\theta_1 + \beta_m\right) - 1\right] \text{ and } r = \frac{R_p\left(1 - \cos\beta_m\right) + a}{\cos\left(\theta_1 + \beta_m\right) + \cos\theta_2} \tag{5.5}$$

In eq 5.5, γ_w, R, T, V_m, θ_1 and θ_2, and P/P_o denote surface tension of water, ideal gas constant, temperature, molar volume of water, contact angle of the particle and substrate surface, and RH, respectively.[9,41]

5.3. Results and Discussion

AFM force measurements revealed the influence of both the electrostatic charge (through the electrical bias application to the system) and the RH on the interaction of a spherical particle, such as gold or silica, with various substrate surfaces, such as mica, silica, and gold. The electrostatic force was theoretically calculated as described in Section 5.2.4 and by using eqs 5.1, 5.2, and 5.3. To investigate the contribution of the electrostatic force to the total adhesion, the calculated electrostatic force was added to the experimentally measured force at 0 V at each level of RH. For the force calculations, the surface charge densities of mica and silica were obtained from literature reports including our previous studies,[14,90] and those of the gold particle or gold surface were calculated by Gauss's Law.[91]

5.3.1. The Normal Load

When an electrical bias is applied to the system through either the surface or the particle, a long-range attraction is observed in both approaching and retracting force-displacement curves. These curves generally overlap each other except for the part that represents the adhesion in the retracting curve (b'-d' in Figure 5.1), unless other events that can change the surface properties at the contact between the particle and the surface occur. As mentioned in the section of Experimental and Modeling Methods (Section 5.2), the normal load (F_n) is estimated from the retracting curve. As the long-range attraction becomes stronger, the curve shifts more towards the attractive region, and therefore the deflection is increased (d'-e' in Figure 5.1). Thus, F_n is greater for the stronger long-range attraction. In addition, the poor overlap of approaching and retracting curves implies that the contribution of the electrical potential of interacting surfaces to the total adhesion force is changed after the contact between the particle and the substrate surface due to modification of the surface properties, probably charge attenuation and charge leakage. This case is described in Section 5.3.2, The Total Adhesion Force.

Figure 5.3 shows randomly chosen data of average normal load values for the systems with mica, silica, and gold substrate surfaces, respectively. In most cases, the normal load increased with an increase of the applied positive bias to gold due to the stronger electrical attraction with the negatively charged surfaces of mica and silica. The change in the interaction of a 1 μm diameter particle with increasing bias was stronger than that of a 2.5 μm diameter particle as the RH was increased from 0 to 80%.

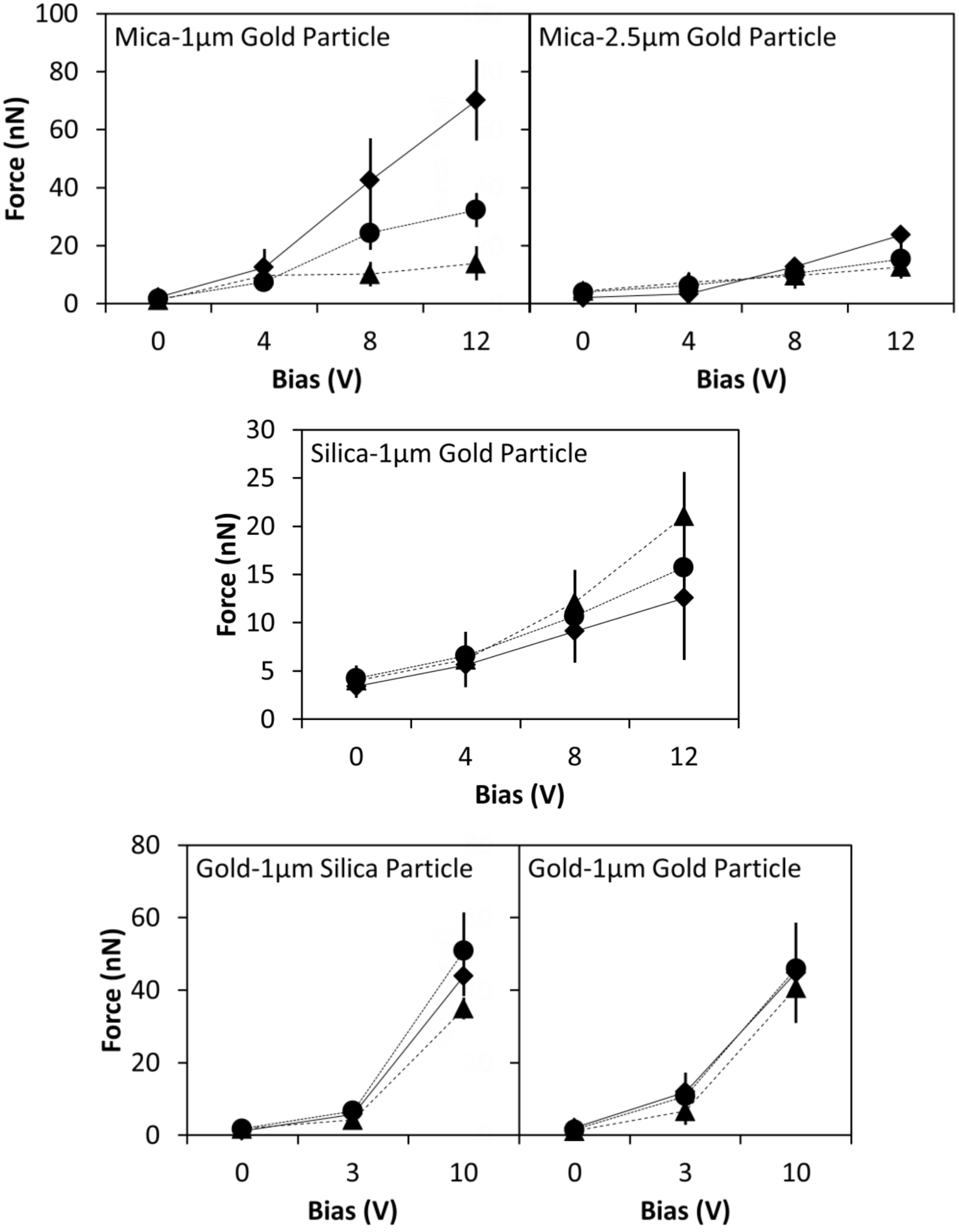

Figure 5.3. Average measurements of the normal load for the interaction of various planar surfaces with gold or silica particles. Diamonds, circles, and triangles represent the measurements at 0, 40, and 80% of RH, respectively.

This difference can be attributed to the large surface-to-volume (S/V) ratio of the 1 μm particle, which is 2.5 times greater than that of the 2.5 μm particle. The calculated surface charge density was also higher for the smaller particle. Thus, the 1-μm diameter particle more strongly responded to the change in the electrical bias. This observation agrees with that by Elfström et al. who reported that smaller nanowires acquire greater sensitivity to local charge changes.[92]

The influence of RH on the normal load (F_n) depends on the hydrophobicity or the contact angle of the interacting surfaces. Adsorption of water molecules can induce an increase in the surface charge density, depending on the material properties. For example, when water molecules are adsorbed, silica is negatively charged due to the formation of silanol groups, and thereby the density of negative charge is increased with increasing RH.[87,88,90] Guoveia et al. also reported charge build-up on silica surface due to water adsorption.[87] When an excessive amount of water molecules is adsorbed at a high RH, however, the charge is dissipated. Our results show that F_n is decreased with an increase of RH, regardless of the applied bias level for systems with mica, whereas F_n is not decreased with the RH for systems with silica or gold as substrate surfaces. This result can be explained by considering that mica is highly hydrophilic, which leads to a greater amount of adsorbed water molecules on mica than that adsorbed on silica or gold at the same level of RH.

Contrary to the general trend of the variation of the normal load (F_n) with the electrical bias, F_n is decreased with increasing bias at 0% RH (Figure 5.4). Mica acquires potassium ions between its unit layers, which balance the net charge between the layers. When mica is cleaved, the potassium ions move to either side of the layers, and therefore

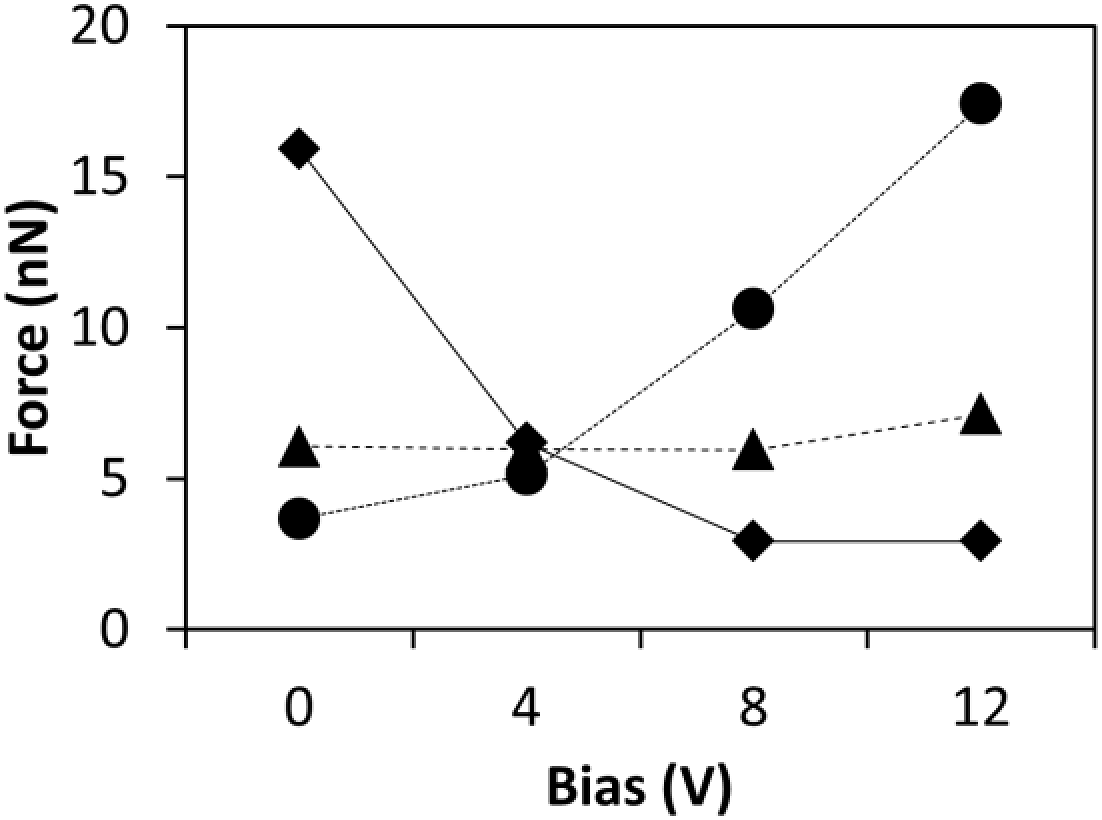

Figure 5.4. The normal load between mica and 2.5 μm gold particles with an opposite trend to the one observed at 0% RH. Diamonds, circles, and triangles represent the measurements at 0, 40, and 80% RH, respectively.

the freshly cleaved mica is either positively or negatively charged. The surface charge of mica is highly localized due to the irregular removal of potassium ions, as well as the inconsistent cleavage rate.[52] The observation at 0% RH implies that the surface charge of mica is positive for the set of experiments shown in Figure 5.4, whereas mica is negatively charged for the sets of experiments shown in Figure 5.3. When RH is increased to 40%, however, the change of the normal force with the bias recovers to the general behavior. When the freshly cleaved mica is covered with water, potassium ions are dissociated into water and the sign of surface charge becomes negative,[93] indiciating that the electrostatic attraction is increased with the positive bias. When RH is increased to 80%, the increase of the bias does not further influence F_n because the amount of adsorbed water molecules is enough to dissipate the surface charge of mica and shield the influence of surface potential.

The electrostatic contribution of interacting surfaces and the influence of water adsorption are discussed further in the following section.

5.3.2. The Total Adhesion Force

The measured total adhesion force (F_{tot}) and the theoretically calculated values of the interaction force between mica and a 1-µm gold particle are shown in Figure 5.5. The total adhesion force is increased with increasing electrical bias at 0 and 40% RH due to the contribution of the electrostatic interaction. At 80% RH, however, the force is increased from 0 to 4 V electrical bias, and is decreased with further increase of the bias. This result suggests that the relationship between surface potential and water adsorption can be explained in two ways: first, the extent of increase in F_{tot} from 0 to 4 V at 0% RH is similar to the one at 40% RH, but the force becomes stronger at 40% RH than

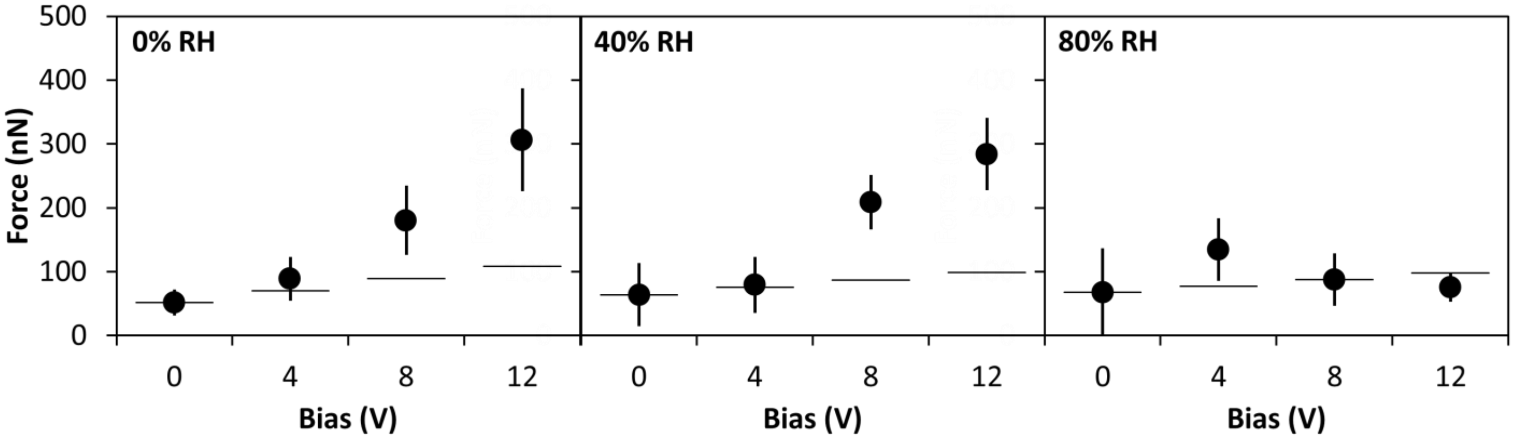

Figure 5.5. Average measurements of the total adhesion force (solid circles) and theoretical values (horizontal bars) of the interaction between mica and a 1-µm diameter gold particle. The horizontal bars are the sums of the measured total adhesion force at 0 V and the theoretically calculated electrostatic force.

at 0% RH, as the bias is increased from 4 to 8 V. A similar behavior was observed at a lower bias application, i.e., from 0 to 4 V, at 80% RH. By considering that RH was the only variable changing in the two cases, this result implies that the amount of adsorbed water molecules increased due to the application of bias, leading to an increase in F_{tot} by the capillary force. This result can be attributed to the high polarity of the water molecules. Beyond a certain amount of adsorbed water molecules due to the increase of RH, however, F_{tot} is reduced. For 40% RH, the adsorbed water molecules shielded the surface potential so that the contribution of the electrostatic force (F_{el}) was reduced.

For 80% RH, the increased amount of water molecules eventually caused charge leakage when the electrical bias was increased over 4 V. The charge leakage can be more clearly identified by comparing the force-displacement curve in the same set of experiments. As Figure 5.6 shows, the long-range attraction was significantly reduced after the first contact of the two surfaces during force measurements. Even though the force measurements were conducted in a randomly chosen area, water molecules adsorbed on the particle surface continuously provide a passage for charge leakage. As a result, at 80% RH F_{tot} was reduced to the force value when no electrical bias was applied.

The relative humidity also affects the total adhesion force (F_{tot}); in general F_{tot} increases with increasing RH, especially at 0 and 4 V. Even though the force was measured prior to the complete formation of a meniscus between the interacting surfaces, water adsorption contributed to F_{tot} by increasing the capillary force. However, the contribution of RH was much smaller than that of the electrostatic force.

The contribution of the electrostatic force (F_{el}) was calculated by the theoretical model. To compare the theoretical forces with the experimental measurements,

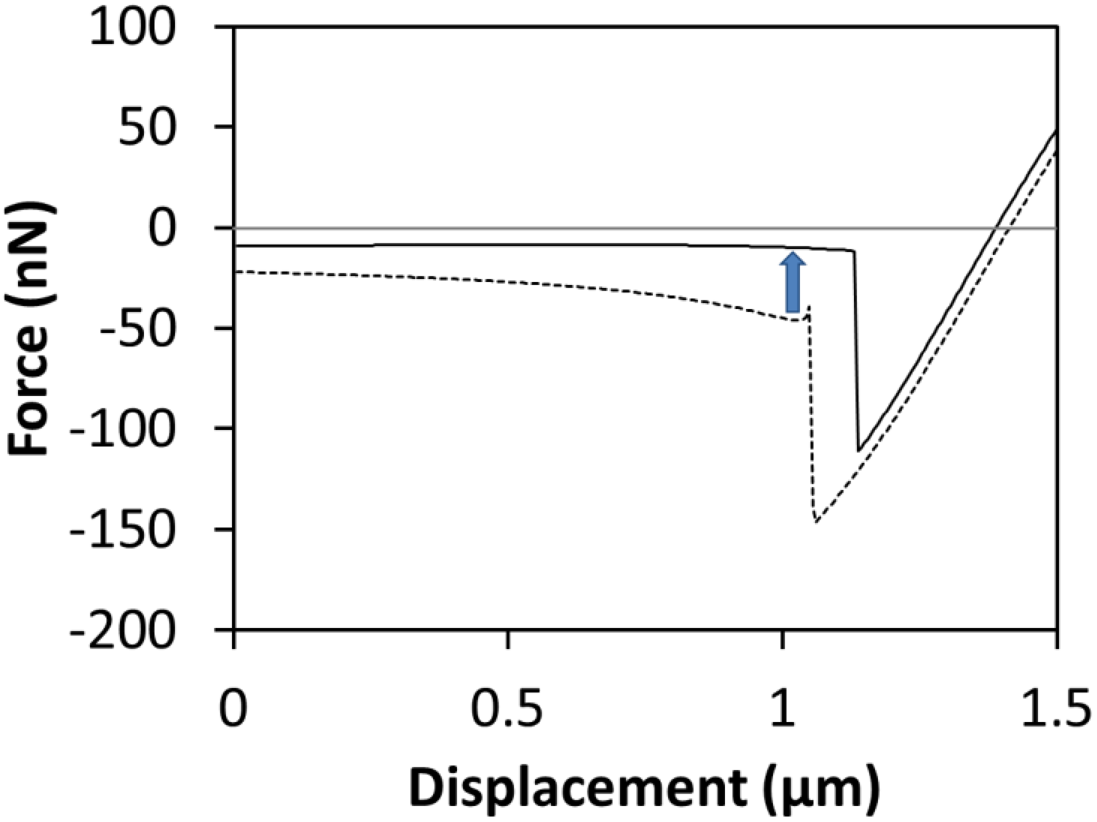

Figure 5.6. Force-displacement curves of the first (dotted line) and second (solid line) measurements in the same set of experiments. The decrease of the normal load and the total adhesion force in the second measurement indicates that charge leakage occurred at the contact of the gold particle and mica.

the calculated F_{el} was added to the measured F_{tot} at 0 V for each level of RH. The horizontal bars in Figure 5.5 are the sums of the measured forces at 0 V and the theoretical F_{el}. The theoretical model can predict the increase of the force with the bias, but it underestimates the contribution of F_{el}, except when charge leakage occurred. Since the surface charge density or surface potential of mica is highly localized, both positive and negative charges exist on the same surface of a freshly cleaved mica.[52] Moreover, the charge density of mica can be varied according to the cleavage rate.[52] Thus, the poor reproducibility for the charge density of mica is inevitable. As a result, the theoretical model is only able to capture the general trend of the variation of force with the electrical bias. The model cannot describe the charge leakage occurring at 8 and 12 V for 80% RH because it does not include terms describing the influence of water adsorption.

Figure 5.7 presents the total adhesion force (F_{tot}) between mica and a 2.5 μm gold particle. It is shown that the force is not influenced by the bias application as much as the total adhesion force found for the mica-1μm gold particle system. The smaller contribution of F_{el} to the interaction force between mica and a 2.5 μm gold particle was expected based on the results of Figure 5.3, where the magnitude of F_n for the 2.5 μm gold particle was much smaller than that for the 1 μm gold particle. In addition, F_{tot} was slightly decreased as the bias was increased from 0 to 4 V. It is unclear what caused this behavior, but a repulsive effect is not likely because the presented results do not include data showing repulsion in the F_n. The total adhesion force was increased with a further increase of the bias voltage. Charge leakage was also observed at 12 V for 80% RH. The influence of RH on F_{tot} was stronger than that of the bias on the interaction force between

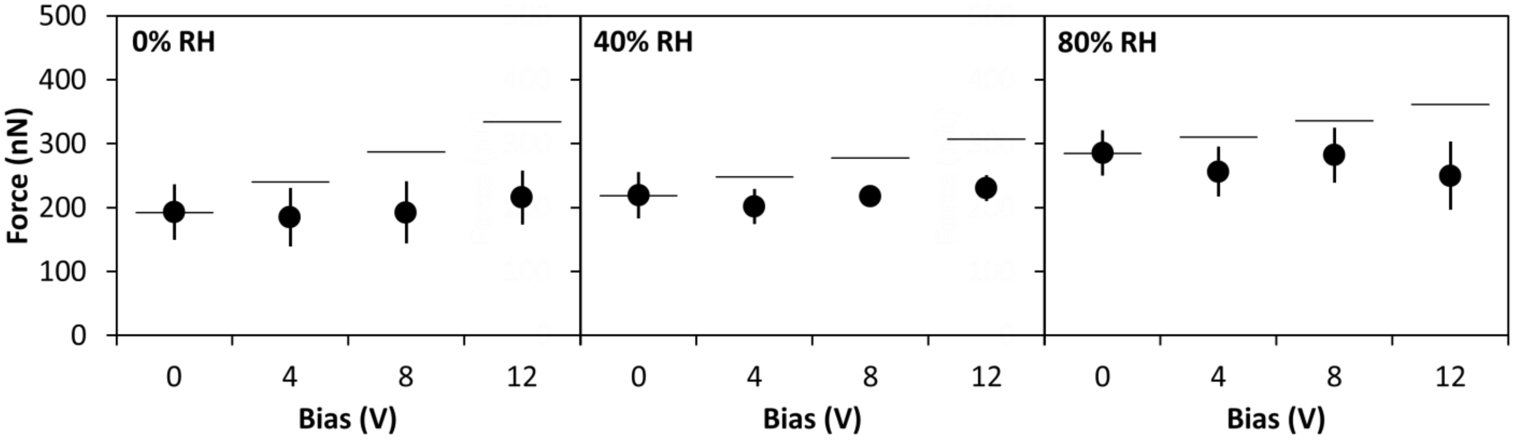

Figure 5.7. Average measurements of the total adhesion force (solid circles) and theoretical values (horizontal bars) of the interaction between mica and a 2.5 µm diameter gold particle. The horizontal bars are the sums of the measured total adhesion force at 0 V and the theoretically calculated electrostatic force.

mica and a 2.5 µm particle, and the magnitude of the force was larger than that of the interaction force between mica and a1 µm gold particle. This is opposite to the behavior of the F_n which is independent from the capillary and van der Waals forces, implying that the capillary force is the major contributor to F_{tot} for the interaction of larger particles. The theoretical model describes only the trend in F_{tot} after 4 V of the applied bias for 0 and 40% RH, and overestimates the magnitude of the force. As explained for the mica-1 µm gold particle system, the discrepancy is due to the poor reproducibility of the surface charge density of mica and the absence of terms that account for the influence of water adsorption on the interacting surfaces.

Figure 5.8 shows the results of the interaction of the fused silica with a 1 µm gold particle. The total adhesion force (F_{tot}) between silica and a 1 µm gold particle showed larger variations than that of mica-gold particles, which may be attributed to the heterogeneous surface properties of silica. It is reported that the surface potential of dielectric surfaces is heterogeneous.[70,88,94] The silica surface also has a surface roughness of about 2 nm in RMS (root mean square), whereas mica is atomically flat.[71] Therefore, the larger variation in the measured force may be due to the roughness of the surface.

As shown in Figure 5.8, the interaction force between silica and a1 µm gold particle was influenced by the increase of the bias application but not as much as that between mica and a 1 µm gold particle. The increase of F_{tot} from 0 to 12 V of the particle bias was up to 18% at 0 and 40% of RH, but only 2% at 80% of RH. This is due to the much lower surface charge density of silica than that of mica.[14,90] The total adhesion force was gradually increased with increasing bias at all RH levels, indicating that the amount of adsorbed water molecules on silica, even at 80% RH, was not enough to cause

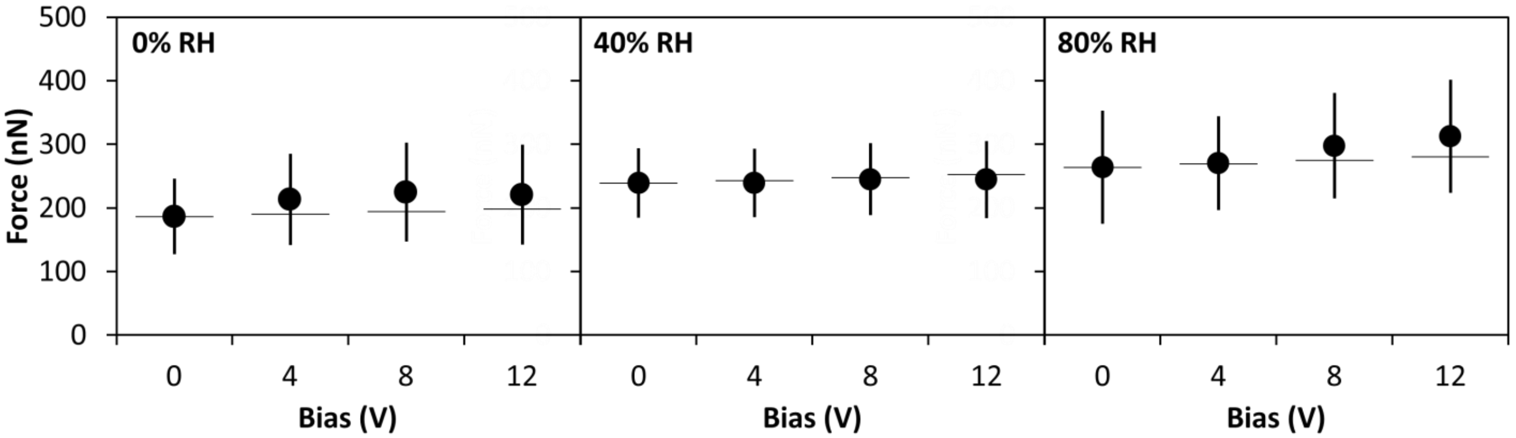

Figure 5.8. Average measurements of the total adhesion force (solid circles) and theoretical values (horizontal bars) of the interaction between silica and a 1 µm diameter gold particle. The horizontal bars are the sums of the measured the total adhesion force at 0 V and the theoretically calculated electrostatic force.

charge leakage. This behavior is different from the results on mica shown in Figure 5.5. Since silica is less hydrophilic than mica, it is thought that silica is not completely covered by a water layer.[71] For this system, a good agreement between the measured force data and the theoretical values implies less interference between water adsorption and surface potential.

The total adhesion force (F_{tot}) for the interaction between silica and a 2.5 µm gold particle was larger than that between silica and a1µm gold particle, but the trend in the force was inconsistent with either the electrical bias or the RH (results not shown). It is unclear what led to this result, but the heterogeneity of silica including surface roughness and electrostatic charge can be a possible reason, as it was reported that it is difficult to reproduce or predict the surface potential of insulating materials.[70]

For the gold foil interaction with a 1 µm silica particle, the trend in the total adhesion force (F_{tot}) with the application of the electrical bias was similar to the interaction between silica and a 1µm gold particle. The total adhesion force increased with increasing bias, as it is described by the theoretical model, and also increased with an increase of RH (Figure 5.9). However, the magnitude of the force was much smaller than that for the interaction between silica and the gold particle. Metals, including gold, have much higher Hamaker constant values (up to an order of magnitude higher) due to their high polarizability,[1] thus the theoretical model (eq. 5.5) predicts a relatively strong adhesion force between gold and a 1 µm silica particle, about 220 nN at 0 V and 0% RH, i.e., at conditions with no contributions from the capillary and electrostatic forces. Due to the high surface energy of the gold surface, however, various gas phase impurities including organic substances easily adsorb to gold, leading to a decrease in the van der

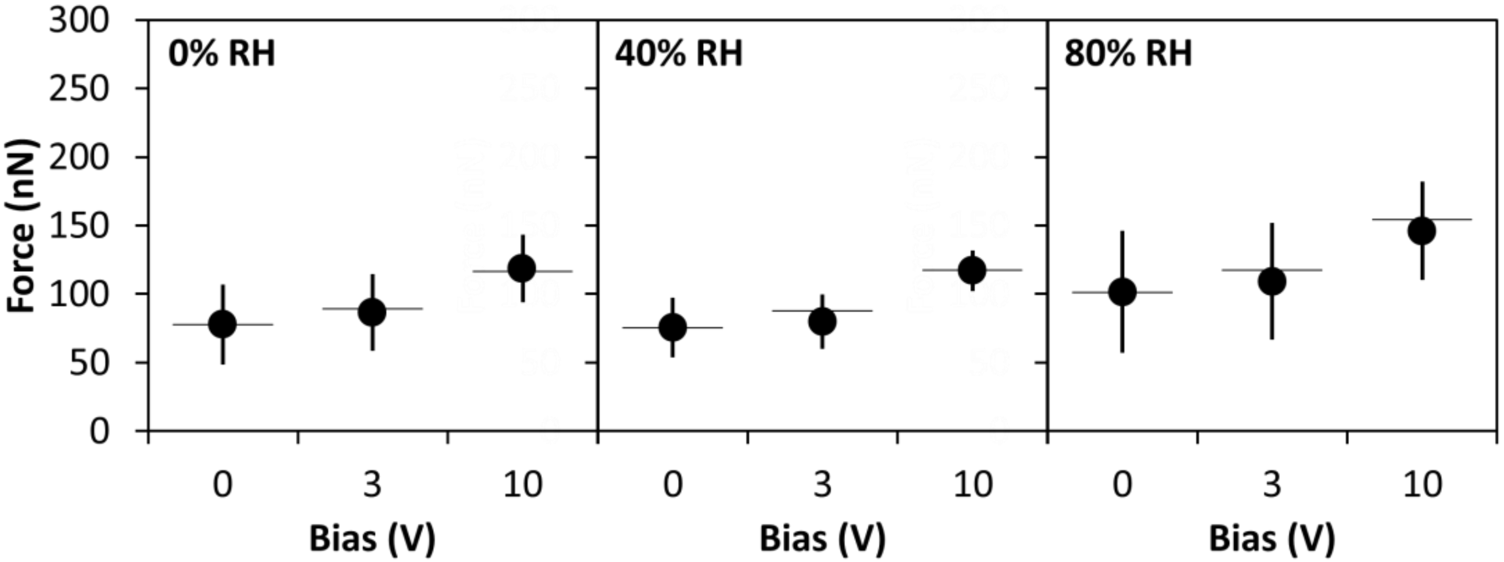

Figure 5.9. Average measurements of the total adhesion force (solid circles) and theoretical values (horizontal bars) of the interaction between gold and a 1-µm diameter silica particle. The horizontal bars are the sums of the measured the total adhesion force at 0 V and the theoretically calculated electrostatic force.

Waals force.[1,65-67] The total adhesion force for the gold-gold particle system was even smaller than that of the gold-silica particle (Figure 5.10). Therefore, surface contamination of both the gold foil and the gold particle was suspected. The total adhesion force increased with RH, regardless of the bias level. However, a good agreement between the measurements and calculated values suggests that the influence of water adsorption on the contribution of the electrostatic force was minimal.

The total adhesion force between a gold substrate and a gold particle also increased with the electrical bias, but it decreased with increasing RH. Theoretical models (eqs. 5.4 and 5.5) show that this trend can be found in the interaction between highly hydrophobic surfaces.[1,9,41] Therefore, the results indicate that the gold surface and gold particle have a higher contact angle than silica surfaces.

5.4. Conclusions and Implications

The influence of surface electrostatic properties on interaction forces was studied by measuring the total adhesion force of sphere-plane systems using AFM. Electrical bias was applied through either a gold particle for dielectric planes or a gold foil to modify the surface potential and subsequently the electrostatic surface charge. For the mica-1 µm gold particle system, the contribution of the electrostatic force increases with the electrical bias, but the extent of the increase is diminished as RH is increased. At 80% RH, the total adhesion force decreases to the value of the adhesion force without bias application due to charge leakage caused by an excessive amount of adsorbed water molecules. When the particle size is increased from 1 µm to 2.5 µm, the influence of the bias is decreased, suggesting that the capillary force is the dominant contributor to the

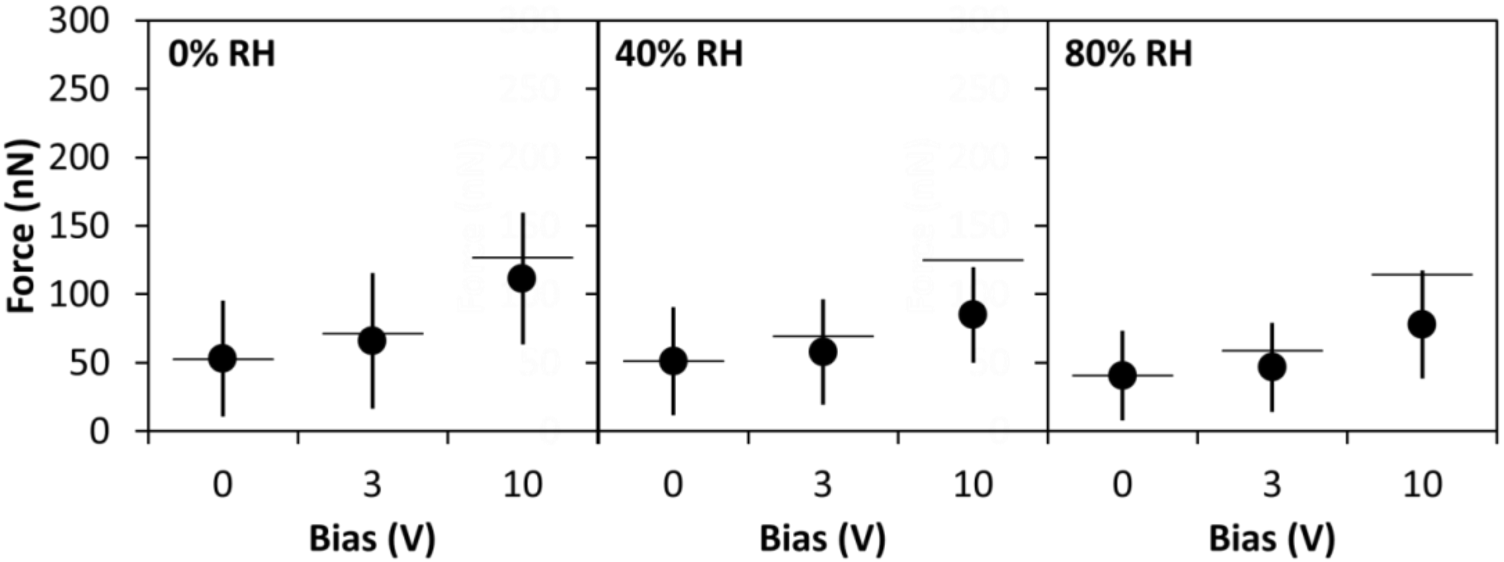

Figure 5.10. Average measurements of the total adhesion force (solid circles) and theoretical values (horizontal bars) of the interaction between gold and a 1µm gold particle. The horizontal bars are the sums of the measured the total adhesion force at 0 V and the theoretically calculated electrostatic force.

total adhesion force. When mica acquires positive charge upon cleavage, the influence of the bias becomes reverse due to the electrostatic repulsion between likely charged surfaces, but regains its general trend due to water adsorption. The total adhesion forces for the other systems with silica substrate-gold particle, gold substrate-silica particle, and gold substrate-gold particle also become stronger with increasing bias, but the change in the forces is smaller than that for the mica-gold particle system because silica and gold substrates acquire a smaller surface charge density. The influence of water adsorption on the contribution of the electrostatic force depends on the hydrophobicity or contact angle of the interacting surfaces.

Theoretical estimations of interaction forces were obtained by adding the electrostatic force to the measured force at 0 V at each level of RH. In most cases, the measured forces agree well with the theoretically calculated values except for the mica-gold particle system because the surface potential of mica is not uniform but localized and cannot be described by a single measurement.[52] The theoretical model does not include contributions from complex phenomena, such as charge attenuation or charge leakage, caused by water adsorption. The amount of water adsorption and its influence on the electrostatic properties of dielectric surfaces become important at high values of RH. A charge leakage model needs to be developed to further improve the theoretical predictions. Our results may be useful for providing insight into the monitoring and control of micron- and submicron-size particles in atmospheric systems where the effects of surface electrostatic charge and RH become important.

5.5. Summary

The influence of electrostatic charge on the adhesion force between spherical particles and interacting planar surfaces was studied using atomic force microscopy. Electrical bias was applied to modify the surface electrostatic charge, and it was found that application of a stronger positive bias to the spherical particle induces a stronger total adhesion force. The sensitivity of the system to changes in the bias was the highest with mica due to its highest surface charge density among the materials investigated. For larger-size particles, the contribution of the electrostatic force was diminished, and thereby the capillary force became the major contributor to the total adhesion force. The influence of water adsorption on the total adhesion force and, specifically, on the contribution of the electrostatic force depends on the hydrophobicity or the contact angle of interacting surfaces. For a hydrophilic surface, water adsorption either attenuates the surface charge or screens the effect of surface potential. An excessive amount of adsorbed water provides a path to surface charge leakage, which may cancel out the electrostatic force, leading to a reduction in the adhesion force. Theoretically calculated forces agree well with measured adhesion forces except for mica which has a highly localized surface potential. The results of this study provide fundamental information on the behavior of charged colloidal particles in atmospheric systems.

CHAPTER 6

CONCLUSIONS AND RECOMMENDATIONS

6.1. Conclusions

The research studies in this thesis focused on surface phenomena between particles and planar surfaces in atmospheric systems and included experimental measurements and theoretical studies. Particles included *Bacillus thuringiensis* spores and spherical particles of silica and gold. Mica, silica, gold, as well as radioactive gold were used as planar surfaces. The interaction forces between surfaces were measured using atomic force microscopy (AFM), and the theoretical calculations were carried out using mathematical equations for the van der Waals, capillary, and electrostatic forces. Based on the research, the factors influencing interfacial interactions were identified and include the physical and chemical properties of interacting surfaces and the conditions of surrounding environments. The force-distance curves obtained by AFM provide information on the changes in the surface properties due to the contact between the particles and planar surfaces. Details about the experimental and theoretical studies carried out in this thesis and specific conclusions are given below.

- The friction and adhesion forces of spores of *Bacillus thuringiensis* and silica particles on planar surfaces, such as mica and silica, in atmospheric systems were investigated at various relative humidity (RH) levels. It was found that the strong surface charge density of mica at low RH induces a long-range attraction between the AFM cantilever and mica, which leads to strong friction forces for the spores and silica particles. As RH increases, water molecules readily adsorb onto the atomically flat hydrophilic mica surface, causing the friction force to decrease. When a rough silica surface is used instead of the atomically flat mica, an increase in RH leads to increasing friction force, which is a result of increasing viscous resistance by adsorbed water molecules and a stronger capillary attraction. As the hydrophobicity of interacting surfaces increases, the significance of RH diminishes. The friction force of the spores shows a linear relationship to the total normal force on a hydrophobic surface. In regard to adhesion force, comparisons between measured and theoretical values indicate the importance of surface charge and contamination. The measurements of single particle interactions with surfaces under controlled relative humidity are extremely useful in understanding the behavior of population of particles. Particle-particle interactions are important and need to be considered in cases of systems with high concentrations of particles.

- The adhesion force of gold was studied to provide a fundamental understanding of the interaction of self-charging radioactive particles with surrounding environmental surfaces in atmospheric systems. Using AFM, the force was measured for gold that acquired surface potential either by irradiation or by application of electrical bias. Radioactivity influences the adhesion force of the irradiated gold because the surface potential generated by irradiation introduces a significant contribution of the electrostatic force to the total adhesion force. Comparisons of experimental measurements with theoretical values reveal a possible relationship between surface potential and water adsorption, which may cause an increase in the capillary force or a reduction in the contribution of the electrostatic force by either screening the surface potential or providing a passage for charge leakage. In the case of likely charged surfaces, an electrostatic repulsive force should exist, making it difficult for these particles to aggregate and settle down on environmental surfaces in close proximity. In addition, particles with higher surface potential should exhibit stronger forces. Therefore, radioactive particles may travel far from their original sources and pollute initially uncontaminated areas by adhering to nonradioactive surfaces that are neutral or oppositely charged.

- The influence of electrostatic properties of interacting surfaces was studied by measuring the total adhesion force of sphere-plane systems using AFM. Electrical bias was applied through either a gold particle for dielectric surfaces or a gold foil in order to modify and control the electrostatic charge of surfaces. Overall, the contribution of the electrostatic force increases with the electrical bias, but the extent of the increase becomes smaller as RH increases. The influence of water adsorption on the contribution of the electrostatic force depends on the hydrophobicity or contact angle of the interacting surfaces. In systems that include mica, which is highly hydrophilic, the total adhesion force is reduced at high levels of RH due to charge leakage caused by the excessive amount of adsorbed water molecules. When the particle size increases, the influence of electrical bias is decreased, suggesting that the capillary force is the dominant contributor to the total adhesion force. When mica acquires positive charge upon cleavage, the influence of electrical bias is opposite due to the electrostatic repulsion between likely charged surfaces, but it regains its general trend due to water adsorption. In systems that include silica or gold substrate, the change in the force due to the electrical bias is smaller than what was observed in systems that include mica because silica and gold substrates have a lower surface charge density. Theoretical values of the forces were calculated by adding the electrostatic force to the measured force at 0 V at each level of RH. In most cases, the measured forces agree well with the theoretically calculated values except for the mica-gold particle system because the surface potential of mica is not uniform but localized. The theoretical models for interaction forces do not include contributions from complex phenomena such as charge attenuation or charge leakage caused by water adsorption. Since the amount of water adsorption and its influence on the electrostatic properties of dielectric surfaces become important at high values of RH, modifications of the models to include the influence of water adsorption on the contribution of electrostatic force are important.

The studies presented in this thesis have important environmental implications in the following areas:

- The interaction forces of particles at microscales and nanoscales were quantified and can be used as a basis in various processes such as aggregation, sedimentation, and deposition of particulate contaminants. A few examples where such processes are involved include indoor air contamination due to poor filtration of particulate aerosols, secondary contamination of areas far from the originally polluted sites, and wear of mechanical equipment and release of particulate debris.
- They can be the building blocks to improve current theoretical models that predict the behavior of particles in atmospheric systems. As our studies show, the

behavior of particles is governed by several factors including surface properties and surrounding conditions.

- They can be useful in suggesting strategies to control and prevent particulate contamination in atmospheric systems.

6.2. Recommendations

The following studies are suggested to strengthen the results found in this thesis.

- The change in the friction of a bacterial spore or a silica particle was explained based on surface properties and the conditions of surrounding environments. The triboelectric effect was not considered, which can also influence friction and adhesion of particles. Thus, it is suggested to study the change of electrical properties of interacting surface due to friction.
- For the capillary force theoretical calculations, only the water meniscus formation between the particle and the surface was considered. Literature studies have suggested that a layer of water covers the entire interacting bodies. The hydrophobicity of interacting surfaces and the relative humidity influence how water is involved in the interactions. Therefore, it is expected that if such effects are included in the models, they will provide a more accurate prediction of the capillary contribution to the particle adhesion.
- For the capillary force calculations, the water meniscus was considered to be free of impurities. In practice, however, various types of contaminants can be dissociated into water, such as organics and ions. Considering that changes in ionic strength can influence the surface tension of water, the inclusion of such an

effect to the theoretical force calculations is expected to improve the agreement between experimental results and theoretical values.

- The adsorption of water molecules, which is not considered in the current theoretical models, can modify the electrostatic properties of interacting surfaces regardless of their contact. Thus, understanding and quantifying how water adsorption influences surface potential can provide important knowledge in predicting particle behavior in atmospheric systems.

Based on the results presented in this thesis, the following future studies are suggested:

- The study of adhesion force can be useful in examining the suitability of materials for various applications. For example, titanium dioxide (TiO_2) can be used as a photocatalyst, and graphene has potential in desalination or in solar cells. Studies of the interaction forces between such materials and other surfaces can help identify their advantages and disadvantages and quantify how they can perform in diverse applications.
- Interaction forces of radioactive materials in atmospheric systems were investigated in this work. Radioactive particles are also expected to contaminate aquatic and subsurface systems. The adhesion force between *Bacillus thuringiensis* (*Bt*) spores and mica in water was studied in our group, and it was found that the surface charge is influenced by such solution variables as pH and ionic strength. In addition, the classical model based on Derjaguin-Landau-Verwey-Overbeek (DLVO) theory was employed to describe the adhesion force of spores in water. Radioactive particles are different from *Bt* spores since they acquire surface charge through a self-charging process that continuously occurs as

radioactivity decays. Therefore, a study of the adhesion force of radioactive particles in water to examine whether their behavior is different from that of non-radioactive particles is of interest.

- Transport of colloidal particles in atmospheric systems is influenced by their interfacial interaction forces at microscales and nanoscales, as well as meteorological conditions, such as the rate and direction of air flow, temperature, and precipitation. Therefore, combining interaction forces of colloidal particles with variations of meteorological conditions can be the next step in this research to provide important information that can predict the behavior of colloidal particles in the environment.

REFERENCES

(1) Israelachvili, J. *Intermolecular and surface forces*; 2nd ed.; Academic Press: London, 1991.

(2) Taboada-Serrano, P.; Vithayaveroj, V.; Yiacoumi, S.; Tsouris, C. *Environ. Sci. Technol.* **2005**, *39*, 6352.

(3) Carpick, R. W.; Salmeron, M. *Chem. Rev.* **1997**, *97*, 1163.

(4) Chung, E.; Kweon, H.; Yiacoumi, S.; Lee, I.; Joy, D. C.; Palumbo, A. V.; Tsouris, C. *Environ. Sci. Technol.* **2010**, *44*, 290.

(5) Li, Q. L.; Elimelech, M. *Environ. Sci. Technol.* **2004**, *38*, 4683.

(6) Taboada-Serrano, P. L. *Colloidal interactions in aquatic environments effect of charge heterogeneity and charge asymmetry*, 2005.

(7) Paajanen, M.; Katainen, J.; Pakarinen, O. H.; Foster, A. S.; Lahtinen, J. *J. Colloid Interface Sci.* **2006**, *304*, 518.

(8) Israelachvili, J. N.; McGuiggan, P. M. *Science* **1988**, *241*, 795.

(9) Orr, F. M.; Scriven, L. E.; Rivas, A. P. *J. Fluid Mech.* **1975**, *67*, 723.

(10) Xu, L.; Lio, A.; Hu, J.; Ogletree, D. F.; Salmeron, M. *J. Phys. Chem. B* **1998**, *102*, 540.

(11) Jones, R.; Pollock, H. M.; Cleaver, J. A. S.; Hodges, C. S. *Langmuir* **2002**, *18*, 8045.

(12) Reed, L. D.; Jordan, H.; Gieseke, J. A. *Journal of Aerosol Science* **1977**, *8*, 457.

(13) Westphal, A. J.; Price, P. B.; Leighton, T. J.; Wheeler, K. E. *Proc. Natl. Acad. Sci. U. S. A.* **2003**, *100*, 3461.

(14) Chung, E.; Yiacoumi, S.; Lee, I.; Tsouris, C. *Environ. Sci. Technol.* **2010**, *44*, 6209.

(15) Butt, H. J.; Berger, R.; Bonaccurso, E.; Chen, Y.; Wang, J. *Adv. Colloid Interface Sci.* **2007**, *133*, 91.

(16) Butt, H. J.; Cappella, B.; Kappl, M. *Surf. Sci. Rep.* **2005**, *59*, 1.

(17) Feiler, A. A.; Stiernstedt, J.; Theander, K.; Jenkins, P.; Rutland, M. W. *Langmuir* **2007**, *23*, 517.

(18) Sirghi, L. *Appl. Phys. Lett.* **2003**, *82*, 3755.

(19) Mo, Y. F.; Turner, K. T.; Szlufarska, I. *Nature* **2009**, *457*, 1116.

(20) Madigan, M. T. *Brock biology of microorganisms*; 11th ed. ed.; Pearson Prentice Hall: Upper Saddle River, NJ :, 2006.

(21) Ubbink, J.; Schar-Zammaretti, P. *Micron* **2005**, *36*, 293.

(22) Turnbull, P. C. B.; Lindeque, P.; Le Roux, J.; Bennett, A. M.; Parks, S. R. *J. Appl. Microbiol.* **1998**, *84*, 667.

(23) Clement, C. F.; Harrison, R. G. *Journal of Aerosol Science* **1992**, *23*, 481.

(24) Chesser, R. K.; Bondarkov, M.; Baker, R. J.; Wickliffe, J. K.; Rodgers, B. E. *Journal of Environmental Radioactivity* **2004**, *71*, 147.

(25) Yoschenko, V. I.; Kashparov, V. A.; Protsak, V. P.; Lundin, S. M.; Levchuk, S. E.; Kadygrib, A. M.; Zvarich, S. I.; Khomutinin, Y. V.; Maloshtan, I. M.; Lanshin, V. P.; Kovtun, M. V.; Tschiersch, J. *Journal of Environmental Radioactivity* **2006**, *86*, 143.

(26) Pagelkopf, P.; Porstendorfer, J. *Atmos. Environ.* **2003**, *37*, 1057.

(27) Lujaniene, G.; Aninkevicius, V.; Lujanas, V. *J. Environ. Radioact.* **2009**, *100*, 108.

(28) Ooe, H.; Seki, R.; Ikeda, N. *Journal of Environmental Radioactivity* **1988**, *6*, 219.

(29) Yoschenko, V. I.; Kashparov, V. A.; Levchuk, S. E.; Glukhovskiy, A. S.; Khomutinin, Y. V.; Protsak, V. P.; Lundin, S. M.; Tschiersch, J. *Journal of Environmental Radioactivity* **2006**, *87*, 260.

(30) Clement, C. F.; Clement, R. A.; Harrison, R. G. *Journal of Aerosol Science* **1995**, *26*, 1207.

(31) Clement, C. F.; Harrison, R. G. *Journal of Aerosol Science* **2000**, *31*, 363.

(32) Gensdarmes, F.; Boulaud, D.; Renoux, A. *Journal of Aerosol Science* **2001**, *32*, 1437.

(33) Mayya, Y. S.; Tripathi, S. N.; Khan, A. *Journal of Aerosol Science* **2002**, *33*, 781.

(34) Chin, C. J.; Yiacoumi, S.; Tsouris, C. *Environ. Sci. Technol.* **2002**, *36*, 343.

(35) Ruan, J. A.; Bhushan, B. *J. Tribol.-Trans. ASME* **1994**, *116*, 378.

(36) Wang, Y. L.; Zhao, X. Z.; Zhou, F. Q. *Rev. Sci. Instrum.* **2007**, *78*.

(37) Meyer, G.; Amer, N. M. *Appl. Phys. Lett.* **1990**, *57*, 2089.

(38) Hazel, J. L.; Tsukruk, V. V. *J. Tribol.-Trans. ASME* **1998**, *120,* 814.

(39) Tocha, E.; Schonherr, H.; Vancso, G. J. *Langmuir* **2006**, *22,* 2340.

(40) Ouyang, Q.; Ishida, K.; Okada, K. *Appl. Surf. Sci.* **2001**, *169,* 644.

(41) Xiao, X. D.; Qian, L. M. *Langmuir* **2000**, *16*, 8153.

(42) Feng, J. Q.; Hays, D. A. *IEEE Trans. Ind. Appl.* **1998**, *34*, 84.

(43) Hays, D. A. *J. Adhes. Sci. Technol.* **1995**, *9*, 1063.

(44) Camesano, T. A.; Liu, Y. T.; Datta, M. *Adv. Water Resour.* **2007**, *30*, 1470.

(45) Sheng, X. X.; Ting, Y. P.; Pehkonen, S. O. *J. Colloid Interface Sci.* **2007**, *310*, 661.

(46) Ong, Y. L.; Razatos, A.; Georgiou, G.; Sharma, M. M. *Langmuir* **1999**, *15*, 2719.

(47) Lee, I.; Chung, E.; Kweon, H.; Yiacoumi, S.; Tsouris, C. *Submitted*.

(48) Lyndenbell, R. M. *Surf. Sci.* **1991**, *244*, 266.

(49) Campbell, P. A.; Sinnamon, L. J.; Thompson, C. E.; Walmsley, D. G. *Surf. Sci.* **1998**, *410*, L768.

(50) Xu, L.; Salmeron, M. *Langmuir* **1998**, *14*, 2187.

(51) Park, S. H.; Sposito, G. *Phys. Rev. Lett.* **2002**, *89*.

(52) Higginbotham, I. G.; Williams, R. H.; McEvoy, A. J. *J. Phys. D-Appl. Phys.* **1975**, *8*, 1033.

(53) Xu, K.; Cao, P. G.; Heath, J. R. *Science* **2010**, *329*, 1188.

(54) Beaglehole, D.; Radlinska, E. Z.; Ninham, B. W.; Christenson, H. K. *Phys. Rev. Lett.* **1991**, *66*, 2084.

(55) Cantrell, W.; Ewing, G. E. *J. Phys. Chem. B* **2001**, *105*, 5434.

(56) Ohnishi, S.; Stewart, A. M. *Langmuir* **2002**, *18*, 6140.

(57) Binggeli, M.; Mate, C. M. *Appl. Phys. Lett.* **1994**, *65*, 415.

(58) Burkhard, D. J. M.; Scherer, T. *J. Non-Cryst. Solids* **2006**, *352*, 241.

(59) Somorjai, G. A. *Chem. Rev.* **1996**, *96*, 1223.

(60) Ando, Y. *Wear* **2000**, *238*, 12.

(61) Jinesh, K. B.; Frenken, J. W. M. *Phys. Rev. Lett.* **2006**, *96*.

(62) Riedo, E.; Levy, F.; Brune, H. *Phys. Rev. Lett.* **2002**, *88*.

(63) Barnette, A. L.; Asay, D. B.; Kim, D.; Guyer, B. D.; Lim, H.; Janik, M. J.; Kim, S. H. *Langmuir* **2009**, *25*, 13052.

(64) Chen, L. J.; Gu, X. H.; Fasolka, M. J.; Martin, J. W.; Nguyen, T. *Langmuir* **2009**, *25*, 3494.

(65) Beaglehole, D.; Christenson, H. K. *J. Phys. Chem.* **1992**, *96*, 3395.

(66) Guzonas, D. A.; Hair, M. L. *Langmuir* **1991**, *7*, 2346.

(67) Liu, Z. G.; Li, Z.; Zhou, H. L.; Wei, G.; Song, Y. H.; Wang, L. *Micron* **2005**, *36*, 525.

(68) Riviére, J. C.; Myhra, S. *Handbook of surface and interface analysis: Methods for problem-solving*; 2nd ed.; CRC Press: Boca Raton, 2009.

(69) Santos, L. P.; Ducati, T. R. D.; Balestrin, L. B. S.; Galembeck, F. *J. Phys. Chem. C* **2011**, *115*, 11226.

(70) Gouveia, R. F.; Costa, C. A. R.; Galembeck, F. *J. Phys. Chem. C* **2008**, *112*, 17193.

(71) Kweon, H.; Yiacoumi, S.; Tsouris, C. *Langmuir* **2011**, *27*, 14975.

(72) Walker, M. E.; McFarlane, J.; Glasgow, D. C.; Chung, E.; Taboada-Serrano, P.; Yiacoumi, S.; Tsouris, C. *J. Colloid Interface Sci.* **2010**, *350*, 595.

(73) Jacobs, H. O.; Leuchtmann, P.; Homan, O. J.; Stemmer, A. *J. Appl. Phys.* **1998**, *84*, 1168.

(74) Lee, I.; Lee, J. W.; Stubna, A.; Greenbaum, E. *J. Phys. Chem. B* **2000**, *104*, 2439.

(75) Liu, B. Y. H.; Pui, D. Y. H. *J. Colloid Interface Sci.* **1977**, *58*, 142.

(76) Yeh, H.-C. *Journal of Aerosol Science* **1976**, *7*, 343.

(77) Sugimura, H.; Ishida, Y.; Hayashi, K.; Takai, O.; Nakagiri, N. *Appl. Phys. Lett.* **2002**, *80*, 1459.

(78) Gustavsson, J.; Altankov, G.; Errachid, A.; Samitier, J.; Planell, J. A.; Engel, E. *J. Mater. Sci.-Mater. Med.* **2008**, *19*, 1839.

(79) Tabor, R. F.; Morfa, A. J.; Grieser, F.; Chan, D. Y. C.; Dagastine, R. R. *Langmuir* **2011**, *27*, 6026.

(80) Tammet, H.; Kimmel, V.; Israelsson, S. *Atmos. Environ.* **2001**, *35*, 3413.

(81) Salthammer, T.; Schripp, T.; Uhde, E.; Wensing, M. *Environ. Pollut.* **2012**, *169*, 167.

(82) He, C.; Morawska, L.; Taplin, L. *Environ. Sci. Technol.* **2007**, *41*, 6039.

(83) McGarry, P.; Morawska, L.; He, C. R.; Jayaratne, R.; Falk, M.; Tran, Q.; Wang, H. *Environ. Sci. Technol.* **2011**, *45*, 6444.

(84) Schripp, T.; Kirsch, I.; Salthammer, T. *Sci. Total Environ.* **2011**, *409*, 2534.

(85) Wallace, L.; Wang, F.; Howard-Reed, C.; Persily, A. *Environ. Sci. Technol.* **2008**, *42*, 8641.

(86) Kok, J. F.; Renno, N. O. *Geophys. Res. Lett.* **2006**, *33*.

(87) Gouveia, R. F.; Costa, C. A. R.; Galembeck, F. *J. Phys. Chem. B* **2005**, *109*, 4631.

(88) Gouveia, R. F.; Galembeck, F. *J. Am. Chem. Soc.* **2009**, *131*, 11381.

(89) Kweon, H.; Yiacoumi, S.; Lee, I.; McFarlane, J.; Tsouris, C. *In preparation*.

(90) Lee, I.; Chung, E.; Kweon, H.; Yiacoumi, S.; Tsouris, C. *Colloid Surf. B-Biointerfaces* **2012**, *92*, 271.

(91) Boyer, L.; Houze, F.; Tonck, A.; Loubet, J. L.; Georges, J. M. *J. Phys. D-Appl. Phys.* **1994**, *27*, 1504.

(92) Elfstrom, N.; Juhasz, R.; Sychugov, I.; Engfeldt, T.; Karlstrom, A. E.; Linnros, J. *Nano Lett.* **2007**, *7*, 2608.

(93) Alcantar, N.; Israelachvili, J.; Boles, J. *Geochim. Cosmochim. Acta* **2003**, *67*, 1289.

(94) Rezende, C. A.; Gouveia, R. F.; da Silva, M. A.; Galembeck, F. *J. Phys.-Condes. Matter* **2009**, *21*.